NAVAL
POSTGRADUATE
SCHOOL

MONTEREY, CALIFORNIA

THESIS

COMPUTATIONAL FLUID DYNAMICS ANALYSIS OF SHOCK PROPAGATION AND REFLECTION IN A PULSE DETONATION ENGINE COMBUSTOR

by

Jimmy K. W. Chan

December 2003

Thesis Advisor:	Chris M. Brophy
Second Reader:	Garth V. Hobson

Approved for public release; distribution is unlimited

THIS PAGE INTENTIONALLY LEFT BLANK

REPORT DOCUMENTATION PAGE			Form Approved OMB No. 0704-0188
Public reporting burden for this collection of information is estimated to average 1 hour per response, including the time for reviewing instruction, searching existing data sources, gathering and maintaining the data needed, and completing and reviewing the collection of information. Send comments regarding this burden estimate or any other aspect of this collection of information, including suggestions for reducing this burden, to Washington headquarters Services, Directorate for Information Operations and Reports, 1215 Jefferson Davis Highway, Suite 1204, Arlington, VA 22202-4302, and to the Office of Management and Budget, Paperwork Reduction Project (0704-0188) Washington DC 20503.			
1. AGENCY USE ONLY ***(Leave blank)***	**2. REPORT DATE** December 2003	**3. REPORT TYPE AND DATES COVERED** Master's Thesis	
4. TITLE AND SUBTITLE: Computational Fluid Dynamics Analysis of Shock Propagation and Reflection in a Pulse Detonation Engine Combustor			**5. FUNDING NUMBERS** N0001403WR20159
6. AUTHOR(S) Jimmy Chan			
7. PERFORMING ORGANIZATION NAME(S) AND ADDRESS(ES) Naval Postgraduate School Monterey, CA 93943-5000			**8. PERFORMING ORGANIZATION REPORT NUMBER**
9. SPONSORING /MONITORING AGENCY NAME(S) AND ADDRESS(ES) Office of Naval Research Ballston Tower One 800 N. Quincy Street Arlinton, VA 22217-5660			**10. SPONSORING/MONITORING AGENCY REPORT NUMBER**
11. SUPPLEMENTARY NOTES The views expressed in this thesis are those of the author and do not reflect the official policy or position of the Department of Defense or the U.S. Government.			
12a. DISTRIBUTION / AVAILABILITY STATEMENT Approved for public release; distribution is unlimited			**12b. DISTRIBUTION CODE**

13. ABSTRACT (maximum 200 words)

The ability to enhance detonation wave transmission at a diffraction plane through various shock reflection/focusing conditions was evaluated numerically. The geometry dimensions were generally representative of the condition existing in a valve-less pulse detonation engine developed by the Naval Postgraduate School and consisted of a small cylindrical "initiator" combustor, which transmitted a shock wave to a larger diameter combustor. The wall cross section of the larger combustor was varied to evaluate the increase in reflected shock temperature and pressure conditions, ultimately revealing the dramatic increase in local temperature for a "scalloped" outer wall condition over the cylindrical cross section cases. The initiator diameter was held constant and the larger combustor diameters varied in order to evaluate the effects of diameter ratio on the shock reflection conditions for both cylindrical and scalloped geometries. A computational fluid dynamics (CFD) solver known as OVERFLOW was used to model the fluid dynamic processes but was limited in capability to shock wave Mach numbers less than about 4.2.

14. SUBJECT TERMS Pulse Detonation Engine, PDE, Combustion, Detonation, Computational Fluid Dynamic, CDF, Overflow, Shock Reflection, Shock Focusing.			**15. NUMBER OF PAGES** 123
			16. PRICE CODE
17. SECURITY CLASSIFICATION OF REPORT Unclassified	**18. SECURITY CLASSIFICATION OF THIS PAGE** Unclassified	**19. SECURITY CLASSIFICATION OF ABSTRACT** Unclassified	**20. LIMITATION OF ABSTRACT** UL

NSN 7540-01-280-5500 Standard Form 298 (Rev. 2-89)
Prescribed by ANSI Std. 239-18

THIS PAGE INTENTIONALLY LEFT BLANK

Approved for public release; distribution is unlimited

COMPUTATIONAL FLUID DYNAMICS ANALYSIS OF SHOCK PROPAGATION AND REFLECTION IN A PULSE DETONATION ENGINE COMBUSTOR

Jimmy K. W. Chan
Singapore Ministry of Defense
B.E., Royal Melbourne Institute of Technology University, 1997

Submitted in partial fulfillment of the
requirements for the degree of

MASTER OF SCIENCE IN ENGINEERING SCIENCE (MECHANICAL)

from the

NAVAL POSTGRADUATE SCHOOL
December 2003

Author: Jimmy K. W. Chan

Approved by: Chris M. Brophy
Thesis Advisor

Garth V. Hobson
Second Reader

Anthony J. Healey
Chairman,
Department of Mechanical and Astronautical Engineering

THIS PAGE INTENTIONALLY LEFT BLANK

ABSTRACT

The ability to enhance detonation wave transmission at a diffraction plane through various shock reflection/focusing conditions was evaluated numerically. The geometry dimensions were generally representative of the condition existing in a valve-less pulse detonation engine developed by the Naval Postgraduate School and consisted of a small cylindrical "initiator" combustor, which transmitted a shock wave to a larger diameter combustor. The wall cross section of the larger combustor was varied to evaluate the increase in reflected shock temperature and pressure conditions, ultimately revealing the dramatic increase in local temperature for a "scalloped" outer wall condition over the cylindrical cross section cases. The initiator diameter was held constant and the larger combustor diameters varied in order to evaluate the effects of diameter ratio on the shock reflection conditions for both cylindrical and scalloped geometries. A computational fluid dynamics (CFD) solver known as OVERFLOW was used to model the fluid dynamic processes but was limited in capability to shock wave Mach numbers less than about 4.2.

THIS PAGE INTENTIONALLY LEFT BLANK

TABLE OF CONTENTS

LIST OF FIGURES

THIS PAGE INTENTIONALLY LEFT BLANK

LIST OF TABLES

THIS PAGE INTENTIONALLY LEFT BLANK

ACKNOWLEDGMENTS

The author would like to thank Professor Chris M. Brophy for his inspiration on pulse detonation engine and invaluable guidance, education and advice provided on the approach and development of this thesis.

The author would like also to thank Professor Garth V. Hobson for his invaluable guidance, education and advice provided on the computational fluid dynamics tools and techniques.

The author would like to also thank his wife, Lay Hua and daughter, Evangeline for their gracious support throughout his education in the Naval Postgraduate School.

Lastly, the author would like to thank the Lord Jesus Christ for the wisdom, strength and endurance provided on discovering new knowledge in this field of research.

THIS PAGE INTENTIONALLY LEFT BLANK

I. INTRODUCTION

A. PURPOSE

The purpose of this thesis was to study the effects of various geometries on the reflected shock conditions for producing high local temperature and pressure regions. The nominal geometry was representative of that existing in a valve-less pulse detonation engine (PDE) developed by the Naval Postgraduate School (NPS). Currently, the NPS PDE uses a small auxiliary combustor known as an initiator, which operates on an oxygen-enriched fuel/air mixture to rapidly and reliably generate a detonation wave, which then re-initiates the less sensitive fuel/air mixture in the combustor. Since the addition of oxygen is treated as "fuel" for specific impulse (ISP) calculation and reduces the overall system performance, it is undesirable on any propulsion platform in terms of performance and practically.

The benefits of modified combustor geometry are to eliminate the requirement for auxiliary oxygen in the initiator and only utilize an exiting fuel/air detonation wave from the initiator into the main combustor. The modified geometry should result in the generation of multiple regions of high temperature due to the reflected/focused shock conditions from its geometry, and they subsequently should allow the initiation of a detonation of the fuel/air mixture in the main combustor.

B. INTRODUCTION TO PULSE DETONATION ENGINE

The interest in PDEs has increased dramatically in recent years due to their high theoretical performance and wide range of potential applications. PDEs use detonation waves that propagate through a premixed fuel/air mixture to produce large increases in chamber pressures and temperatures. The expansion of these products produces thrust. They offer the potential for high performance because the rapid detonation process results in a very efficient combustion process with high operating frequencies and combustor chamber pressures. They offer the potential of good thrust characteristics across subsonic to supersonic flight regimes. They have the potential to operate at very high energy

densities, allowing the use of simple and compact combustor designs. They also offer instant throttleability due to cycle-to-cycle control.

The valve-less PDE developed at the NPS uses a continuous air flow design, which eliminates the need for valves to supply fuel/air mixture to the combustor. The initiator operates on an oxygen-enriched fuel/air mixture to rapidly and reliably generate a detonation wave, which re-initiates the less sensitive fuel/air mixture in the combustor. Without a large valve on the air flow, a convenient flow path is allowed to rapidly fill, detonate, and purge the combustion chamber at rates up to 100 Hz cycle frequency.

C. INTRODUCTION TO COMPUTATIONAL FLUID DYNAMIC TOOLS

Computational Fluid Dynamics (CFD) is a powerful tool for fluid flow analysis. The CFD process involves many primary and secondary programs used on Silicon Graphic Iris (SGI) workstations at the NPS. The lists of programs used for this thesis are as follows:

- GRIDGEN – Grid generation program
- GRIDED – Grid editing program
- OVERFLOW – Flow solver program
- FAST – Flow solution visualization program

The interpretation of CFD results requires much scientific judgment and knowledge. The CFD results can be improved by modifying the grid mesh, boundary conditions, numerical differencing scheme, time step and more.

The OVERFLOW flow solver program is based on prefect gas law algorithm; solution will be stable for flow less than Mach 5 and it is not capable of handling chemical reaction. Due to its limitations, the model is not capable of simulating the operating conditions of the actual PDE. But it is believed to be adequate to study the efforts of combustor geometry on shock reflecting/focusing to generate regions of high vorticity and subsequently regions of high temperature also know as “hot spots”, transmitted from the initiator into the main combustor through a weaker supersonic shock wave.

II. DETONATION PHYSICS

A. INTRODUCTION

This chapter discusses the physics, properties, structure and development of detonation. Detonation is a supersonic combustion wave that typically propagates at a few thousand meters per second, closely coupled to a thin flame front. Detonation waves travel in this manner, which are locally three-dimensional and non-steady. Short deflagration to detonation transition (DDT) length is desirable for propulsion system design and can be achieved by increasing the chemical reaction rate of premixed gases through turbulence and increasing the temperature through shock reflection.

B. EXPLOSION, DFLAGRATION AND DETONATION

The chemical reactions relating to the combustion of premixed gases generally fall into one of the three categories namely explosion, deflagration and detonation. The three categories can be further described as follows. The chemical-reaction zone is often called the “flame zone”, “flame front” or “reaction wave”, which often emits visible light [Ref. 1]. There are generally two types of flames namely premixed flames, where reactants are perfectly mixed before chemical reaction and diffusion flames, which reactants diffuse and mix into each other during the chemical reaction [Ref. 1].

1. Explosion

Explosion is a term that corresponds to a rapid heat release or pressure rise but it does not require the passage of a combustion wave through the exploding medium. Certain fuel and oxidizer gas mixtures will not propagate a burning zone or combustion wave and are outside the flammability limits of the explosive gas [Ref. 2].

2. Deflagration

Deflagration is a combustion wave propagating at subsonic speed and is the most common type of combustion [Ref. 1]. Deflagration flame speeds at the order of one or more meters per second for most typical hydrocarbon/air mixtures. The propagation of a deflagration flame is governed by laminar or turbulent diffusion of unburned gases ahead

of a flame and burned gases behind the flame. Deflagrations produce small decreases in pressure and can be modeled as nearly isobaric or constant pressure processes [Ref. 1]. Some examples of deflagrations are gas stove flames and a camp fire flame.

3. Detonation

Detonation is a supersonic combustion wave that typically propagates at a few thousand meters per second relative to an unburned fuel/air mixture [Ref. 1]. Detonations are much more energetic than deflagrations and produces large overpressures because the combustion region is closely coupled to a supersonic shock wave [Ref. 3].

A detonation wave compresses a fluid, increasing its pressure, density and temperature. The rapid compression and heating of the reactants greatly accelerates the combustion process. Detonations can be approximated as normal shock waves that initiate and are closely coupled to a thin flame front or combustion region. A one-dimensional model of such a structure is known as a Zel'dovich, von Neumann and Döring (ZND) model, which is further described later in this chapter. Due to the high-speed nature of a detonation wave, a detonation closely approximates a constant volume combustion process, thereby producing a lower entropy rise of the working fluid versus a deflagration combustion mode. The result is an improved thermodynamic efficiency [Ref. 1].

4. Qualitative Differences between Detonation and Deflagration

A schematic diagram of a one-dimensional combustion wave is shown in Figure 1 [Ref. 1]. In this reference frame, the unburned reactants move towards the stationary combustion wave at velocity, u_1, and the burned reactants move away from the combustion wave at velocity, u_2. The difference between these two velocities can be large depending on whether the combustion process occurs as deflagration or detonation.

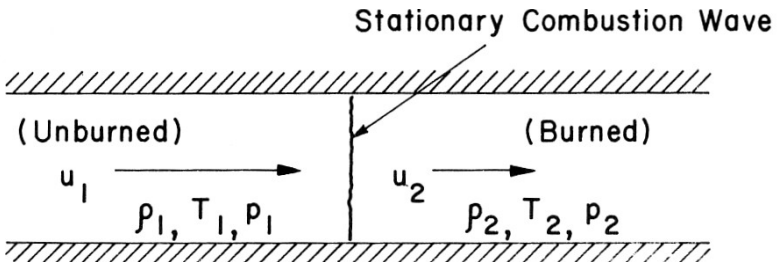

Figure 1. Schematic of Stationary One-Dimensional Combustion Wave.

A comparison of thermodynamic properties between deflagration and detonation is shown in Table 1 [Ref. 1]. The terms u, c, p, T and ρ are velocity, sonic velocity, pressure, temperature and density respectively.

Ratio	Detonation	Deflagration
u_1/c_1	5-10	0.0001-0.03
u_2/u_1	0.4-0.7 (deceleration)	4-6 (acceleration)
p_2/p_1	13-55 (compression)	≈0.98 (slight expansion)
T_2/T_1	8-21 (heat addition)	4-16 (heat addition)
ρ_2/ρ_1	1.7-2.6	0.06-0.25

Table 1. Qualitative Differences between Detonation and Deflagration in Gases.

C. HUGONIOT CURVE AND CHAPMAN-JOUGUET POINTS

A detonation wave can be approximated as a normal shock wave that is closely followed by a deflagration. However, detonation waves are actually complex, oscillatory phenomena with three-dimensional cellular structure [Ref. 3].

Detonation waves can be modeled as discontinuities in the flow of an ideal gas at which heat addition occurs [Ref. 4]. This treatment of detonation waves is a reasonable approximation for studying engine performance since the significant changes in the fluid properties occur over a very short distances. The analysis is based on the conservation equations for mass, momentum, and energy across the detonation in a constant cross section tube and on the equation of state [Ref. 3].

Conservation of Mass:

$$\rho_1 u_1 = \rho_2 u_2 \equiv \dot{m} \tag{1}$$

Conservation of Momentum:

$$P_1 + \rho_1 u_1^{\,2} = P_2 + \rho_2 u_2^{\,2} \tag{2}$$

Conservation of Energy:

$$\begin{aligned} C_p T_1 + \frac{1}{2} u_1^{\,2} + q &= C_p T_2 + \frac{1}{2} u_2^{\,2} \\ h_1 + \frac{1}{2} u_1^{\,2} + q &= h_2 + \frac{1}{2} u_2^{\,2} \end{aligned} \tag{3}$$

$$C_p = \frac{R}{\left(1 - \frac{1}{\gamma}\right)} = \left(\frac{\gamma}{\gamma - 1}\right) R \tag{4}$$

where

subscript 1 refers to state of unburned gas upstream of the detonation wave

subscript 2 refers to state of burned gas immediately downstream of detonation

ρ = density, ν = specific volume = $1/\rho$

u = one-dimensional velocity

h = enthalpy of the gas (per unit mass)

q = heat addition (per unit mass)

Combining the conservation of mass (1) and conservation of momentum (2) equations produces the Rayleigh-line relation [Ref. 1] as defined in equations (4) and (5) in terms of Mach number. Since $(\rho_1 u_1)^2$ and $(\rho_2 u_2)^2$ are always positive, the terms $(P_2\text{-}P_1)$ and $(\nu_2\text{-}\nu_1)$ must be of opposite sign.

$$P_2 - P_1 = \rho_1 u_1^{\,2} - \rho_2 u_2^{\,2} = \frac{\left(\rho_1 u_1\right)^2}{\rho_1} - \frac{\left(\rho_2 u_2\right)^2}{\rho_2} = \left(\frac{1}{\rho_1} - \frac{1}{\rho_2}\right) \dot{m}^{\,2}$$

$$\therefore \left(\rho_1 u_1\right)^2 = \left(\rho_2 u_2\right)^2 = \dot{m}^{\,2} = -\left(\frac{P_2 - P_1}{\nu_2 - \nu_1}\right) \tag{4}$$

$$M_1 \equiv \frac{u_1}{c_1}, c_1 \equiv \sqrt{\gamma R_1 T_1} = \sqrt{\gamma \left(\frac{P_1}{\rho_1}\right)}$$

$$\frac{\gamma}{\gamma}\frac{\rho_1^2 u_1^2}{\rho_1 P_1} = \frac{\frac{P_2}{\rho_1} - 1}{1 - \frac{\rho_1}{\rho_2}}$$

$$\gamma M_1^{\,2} = -\frac{\left(\frac{P_2}{P_1} - 1\right)}{\left(\frac{v_2}{v_1} - 1\right)} \tag{5}$$

A deflagration produces a net decrease in both pressure and density as a result of combustion process. Therefore deflagrations are classified as being weak because they are nearly isobaric and result in only small decrease in pressure. However, a detonation produces a net increase in both pressure and density because the shock wave, which precedes the flame region of the detonation wave, both compresses and pressurizes the un-reacted gas prior to the heat addition process [Ref. 3].

Combining and rearranging the conservation of mass (1), conservation of momentum (2) and conservation of energy (3) equations forms the Hugoniot equations for flow in a constant cross-sectional tube with heat release. Equations (6) and (7) relate the thermodynamic properties upstream and downstream of a combustion region [Ref. 1].

$$h_1 - h_2 + q = \frac{1}{2}\left(P_1 - P_2\right)\left(v_2 - v_1\right) \tag{6}$$

$$e_1 - e_2 + q = \frac{1}{2}\left(P_1 + P_2\right)\left(v_1 - v_2\right) \tag{7}$$

where

e = internal energy of gas per unit volume

h = enthalpy = e+p/ρ = e+pv

Champan (1899) and Jouguet (1905) [Ref. 3] independently determined that the tangency point of the Rayleigh line and the Hugoniot curve for the detonation reaction products represented the stable end state for self-sustaining detonation waves. The schematic diagram depicting the various sections of the Hugoniot curve is shown in Figure 2 [Ref. 4]. The Chapman-Jouguet (CJ)

condition for detonation is indicated by point B (P_+, v_+). A Rayleigh line through the point (1,1) will not intersect the Hugoniot curve if the magnitude of its slope is less than the tangent line's slope, which implies a minimum wave speed, μ, for detonations. There are two possible detonation end states at higher wave speeds: one on curve A-B representing strong detonation and another on curve B-C representing weak detonations. The summary of the properties of Hugoniot curves is shown in Table 2 [Ref. 4].

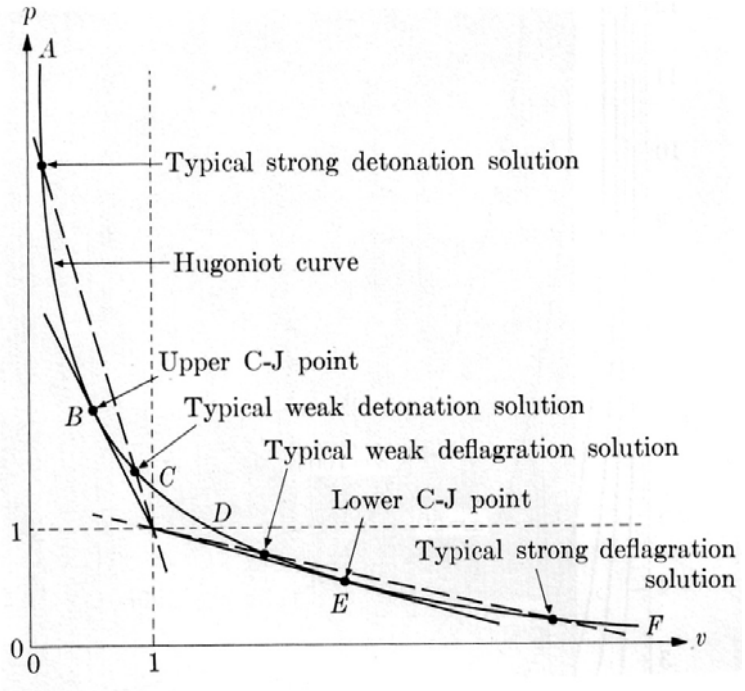

Figure 2. Rayleigh Line – Hugoniot Curve Flow Solutions.

	Section in Figure 2	Pressure Ratio $p\equiv(p_\infty/p_0)$	Velocity and density ratios $v\equiv(v_\infty/v_0)=(\rho_0/\rho_\infty)$	Propagation Mach number $M_0=(v_0/a_{f0})$	Downstream Mach Number $M_\infty=(v_\infty/a_{e,\infty})$	Remarks
Strong detonations	Line A-B	$p_+<p<\infty$	$\min<v<v_+$ ($v\min>0$)	$M_{0+}<M_0<\infty$	$M_\infty<1$	Seldom observed; required special experimental arrangement
Upper Chapman-Jouguet point	Point B	$p=p_+$ ($p_+>1$)	$v=v_+$ ($v_+<1$)	$M_0=M_{0+}$ ($M_{0+}>1$)	$M_\infty=1$	Usually observed for waves propagating in tubes
Weak detonations	Line B-C	$p_1<p<p_+$ ($p_1>1$)	$v_+<v<1$	$M_{0+}<M_0<\infty$	$M_\infty>1$	Seldom observed; requires very special gas mixtures.
Weak deflagrations	Line D-E	$p_-<p<1$	$v_1<v<v_-$ ($v_1>1$)	$0<M_0<M_{0-}$	$M_\infty<1$	Often observed; $p\approx1$ in most experiments.
Lower Chapman-Jouguet point	Point E	$p=p_-$ ($p_-<1$)	$v=v_-$ ($v_->1$)	$M_0=M_{0-}$ ($M_{0-}<1$)	$M_\infty=1$	Not observed.
Strong deflagrations	Line E-F	$0<p<p_-$	$v_-<v<v_{max}$ ($v_{max}<\infty$)	$M_{0min}<M_0<M_{0-}$ ($M_{0min}>0$)	$M_\infty>1$	Not observed; forbidden by considerations of wave structure.

Table 2. Properties of Hugoniot Curves.

D. DETONATION WAVE PROPERTIES

A general pressure distribution of a detonation initiated at the closed end of a tube and propagating left to right toward the open end is shown in Figure 3 [Ref. 1].

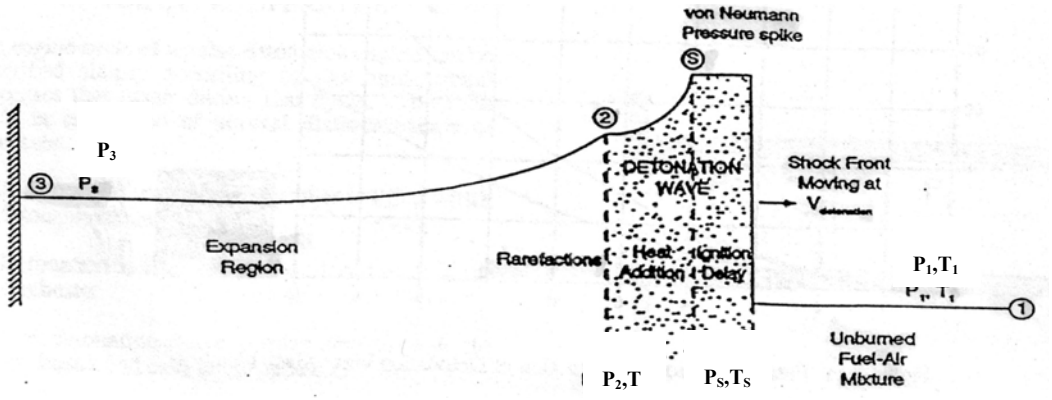

Figure 3. Detonation Chamber Pressure Profile.

The transitory von Neumann pressure increase across the leading shock of the leading shock of the detonation wave can be defined from the conservation equations (1), (2) and (3) and the perfect gas relation as:

$$\frac{P_S}{P_1} = 1 + \frac{2\gamma_1}{\gamma_1 + 1}\left(M_1^{\,2} - 1\right) \tag{8}$$

where

γ_1 = specific heat ratio in unburned gas

M_1 = Mach number of detonation wave relative to unburned gas

The following relations can be expressed for pressure and temperature ratios across a Chapman-Jouguet detonation wave in an ideal gas:

$$\frac{P_2}{P_1} = \frac{1 + \gamma_1 M_1^{\,2}}{1 + \gamma_2} \tag{9}$$

$$\frac{T_2}{T_1} = \frac{m_2}{m_1}\frac{\gamma_2}{\gamma_1}\frac{1}{M_1^{\,2}}\left(\frac{1 + \gamma_1 M_1^{\,2}}{1 + \gamma_2}\right)^2 \tag{10}$$

where

γ = ratio of specific heats

m = molecular weight of gaseous mixtures

Relating the speed of the unburned gases just behind the detonation to the speed of the wave and accounting for the initial velocity due to fuel/air injection yields:

$$M_{2C} = \left(M_0 + M_1\right)\left(\frac{m_2}{m_1}\frac{\gamma_1}{\gamma_2}\frac{T_1}{T_2}\right)^{\frac{1}{2}} - 1 \tag{11}$$

where

M_{2C} = Mach number of burned gas w.r.t. detonation chamber wall

M_0 = Mach number of unburned gas w.r.t. detonation chamber wall

M_1 = Mach number of detonation wave w.r.t. unburned gas

Mach number of the burned gas relative to the detonation chamber wall, M_{2C} is in the high subsonic range for detonations initiated within tubes, which contain a fuel/air mixture with no initial velocity. M_{2C} can be more than one if the velocity of the unburned gas is not zero.

The von Neumann spike pressure, P_S, is typically a large value. Due to the boundary condition, the static pressure at the closed end is reduced to P_3 by a series of rarefaction waves that forms in order to ensure the normal velocity is zero at the closed end. The pressure just behind the detonation wave, P_2, is therefore reduced to the plateau pressure, P_3, at the wall. P_3 can be deduced from the following pressure ratio:

$$\frac{P_3}{P_1} = \frac{P_2}{P_1}\left(1 - \frac{\gamma_2 - 1}{2}M_{2C}\right)^{\frac{2\gamma_2}{\gamma_2 - 1}} \tag{12}$$

.

E. DETONATION WAVE STRUCTURE

1. ZND One-Dimensional Detonation Wave Structure

Zel'dovich (1940), von Neumann (1942) and Döring (1943) independently assumed that the flow is strictly one-dimensional and steady relative to the detonation

front [Ref. 1]. The variation of physical properties through one-dimensional ZND detonation wave is shown in Figure 4 [Ref. 1].

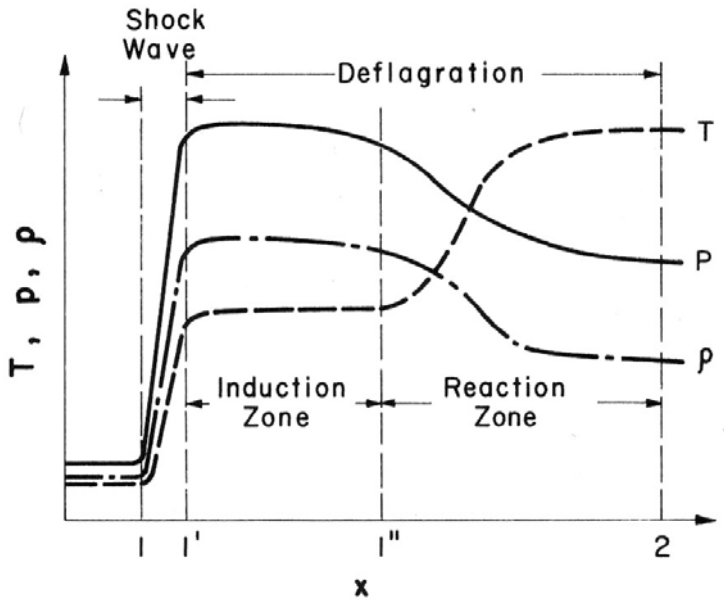

Figure 4. Variation of Physical Properties through a ZND Detonation Wave.

The shock wave moves at the detonation velocity, with chemical reaction occurring behind it in a region much thicker than a typical shock wave. It initially heats the reactants to a temperature at which they can react at a high enough rate for deflagration to locally propagate as fast as the wave. Its thickness is usually very small, in the order of a few mean free paths of the gas molecules. Thus the major heat release occurs in a substantially thicker region behind it [Ref. 1]. The pressure, temperature and density at state 1 increase sharply behind the shock at state 1'. According to Arrhenius law as shown below in equation (13), the reaction rate increases in the region immediately behind the shock, where the temperature is not extremely high. This region is called the induction zone because the pressure, temperature and density profile are relatively flat immediately behind the shock front. At the reaction zone, the gas properties change sharply as the reaction rate increases drastically to high values and reaches equilibrium values at the end of the reaction. The distance between the shock front and the fully reacted state for most fuel/air mixtures is in the order of 1cm [Ref. 1].

The locus of the reacting mixture on the Hugoniot curve is shown in Figure 4 [Ref. 1]. Paths (a), (b), (c) and (d) pass through the detonation wave from un-reacted state to fully reacted state, therefore they satisfy the conservation equations. Path (a) is unlikely to have sufficiently fast reaction rates to sustain the wave whereas paths (b) and (c) represent mixtures with fast and slow chemical kinetics respectively. The peak pressure behind the shock wave is known as the von Neumann spike.

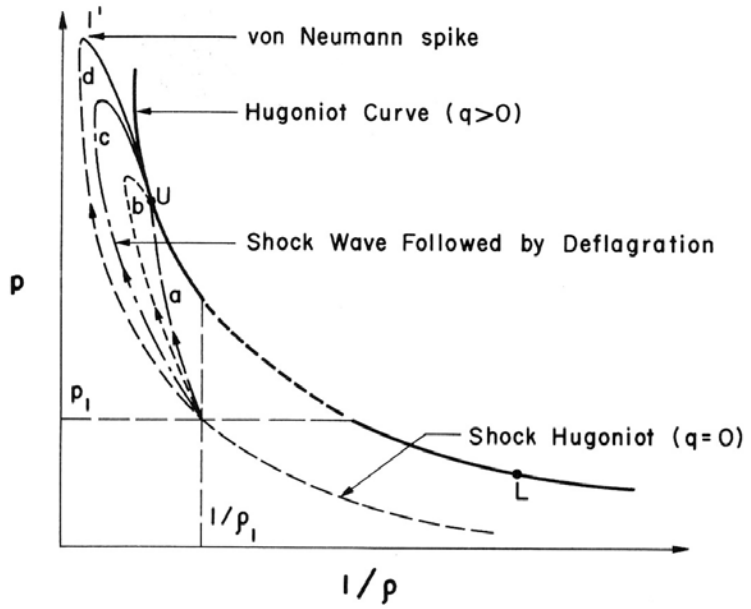

Figure 5. ZND Detonation Structure on (p,1/ρ) Diagram.

The Arrhenius rate law [Ref. 1] is defined as:

$$k = Ae^{\left(\frac{-E_a}{R_u T}\right)} \tag{13}$$

where

k = rate of reaction

A = constant to each chemical

Ea = activation energy

R_u = universal gas constant

T = temperature

Therefore the chemical reaction rate increases exponentially as the temperature of the mixture increases. The constant, A, generally increases as P^2.

2. Multi-Dimensional Detonation-Wave Structure

By observing spin in limit mixtures in circular tubes, they showed that detonation waves might prefer to travel in a manner, which is locally three-dimensional and non-steady [Ref 1]. Through the smoked-foil method, a propagating detonation wave is able to write on the walls due to the presence of triple points at the intersecting lines of three shock waves as shown in Figure 6 [Ref 1]. A steady supersonic two-dimensional flow, passing through a convergent ramp section from right to left, produces a shock-wave pattern, when the ramp is very steep as shown in Figure 7 [Ref 1]. The triple point is the intersection point of Mach-stem, incident and reflected shocks. A slipstream is also generated.

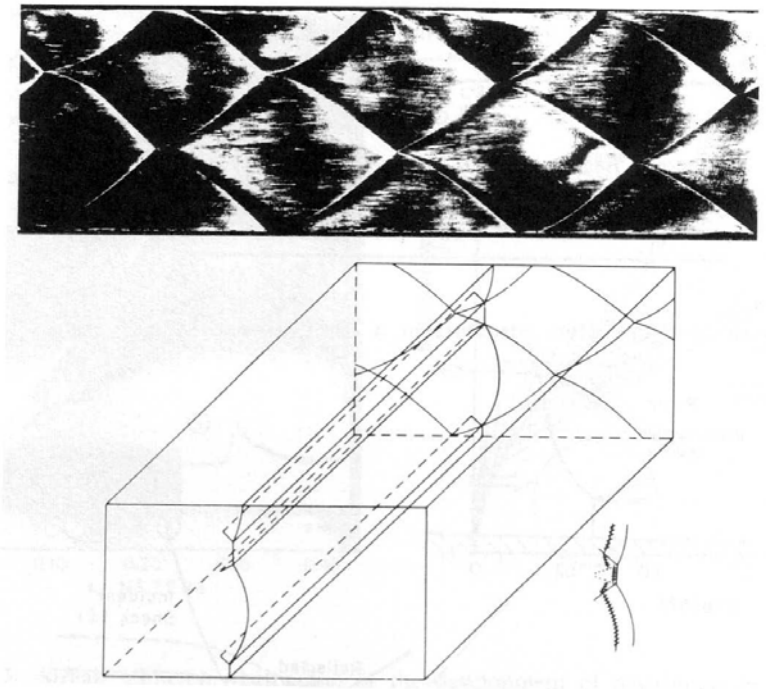

Figure 6. Smoked-Foil Record and Schematic Diagram of Symmetric Planer Interaction.

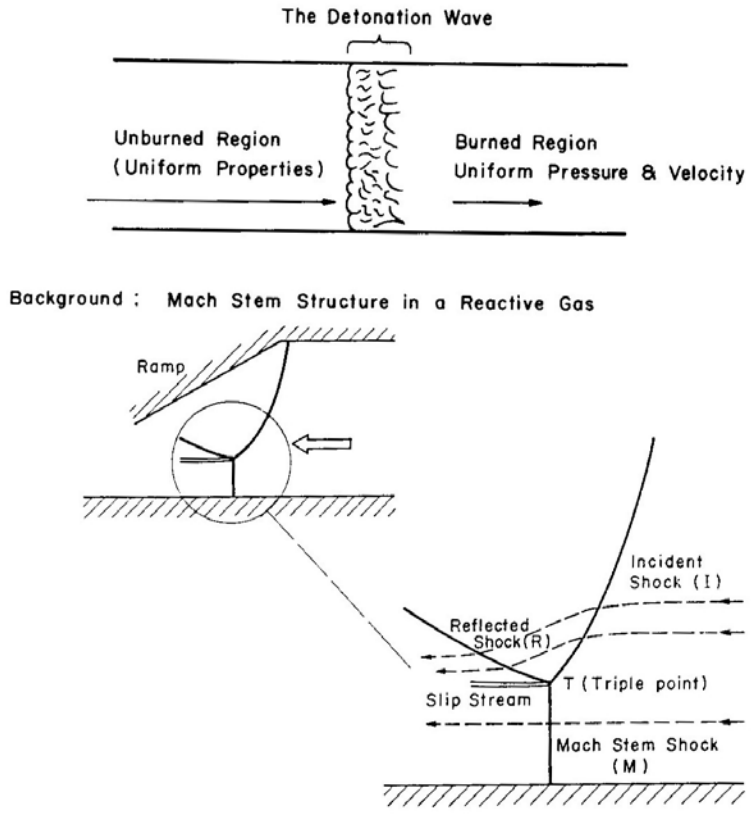

Figure 7. Schematic Diagram Showing the Shock-Wave Pattern and Triple Point in a Two-Dimensional Supersonic Flow Passing through a Convergent Ramp Section.

Cell length, L_C, is defined as the cell dimension along the axis of detonation propagating and cell size, λ, also known as cell width, is defined as the cell dimension perpendicular to the direction of propagation as shown in Figure 8. The chemical reactions are essentially completed within one cell length, and $\lambda = 0.6\ L_C$. The minimum cell size, λ, usually occurs at equivalence ratio, φ, of 1. Equivalence ratio, φ, is defined as the ratio of actual fuel-oxidant ratio to the fuel-oxidant ratio for a stoichiometric process. Cell size, λ, is also representative of the sensitivity of the mixture. It increases as the sensitivity of the mixture decreases [Ref. 2]. Figure 9 shows the detonation cell size against equivalence ratio for common fuels [Ref. 6].

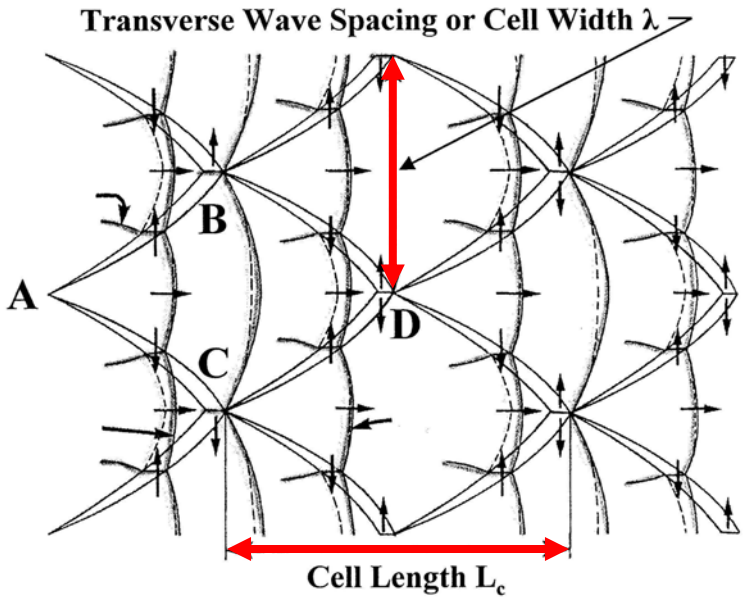

Figure 8. Cellular Structure of Detonation.

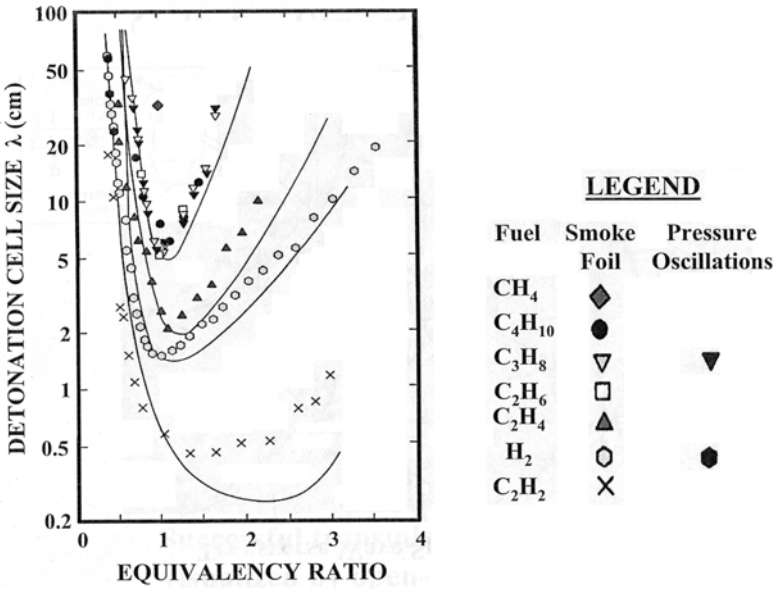

Figure 9. Cell Size Measurements for Common Fuel.

F. DEVELOPMENT OF DETONATION WAVE

Direct ignition and deflagration-to-detonation transition (DDT) process, also known as thermal ignition, are primarily the two ways to initiate a detonation wave. DDT length, X_{DDT}, is dependent on the type of combustible mixture used and its equivalence ratio, the internal combustor geometry and possible heat addition. Figure 10 shows a

series of schlieren images taken of a deflagration-to-detonation transition for hydrogen/oxygen mixture [Ref 1].

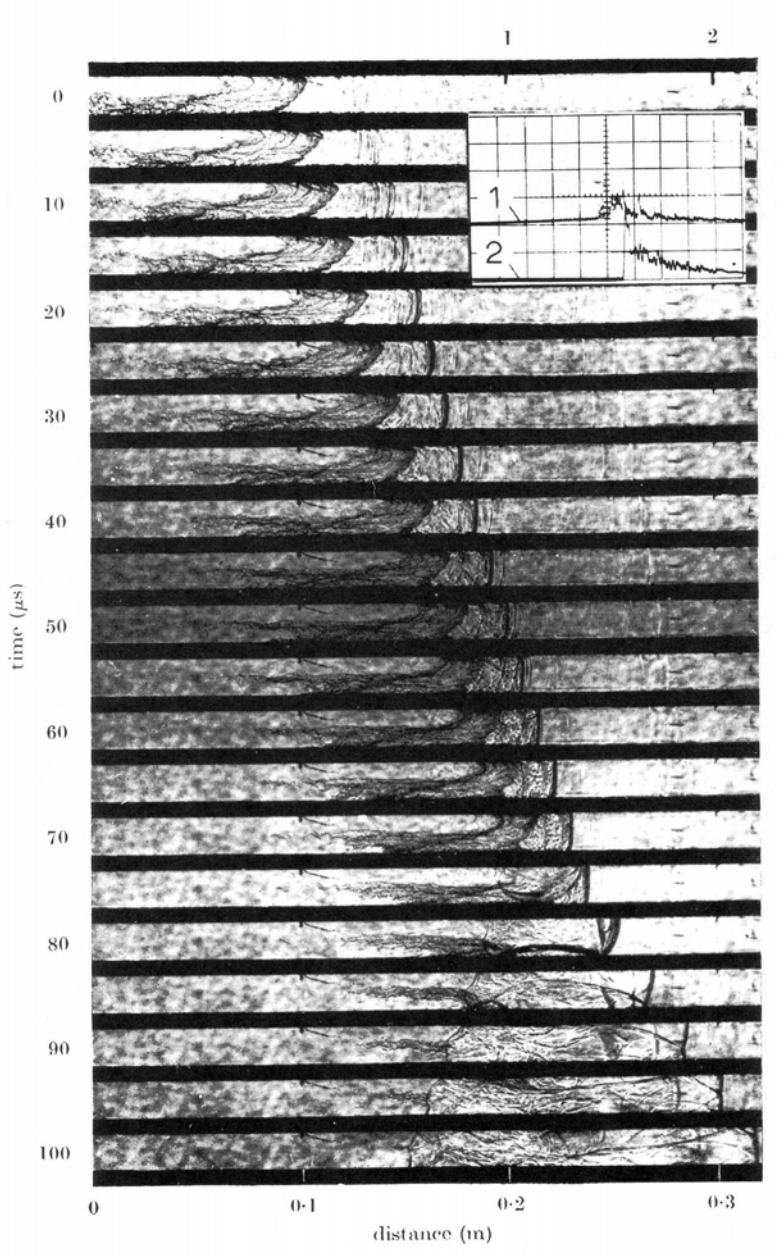

Figure 10. Deflagration-to-Detonation Transition for Hydrogen/Oxygen Mixture.

A cylindrical tube contains a combustible mixture, which is ignited with a spark plug at the closed end and the other end opens. A combustion wave initially propagates as a laminar flame front and rapidly transit into a turbulent flame front, propagating at 5 to 10 times that of the laminar speed. This flame produces weak compression waves, which

propagate at the local sonic velocity and increases the temperature of the unburned mixture slightly after each wave passes. A shock wave rapidly develops as these compression waves coalesce. Based on the local sonic velocity defined in equation (14), the increased temperature behind the shock front increases the sonic velocity further [Ref. 5].

$$c = \sqrt{\gamma RT} \tag{14}$$

where

c = local sonic velocity

γ = ratio of specific heats for reactants and hot products throughout reaction

R = gas constant

T = local temperature

A combustion driven shock is generated as the turbulent flame continues to accelerate through the shock-heated and compressed mixture. The combustion wave continues to produce compression waves, which propagate towards the shock and further increase the temperature of the unburned mixture. When a sufficient temperature rise occurs between the shock and the combustion front, a thermal explosion will occur in the unburned mixture, producing strong secondary shock waves in all directions and allowing the combustion zone to occur immediately after the leading shock wave forming a detonation wave. The detonation will overdrive itself momentarily, but then propagates at about Mach 5 relative to the unburned mixture. The reaction zone then becomes located close behind the leading shock of the detonation wave. The detonation shock wave preheats the unburned mixture to extremely temperature as it propagates through causing the reactants to combust extremely fast. The equations governing the Mach number and temperature ratio before and after the shock in a prefect gas are defined in equations (15) and (16) [Ref. 5].

$$M_2^{\,2} = \frac{M_1^{\,2} + \dfrac{2}{(\gamma - 1)}}{\left(\dfrac{2\gamma}{\gamma - 1}\right) M_1^{\,2} - 1} \tag{15}$$

$$\frac{T_2}{T_1} = \frac{1 + \frac{(\gamma - 1)}{2} M_1^{\,2}}{1 + \frac{(\gamma - 1)}{2} M_2^{\,2}} \tag{16}$$

where

M_1 = Mach no. of the leading shock

M_2 = Mach no. after the shock

T_1 = temperature before the shock

T_2 = temperature after the shock

Typical, X_{DDT} for most hydrocarbon/air combustion is ten tube diameter or more for a tube diameter greater than the cell size, λ [Ref. 6]. X_{DDT} must take place within about 0.3 m as the practical lengths for propulsion purposes are about 1 m. Short X_{DDT} is desirable for propulsion system design and can be achieved by increasing the global reaction rates through turbulence and increasing the temperature through shock reflection [Ref. 5]. High-speed turbulent combustible mixtures injected through orifices into the combustor can also increase the overall reaction rate as can reflected shock scenarios due to combustor geometry [Ref. 5].

III. PULSE DETONATION ENGINES

A. INTRODUCTION

This chapter discusses the operating principles of PDEs. PDEs have received renewed interest during the past 10 years. They use detonation waves that propagate through a premixed fuel/air mixture to produce large chamber pressures, which then produce thrust [Ref. 3]. They offer the potential for high performance because the rapid detonation process results in nearly constant volume combustion with high operating frequencies and combustor chamber pressures. They are predicted to be very efficient and offer good thrust characteristics from subsonic to the supersonic flight regimes. They have the potential to operate at very high energy densities, allowing the use of simple and compact combustor designs [Ref. 3]. They also offer instant throttleability due to cycle-to-cycle control.

B. STEADY AND UNSTEADY STATE ENGINES

Air-breathing engines can be classified according to the type of combustion process employed in the device. The combustion process can be characterized as either steady (quasi-steady) or unsteady. Propulsion systems may be further classified according to whether a deflagrative or detonative mode of combustion is utilized [Ref. 3].

The most commonly used class of engines is steady state combustion propulsion systems. A continuous, constant pressure, deflagration combustion process, characterizes these engines. Examples of this class of engines are the turbojets and ramjets.

The second class of engines is the unsteady combustion propulsion systems. Combustion occurs in an intermittent manner and is governed by the fuel/air flame speeds and combustion chamber characteristics. Unsteady combustion propulsion systems can be based on either deflagration combustion (pulse jets) or detonation combustion (pulse detonation engines) [Ref. 3].

C. ENGINE EFFICIENCY

The constant volume detonation and constant pressure deflagration processes can be modeled as the Humphrey and Brayton cycles respectively. Figures 11 and 12 compare the temperature, pressure and specific volume characteristics of the Brayton and Humphrey cycles [Ref. 1]. The Brayton cycle (0-1-4-5-0) consists of two constant pressure cycle (1-4 and 5-0) and two isentropic processes (0-1 and 4-5). The Humphrey cycle is similar, except the constant pressure combustion process (1-4) is replaced by a constant volume heat addition process (1-2).

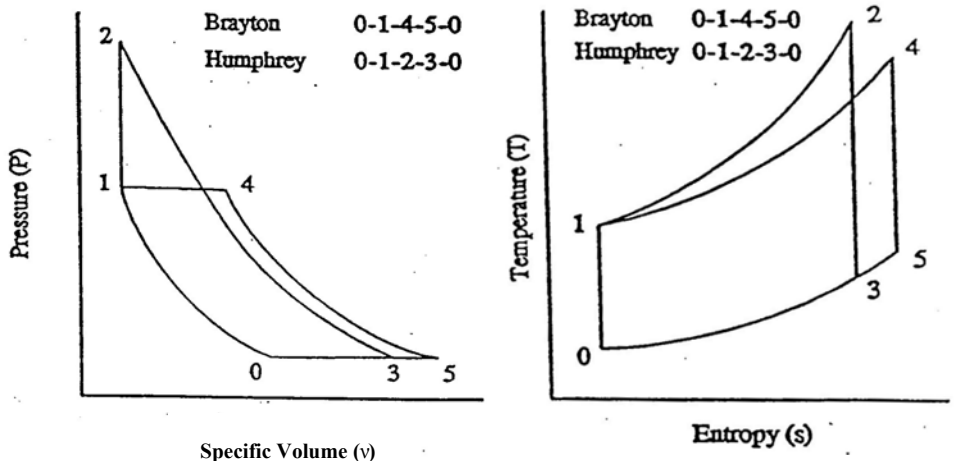

Figure 11. Pressure-Volume Cycle Diagram (Left).
Figure 12. Temperature-Entropy Cycle Diagram (Right).

The efficiencies of the constant pressure Brayton and constant volume Humphrey cycles can be computed from the pressure-volume and temperature-entropy diagrams in Figures 11 and 12. The efficiency of a cycle is defined as the useful work output divided by the total heat energy input.

The efficiency of the Brayton cycle defined in equation (17) depends only on the temperature change during either of the two isentropic compression or expansion processes (i.e. $T_0/T_1 = T_4/T_5$) [Ref. 3].

$$\eta_{BRAYTON} = 1 - \frac{T_0}{T_1} \tag{17}$$

The efficiency of the Humphrey cycle [Ref. 3] is defined as:

$$\eta_{HUMPHREY} = 1 - \gamma \frac{T_0}{T_1} \left[\frac{\left(\frac{T_2}{T_1} \right)^{\frac{1}{\gamma}} - 1}{\frac{T_2}{T_1} - 1} \right] \tag{18}$$

The efficiency of the Humphrey cycle depends not only on the isentropic compression temperature ratio, T_0/T_1, but also on the ratio of specific heats, γ, and the temperature change due to the constant volume combustion (i.e., the detonation temperature ratio T_2/T_1).

The difference between the Brayton and Humphrey cycle efficiencies is the following T_0/T_1 multiplier:

$$\gamma \left[\frac{\left(\frac{T_2}{T_1} \right)^{\frac{1}{\gamma}} - 1}{\frac{T_2}{T_1} - 1} \right] \tag{19}$$

The value of this expression is always less than one for typical detonation combustion. As a result, the typical efficiency of a detonation cycle is greater than the efficiency of the Brayton cycle. Based on initial combustion conditions of 1 atmosphere and 300 °K, the Brayton and Humphrey cycle efficiencies are calculated to be 36.3 % and 56.4 % respectively with a difference of 20.1 % for JP-10/air mixtures. Thus thermodynamic efficiency of a PDE combustion cycle is very high.

D. BASIC ENGINE OPERATION

Cycle frequency is defined as the inverse of the time required to complete a full detonation cycle. Cycle time is defined as the time required to fill the combustor with fresh fuel/air mixture, to initiate detonation, to allow the detonation to traverse the length of the tube and allow the unburned gases to expand and reduce the chamber pressure to permit the refill process to occur [Ref. 3].

$$T_{CYCLE} = T_{DETONATION} + T_{EXPANSION} + T_{FILL} \tag{20}$$

The instantaneous peak thrust can be approximated by examining the pressure differential acting upon the interior surfaces of the combustor. The instantaneous thrust [Ref. 3] which acts during the positive P_3, or head end pressure, portion of the cycle can be estimated for a detonation chamber of constant cross-sectional area, A, is defined:

$$F_{INST} = \left[P_3(t) - P_1 \right] A - Drag(t) \tag{21}$$

Drag forces include all inviscid and viscous forces associated with flow about and through the vehicle. The average thrust [Ref. 3] is defined:.

$$F_{AVG} = \int_0^{T_{CYCLE}} F_{INST}(t)\,dt \times f \tag{22}$$

where

F_{INST} = instantaneous or unsteady thrust

f = cycle frequency

The specific impulse (ISP) can be computed from the average thrust level and the fuel consumption or mass flow-rate by accounting for the fuel in the combustor and second by accounting for the fuel and auxiliary oxygen used in the initiator as shown in equation (23) [Ref 7].

$$I_{SPf} = \frac{F_{AVG} / f}{\left(m_f + m_{f\_INIT} + m_{O2\_AUX} \right) g} \tag{23}$$

where

f = cycle frequency

m_f = mass flow-rate of fuel in the combustor

m_{f_INIT} = mass flow-rate of fuel in the initiator

m_{O2_AUX} = mass flow-rate of auxiliary oxygen in the initiator

E. DETONATION INITIATION

An initiator consists of a small auxiliary combustor filled with sensitive mixture. The unit is used to rapidly generate and transmit a detonation as the means to initiate a detonation in a larger main combustor containing less sensitive fuel/air mixture. Initiator concepts vary from the coaxial to transverse or splitter a plate design and typically operate on fuel/oxygen mixtures or a blend of oxygen-enriched air as the oxidizer [Ref. 7]. The use of auxiliary oxygen provides excellent reliability, repeatability and rapid ignition but its minimization is required since it is treated as "fuel" for specific impulse (I_{SP}) calculations and reduces the overall system performance [Ref. 7].

Some examples of initiators concepts using fuel/oxygen, fuel/air and hybrid are shown in Figure 13 [Ref. 8]. Concept (a) uses an oxygen/fuel "plug" as the head-end of the combustor; which works well but uses a substantial amount of oxygen. Concepts (b) and (c) use a fuel/oxygen mixture in a smaller combustor to rapidly generate a strong detonation wave to initiate the fuel/air mixture in the combustor. Concept (b) possesses a solid black wall at the diffraction plane whereas concept (c) allows the wave to diffract initially to slight larger diameter. The splitter plate and lateral tube concepts shown in (d) and (e) respectively have been explored on a limited scale. Both hybrid designs of concept (f) use wall shaping and shock focusing to promote the generation of detonation wave. Air can solely be used as the oxidizer in both designs but they are likely to be limited in the operational frequency, reliability and their requirement for additional axial length for DDT process to occur.

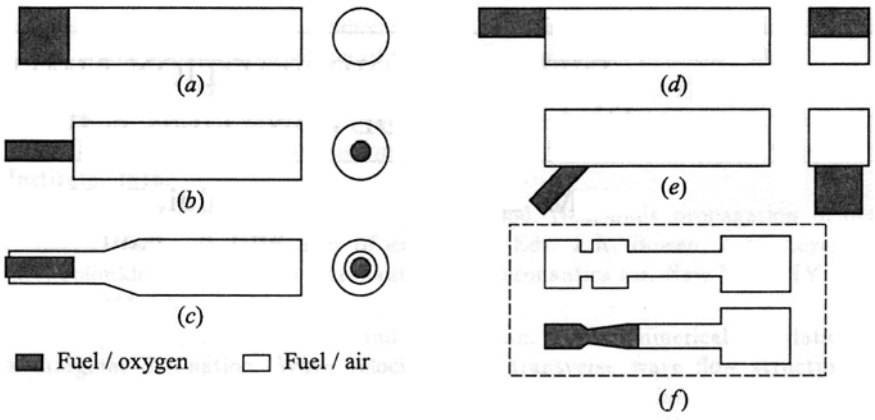

Figure 13. Examples of Initiator Concepts.

Generally, detonation waves produced in a hydrocarbon fuel/oxygen initiator propagate at about 2800 to 3000 m/s and typically near 1800 m/s using hydrocarbon fuel/air mixtures. Therefore temperature increases across the detonation shock wave for fuel/oxygen initiators are on the order of 3.5 times more than for fuel/air initiators based on equations (15) and (16).

A critical area of concern is at the initiator exit plane where the exiting detonation wave diffracts into the combustor and is the motivation for characterizing the effects of the diffraction condition between an initiator of diameter, D_i, and the main combustor of diameter, D, at the diffraction plane. Adequate conditions can exist through a combination of diameter ratio (D/D_i), mixture variation (overdrive) and varying degrees of confinement [Ref. 7]. The successful and unsuccessful test conditions for which detonation transmission occurred for the ethylene-air mixture for single-shot cases are shown in Figure 14 [Ref. 7]. It shows that a diffraction ratio, Y/Y_o, of 1.8 should have a successful detonation transition from the initiator to the combustor for an initiator operating at equivalence ratio of 1.0.

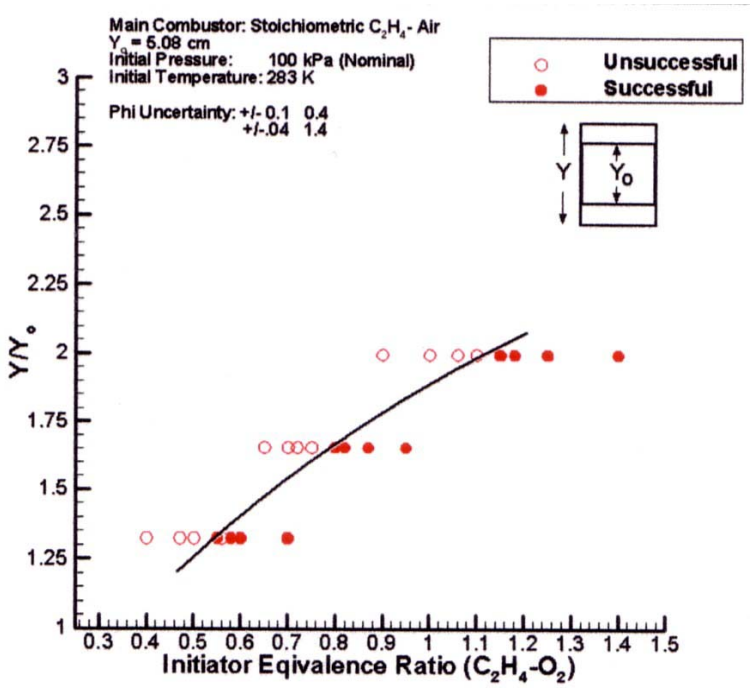

Figure 14. Results for Two-Dimensional Single-Shot Diffraction Tests.

The critical diameter value of 13 times the cell size, λ, of a mixture has been verified many times for the transmission of a detonation wave to an unconfined volume [Ref. 7]. The rule holds for most mixtures and is especially valid for mixtures containing more irregular cell spacing, typically fuel/air mixtures with higher activation energies. Mixtures containing highly regular detonation cell structure, such as argon diluted fuel/oxygen mixtures often require a larger critical diameter than the 13λ rule, thus emphasizing the importance of wave front structure during the diffraction processes in generating gas dynamic hot spots for spontaneous re-ignition to occur. The increased irregularity in the cellular structure for fuel/air mixtures often assists in the adjustment to sudden expansion conditions and possessing more levels of instability, therefore more modes by which spontaneous re-initiation may occur near a critical diameter value [Ref. 7].

Studies on the re-initiation mechanisms of shock wave reflections at a rigid wall from the propagation of a quasi-detonation in an obstacle-laden channel and in an imparting spherical blast wall on a rigid wall emphasize the importance of rapid re-ignition sites immediately behind the generated Mach stems at the wall [Ref. 7]. Additional research on the effects of overdriving a detonation wave during diffraction from a smaller combustion tube to a large volume have shown that a definitive benefit exists when a detonation wave is allowed to propagate into a less reactive mixture immediately before diffraction occurs, thus creating an overdrive condition in the less reactive mixture [Ref. 7]. Therefore a combination of shock wave reflections and overdriven conditions would be the mechanisms that govern successful initiator transmissions on most PDEs.

F. VALVE-LESS PULSE DETONATION ENGINE

The valve-less PDE developed at the Naval Postgraduate School uses a continuous air flow design, which eliminates the need for a large air valve to supply a fuel/air mixture to the combustor as shown in Figure 15 [Ref. 7]. The initiator, which is similar to Figure 13(c), operates on an oxygen-enriched fuel/air mixture to rapidly and reliably generates a detonation wave, which initiates the less sensitive fuel/air mixture in the combustor. Without a large valve on the air flow, a convenient flow path is allowed to

rapidly fill, detonate, and purge the combustion chamber at rates up to 100 Hz cycle frequency [Ref. 7]. The operational cycle of the valve-less PDE is shown below in Figure 16 and explained in Table 3 [Ref. 7].

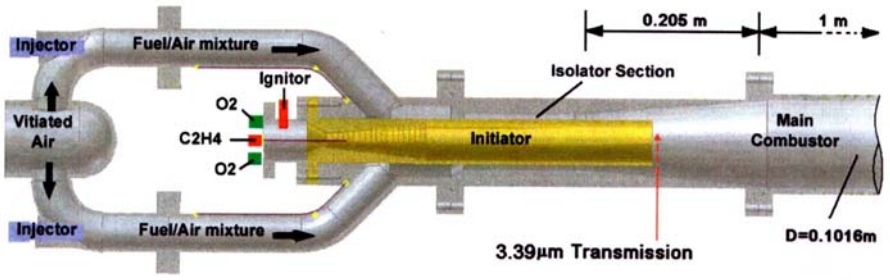

Figure 15. Valve-less PDE Configuration.

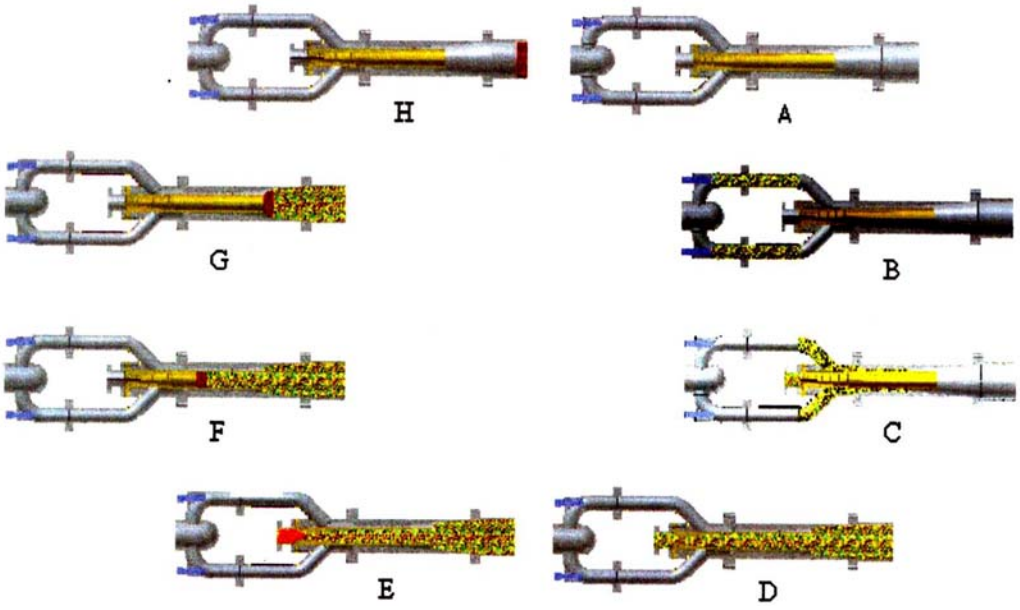

Figure 16. Valve-less PDE Operational Cycle

Stage	Description
A	Air flows through the combustor and purge the previous combustion products
B	Fuel is injected into the incoming air and flows into the combustor
C	Fuel/air mixture fully fills the combustor
D	A highly detonable mixture is rapidly injected into the initiator
E	Mixture in the initiator is ignited and a detonation wave forms
F	Detonation wave continue to propagate in the initiator
G	Detonation wave exits the initiator and initiates the fuel/air mixture residing in the combustor
H	After the detonation exits the combustor, a series of rarefaction waves reduce the pressure inside the combustor and the combustion products are purged. The process is then repeated.

Table 3. Valve-less PDE Operational Cycle.

Immediately after the detonation wave from the initiator diffracts into the combustor, a combustion-driven shock wave begins to propagate upstream into the incoming air stream. The propagation of the shock can be limited to a certain axial location if an inlet venturi is used. After the detonation wave exits the main combustor, rarefaction waves reduce the combustor pressure and allow the purging process to begin. The process then repeats.

THIS PAGE INTENTIONALLY LEFT BLANK

IV. COMPUTATIONAL FLUID DYANMICS TOOLS AND TECHNIQUES

A. INTRODUCTION

This chapter discusses the computational fluid dynamics (CFD) tools used and the techniques employed in modeling the various combustors. CFD is a powerful tool for fluid flow analysis. The CFD process involves many primary and secondary programs used on Silicon Graphic Iris (SGI) workstations at the NPS. The interpretation of CFD results requires much scientific judgment and knowledge. The CFD results can be improved by modifying the grid mesh, boundary conditions, numerical differencing scheme, time step and more.

B. GRIDGEN (GRID GENERATION PROGRAM)

GRIDGEN, version 9.6 is a grid generation program developed by John P. Steinbrenner and John R. Chawner at MDA Engineering and supported by NASA Ames Research Center via Computer Sciences Corp [Ref. 9]. It is a software system for the generation of 3D, multiple block, and structure grids and may also be used to generate single block structured grids, single surface structure grids and overset structured grids. It is an interactive code used to decompose a three-dimensional domain into blocks, distribute grid points on curves, initialize and refine grid points on surfaces and initialize volume grid points. It is menu driven but does not have advance features like a CAD system to model complex geometries. However it can read IGES files, which are CAD generated.

1. Grid Point Distribution Function

A hyperbolic tangent function method developed by Vinokur is based on a tangent function, which either has a read (tangent) or a purely imaginary (hyperbolic tangent) argument. The method allows the user to specify both the spacing between the first and second grid points and the spacing between the next-to-last and last grid points. The function is very robust and results in smooth transition of grid point clustering along the edge. It is used extensively to incrementally distribute the grid points at both edges of

the connectors along the axes of the model by specifying the respective distribution factor at each edge [Ref 9].

2. Connectors

Connectors are three-dimensional space curves, which represent edges of the surface grids used to define the surfaces or domains. A connector is created by drawing the shape, assigning the number of grid points and distributing the grid points. Connectors are constructed from one or more segments. The frequently used segments are line, three point circular arc and conic section as shown in Table 4 [Ref. 9].

Type of Segment	Description
Line	This type of segment passes a linear polynomial between control points. At least two control points are needed to specify this segment.
Three Point Circular Arc	This type of segment allows the user to define a circular arc of not more than 180° by selecting three control points that lie on the circle as shown in Figure 17 [Ref. 9]. It is constructed that begins at the first input control point, ends at the second point, and passes through a third control point elsewhere in space. Cursor movement of the third control point is constricted so that circle will subtend an angle of not more than 180°.
General Conic Section	This type of segment is used to create a general conic section spanning an arc less than 180° as shown in Figure 18 [Ref. 9]. It is constructed from three (or four) input control points. The resulting conic section begins and ends on the first and second control point. The third control point is used to control the tangent intersection point, and the fourth input values is used to specific the ρ value that determines the type of conic section.

Table 4. Type of Segment and Description.

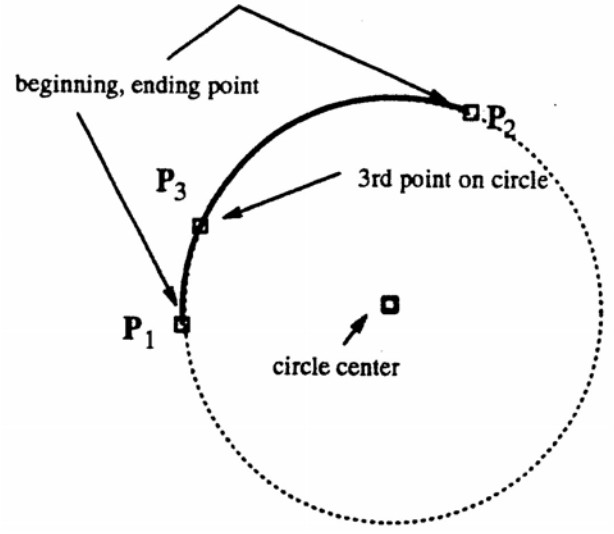

Figure 17. Three Point Circular Arc Segment.

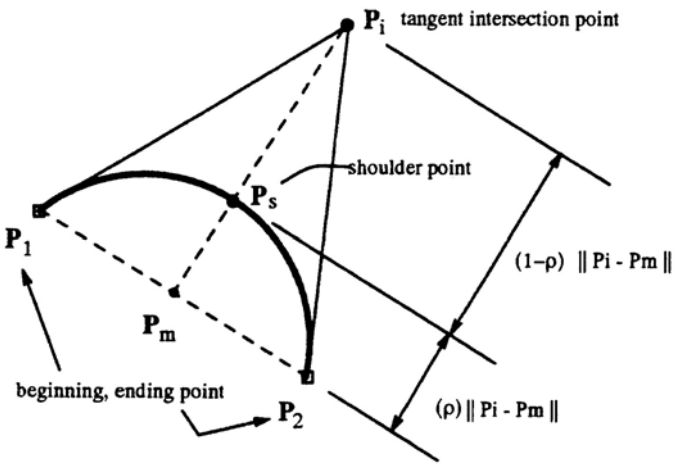

Figure 18. General Conic Segment.

3. Domains

A domain represents a dimensionally rectangular patch of grid points which is constructed by four edges with each edge consists of a string of connectors that connect end to end as shown in Figure 19 [Ref 9]. The copy menu button is frequently used to copy an existing domain and move it to a new location.

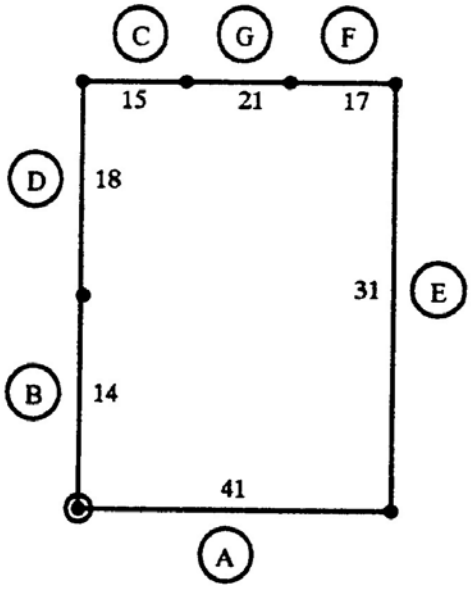

Figure 19. Domain Construction.

4. Blocks

A block is constructed by piecing together the groups of domains that represent the outer shell of the block. It consists of six individual faces that comprise the block shell and a face can comprise of more than one domain as shown in Figure 20 [Ref. 9].

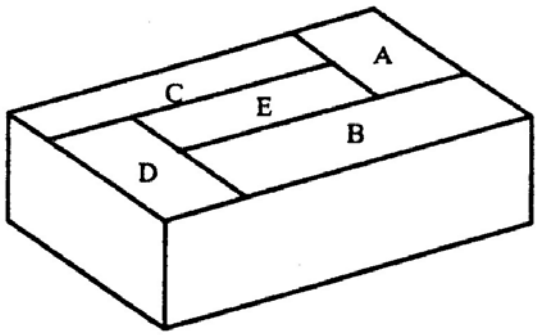

Figure 20. Block Construction with a Face with Multiple Domains.

C. GRIDED (GRID EDITING PROGRAM)

GRIDED, version 3.0d is a very useful menu-orientated grid editing program. It is capable of converting formatted grid files to unformatted grid files and vice versa. It can covert two or three-dimensional whole or plane grid by interchanging the grid families, reserving index direction, adding extra planes by reflected symmetry and more. An example of the GRIDED menu is shown in Appendix D.

D. OVERFLOW (FLOW SOLVER PROGRAM)

The OVERFLOW program, version 1.8w, is an implicit conservative Navier-Strokes (NS) flow solve. It is a complete rewrite of F3D/Chimera code developed by Joseph L. Steger and his team at NASA Ames Research Centre. The viscous terms, which are partially defined by the shear expressions, are set to zero for inviscid test cases. It is based on prefect gas law algorithm, thus solution will be stable for flow less than Mach 5. It is not capable of handling chemical reactions. Table 5 shows a list of input and output files commonly used and generated by the OVERFLOW program [Ref. 11].

Filename	File Type	Description
Filename.inp	Input	NAMELIST inputs and boundary conditions
grid.in	Input	Grid file in single or multiple grid PLOT3D format.
q.restart	Input	Q restart file in modified single or multiple grid PLOT3D format.
q.save	Output	Q save file in single or multiple grid modified PLOT3D format.
q.bomb	Output	Q bomb file in modified PLOT3D format. It is only written if a negative density or pressure is detected or if the specific heat ratio, γ, falls below one.
resid.out	Output	Flow solver residual history.
fomo.out	Output	Force, moment and mass flow coefficient history per wall.
rpmin.out	Output	Minimum density, pressure and gamma history.
Filename.out	Output	Summary of NAMELIST inputs, boundary conditions and status of solution

Table 5. OVERFLOW Program Input/Output Files.

The input parameter specifications to OVERFLOW program are done using NAMELIST inputs as shown in Appendix A and are written in the input files such as filename.inp. Variables generally have a default value unless specify by the user. The boundary conditions and turbulence model specifications for the input files are shown in Appendix B. A batch file such as filename.batch is usually used to run the OVERFLOW program with the input files and generate the output files such as filename.out and other output files listed in Table 5. The filename.out output file contains the summary of the NAMELIST inputs, boundary conditions and status of the solution.

The various flow quantities used by the flow solver are based on the perfect gas law assumption as shown below:

$$p = \rho RT = (\gamma - 1)\rho e_i = (\gamma - 1)\rho c_v T \tag{24}$$

$$a^2 = \gamma RT = \frac{\gamma p}{\rho} \tag{25}$$

$$e_i = c_v T \tag{26}$$

$$\gamma = \frac{c_p}{c_v} \tag{27}$$

$$R = c_p - c_v = (\gamma - 1)c_v = \frac{(\gamma - 1)}{\gamma} c_p \tag{28}$$

Some of the frequently used non-dimensional thermodynamic equations [Ref. 11] are:

$$t^* = \frac{ta_\infty}{L} = DT \tag{29}$$

$$\rho^* = \frac{\rho}{\rho_\infty} \tag{30}$$

$$p^* = \frac{p}{\rho_\infty a_\infty{}^2} = \frac{p}{\gamma_\infty p_\infty} \tag{31}$$

$$T^* = \frac{TR_\infty}{a_\infty{}^2} = \frac{T}{\gamma_\infty T_\infty} \tag{32}$$

$$V^* = \frac{V}{a_\infty} \tag{33}$$

E. FAST (FLOW SOLUTION VISUALIZATION PROGRAM)

FAST (Flow Analysis Software Toolkit) is a software environment for data visualization. A series of module runs allows the user to examine the results of both numerical and experimental simulation. Users can load data files, perform data calculations, visualize the calculated results, construct scenes of three-dimensional objects, and plot, animate and record scenes. A list of frequently used FAST modules and their functions is shown in Table 6.

Modules	Functions
File IO	It loads grid, solution and PLOT3D function files into the shared memory and also writes out files. Grids can be structured or unstructured.
Calculator	It is used to calculate CFD functions. PLOT3D functions are offered, and custom functions can be programmed. Non-CFD functions can also be created.
Surfer	It visualize the grid data that has been loaded with file IO and the functions that have been calculated with calculator from the solution data loaded with file IO. Surfer renders optional shading using interactive system light sources.
Viewer	It is used for transformations and for setting lighting, color, clipping, mirroring, transparency, center of rotation, anti-aliasing and scene contents
Plotter	It attaches to scalar fields in shared memory or reads xy ASCII files and generates two-dimensional line plots and histograms in computational space.

Table 6. FAST Modules.

F. MODELING TECHNIQUES

The approach is to model a Mach 2.8 supersonic shock wave transmitted from the initiator to the combustor through an initial pressure ratio and density ratio of 20 and 6 respectively between the initiator and combustor using the OVERFLOW flow solver program. A total of ten combustor models were generated with four cylindrical combustor wall geometries and six scalloped combustor wall geometries, which are described later in the chapter. The effects of shock reflection/focusing were studied by fixing the diameter of the initiator at 1.875 inches and varying the inner diameter of the cylindrical and scalloped combustor at 2.25, 2.5, 2.75 and 3 inches, forming eight combustor models. Another two combustor models with the scallop edges of the 2.75 and 3 inches scalloped combustor wall geometries modified were added.

1. Grid Construction

To save computational space and time, only a quarter of the combustor was modeled using the GRIDGEN program with both the extra horizontal and vertical planes being defined as symmetry planes through the boundary conditions of the OVERFLOW program. Figures 38 and 39 of Appendix C show the grid construction models of a cylindrical and scallop combustors respectively. Table 10 of Appendix C shows the coordinates of the grid points of the combustors. The grid mesh constructions of both the cylindrical and scallop combustors are tabulated in Tables 11 and 12 of Appendix C. Both the general conic and 3 point circular arc segments were used to construct the quarter arcs and the scallop arcs of the combustors. Figures 21 and 22 show the grid meshes of the 2.25 inches diameter cylindrical and scallop combustors respectively. The red and blue grid mesh represents the initiator and combustor respectively.

GRIDED was used to add extra planes by reflected symmetry on the horizontal and vertical plane of the combustor, increasing the grid planes in the circumferential index (L index) from 81 to 83 so that the OVERFLOW program could recognize the extra planes as symmetry planes through the definition of the boundary conditions.

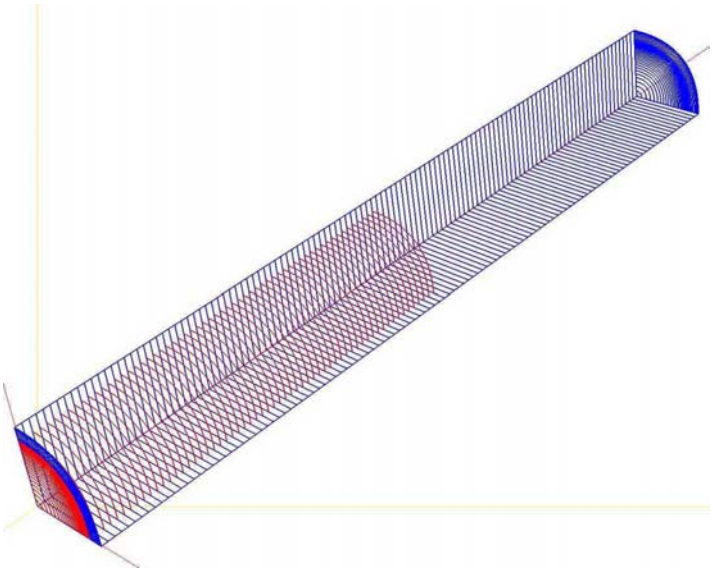

Figure 21. Grid Mesh of 2.25 inches Diameter Cylindrical Combustor.

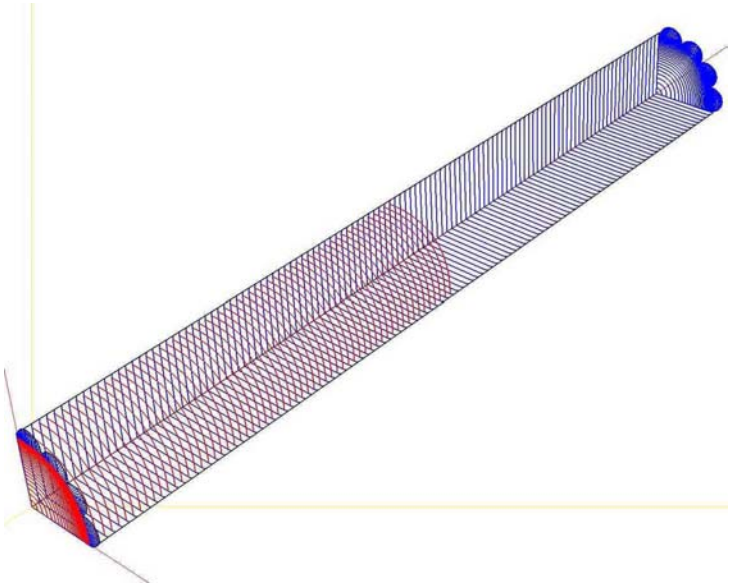

Figure 22. Grid Mesh of 2.25 inches Diameter Scallop Combustor.

2. Grid Refinement

Grid refinement is more like an art than a science with no definite technique or procedure. The Courant-Friedrichs-Levy number, CFL is defined as:

$$|\lambda| = \left| \frac{a \times \Delta t}{\Delta x} \right| \tag{34}$$

where

Δt = time step of the integration, known as DT in OVERFLOW program

Δx = grid size

a = wave speed of the following first order wave equation

$$\frac{\partial u}{\partial t} + a \frac{\partial u}{\partial x} = 0 \tag{35}$$

The convergence and stability of the solution depends extensively on the combination of the CFL and DT and finding their optimal combination may differ from case to case depending on the Mach number. The general guideline is that grid mesh can be refined at locations of sharp edges, sharp corners, flow transition, interest and both viscid and inviscid walls.

3. Boundary Conditions

Table 13 of Appendix D shows the boundary conditions of the combustors used in the OVERFLOW program. The core axis was defined as axis around L index and both the extra horizontal and vertical grid planes were defined as symmetry planes. The cylindrical and scallop combustor walls were defined as viscous adiabatic wall with pressure extrapolation and the closed rear wall of the initiator was defined as inviscid adiabatic wall with pressure extrapolation. The combustor main front and annular rear outlets were defined as outflow with extrapolation. The boundary conditions used were similar to the validated shock tube test case shown in the README file of Appendix E.

4. Numerical Differencing Scheme

Table 7 shows a list of numerical differencing schemes used in the validated shock tube test case as shown in the Appendix G. The ability of Newton sub-iterations to decrease factorization errors in the cross flow directions was tested. Each addition of Newton sub-iteration took the same amount of CPU time as one step of the original

method. Thus a ten Newton sub-iterations run would take ten times as long as a run with no sub-iteration.

Base Name	No. of Newton Sub-Iterations	Numerical Differencing Scheme
Central	Nil	Central Differencing, Scalar Dissipation, Diagonal, LHS
Central 3	3	Central Differencing, Scalar Dissipation, Diagonal, LHS
Central 5	5	Central Differencing, Scalar Dissipation, Diagonal, LHS
Central 10	10	Central Differencing, Scalar Dissipation, Diagonal, LHS
Matrix	Nil	Central Differencing, Matrix Dissipation, Diagonal, LHS
Matrix 3	3	Central Differencing, Matrix Dissipation, Diagonal, Left Hand Side
Matrix 5	5	Central Differencing, Matrix Dissipation, Diagonal, Left Hand Side
Matrix 10	10	Central Differencing, Matrix Dissipation, Diagonal, Left Hand Side
Matrix 30	30	Central Differencing, Matrix Dissipation, Diagonal, Left Hand Side
Roe	Nil	Central Differencing, Matrix Dissipation, Diagonal, Left Hand Side
Roe 3	3	Roe Upwinding, Diagonal, Left Hand Side
Roe 5	5	Roe Upwinding, Diagonal, Left Hand Side
Roe 10	10	Roe Upwinding, Diagonal, Left Hand Side
Roe 30	30	Roe Upwinding, Diagonal, Left Hand Side
Lu Roe 3	3	Roe Upwinding, LU-SGS Algorithm, Diagonal, Left Hand Side
Lu Roe 10	10	Roe Upwinding, LU-SGS Algorithm, Diagonal, Left Hand Side

Table 7. Numerical Differencing Scheme of Shock Tube Test Case.

The density, velocity and pressure line plots of the various scheme of the test case were evaluated against the experimental results of Appendix G. It was observed that the central differencing scheme coupled with scalar dissipation and three Newton sub-iterations was sufficient to remove factorization errors. Central differencing scheme with matrix dissipation took five Newton sub-iterations and Roe upwinding scheme took ten sub-iterations. The residual files showed that the convergence of the Newton sub-iterations slowed down greatly after the first three iterations, indicating not much benefit from additional sub-iterations for the larger time step part of the run. However, for the first ten steps with the smaller DT, additional sub-iterations continued to help convergence. This showed that the time step of 0.01 might be too large for maximum benefit of the Newton sub-iteration procedure.

The numerical differencing scheme chosen for all the combustor models was central differencing scheme coupled with matrix dissipation and ten Newton sub-iterations. It was selected based on its test case solution accuracy against the experimental results and its relatively shorter computation time. The first ten steps were taken with

time step, DT of 0.0001 and the subsequent steps were taken with time step, DT of 0.001 as shown in central.1.inp, central.2.inp and central.3.inp of Appendix F.

5. Input Thermodynamic Parameters and Assumptions

All the combustor models had the same initial thermodynamic parameters with the high pressure, temperature and density region filling the initial half of the initiator and the nominal ambient pressure, temperature and density region filling the rest of the initiator and combustor as shown in Figure 23. The pressure and density ratios of 20 and 6 between these regions shown in Table 8 would work out the temperatures to be 960 °K and 288 °K respectively based on the perfect gas relation. The specific heat ratios, γ for both regions were assumed to be 1.4 for air. These initial input thermodynamic parameters were edited in the makeq.f. file as shown in Appendix F and was later complied to makeq executable file using the Fortran 77 complier. The execution of the makeq file would generate the q.save solution file with the initial input thermodynamic parameters set in place. The central.1.batch file as shown in Appendix F would rename the q.save solution file to q.restart solution input file, which would be ready to feed into the OVERFLOW flow solver program.

	High Density, Pressure & Temperature Region	**Nominal Density, Pressure & Temperature Region**
Density, ρ (kg/m^3)	7.350	1.225
Density, ρ^* (non-dimension)	6.00	1.00
Pressure, p (kPa)	2026.500	101.325
Pressure, p^* (non-dimension)	20.00	1.00
Temperature, T (°K)	960.677	288.150
Specific Heat Ratio of Air, γ	1.4	1.4

Table 8. Initial Input Thermodynamic Parameters

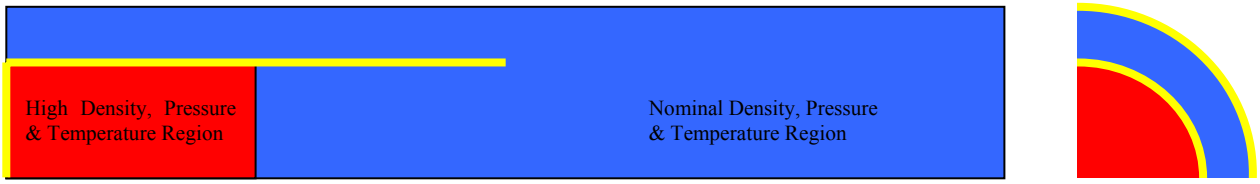

Figure 23. Initial Thermodynamic Parameters of Combustors.

6. Flow Solver Program Solutions at Different Stages

At the start of the run, the high density, pressure and temperature region in the initial half of the initiator would expand and generate a normal shock wave propagating towards the opened end of the initiator. The pressure behind the normal shock wave would be rapidly reduced to a plateau pressure of approximately six atmospheres due to the series of rarefaction waves that forms at the closed end of the initiator as shown in Figure 24. The velocity of the normal shock wave, driven by the reduced plateau pressure behind it, is approximately Mach 2.8 before exiting the initiator.

Subsequently, the normal shock wave from the initiator would be diffracted into the main combustor. The diffracted shock would be reflected by the combustor wall geometry and would form two normal shock waves, one propagating upstream into the coming air stream of the annular combustor outlet and another propagating downstream towards the main outlet of the combustor. The velocities of both the propagating normal shock waves would decrease as the diameter of the combustor wall increases.

Due to the limitations of the flow solver, the model is not capable of simulating the operating condition of the actual PDE. But it is adequate to study the efforts of reflected shock/focusing in generating regions of high vorticity and subsequently regions of high temperatures, transmitted from the initiator into the combustor through a weaker supersonic shock wave.

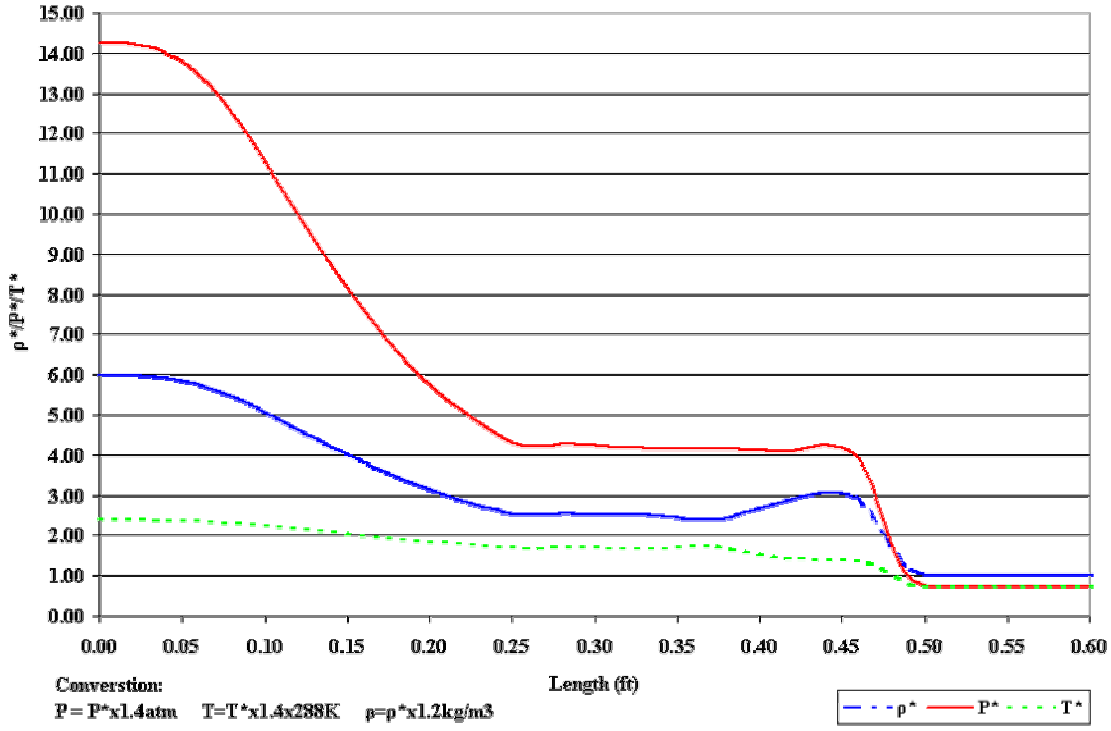

Figure 24. Thermodynamic Parameters Before Normal Shock Wave Exits Initiator.

7. CFD Procedure Flow Chart

Figure 25 shows a CFD procedures flow chart. The grid mesh was generated using GRIDGEN and edited using GRIDED. Appendix E shows the procedures of converting grid.grd to grid.in through the reserving the directions of the grid indexes, adding extra planes by reflected symmetry on the horizontal and vertical plane and etc. FAST was used to check the grid construction, grid distribution and directions of the grid indexes. The executable makeq file was used to create the q.save solution file, which set up the initial thermodynamic parameters and the q.save solution file was later renamed to q.restart solution input file through the execution of the central.1.batch file. FAST was used to check the initial density, pressure and temperature values of the combustor. The high density, pressure and temperature region would be shaded in white and rest in black.

There were three input files, each containing identical boundary conditions. The central.1.inp input file had 10 steps with time step, DT, of 0.0001 to help convergence. Both the central.2.inp and central.3.inp input files had the same time step, DT, of 0.001 but a different number of steps, NSTEPS, of ten and one respectively to save the

solutions accordingly. The OVERFLOW flow solver program would read the q.restart solution input file, grid.in grid file and the relevant central.1.inp, central.2.inp or central.3.inp input file and initiate the run through the execution of the central.1.batch file. The solver would stop the run at each designated steps as specified by the central.1.batch file, save and copy the q.save solution file to a new file name to prevent it from being overwritten and rename it to q.restart solution input file. The program, re-initiated by the central.1.batch file, would read the next q.restart solution input file, grid.in grid file and the relevant input file out of the three as stated above and the cycle continues until the last command of the central.1.batch file was executed.

If the solution failed due to a negative density or pressure or less than one specific heat ratio, γ, the previous step of the solution would be saved as q.bomb solution file. All the central output files and the residual file would be evaluated to determine the need to increase the number of first steps and reduce the time step, DT. If the need arises, all the central input files would be modified accordingly. Subsequently, FAST was used to check the grid mesh locations where negative density or pressure or the less than one specific heat ratio, γ, occurred. That region of the grid mesh might need to be refined using GRIDGEN. The process of determining the optimal time step, DT, and grid mesh size was indefinite and was usually based on trial and error attempts.

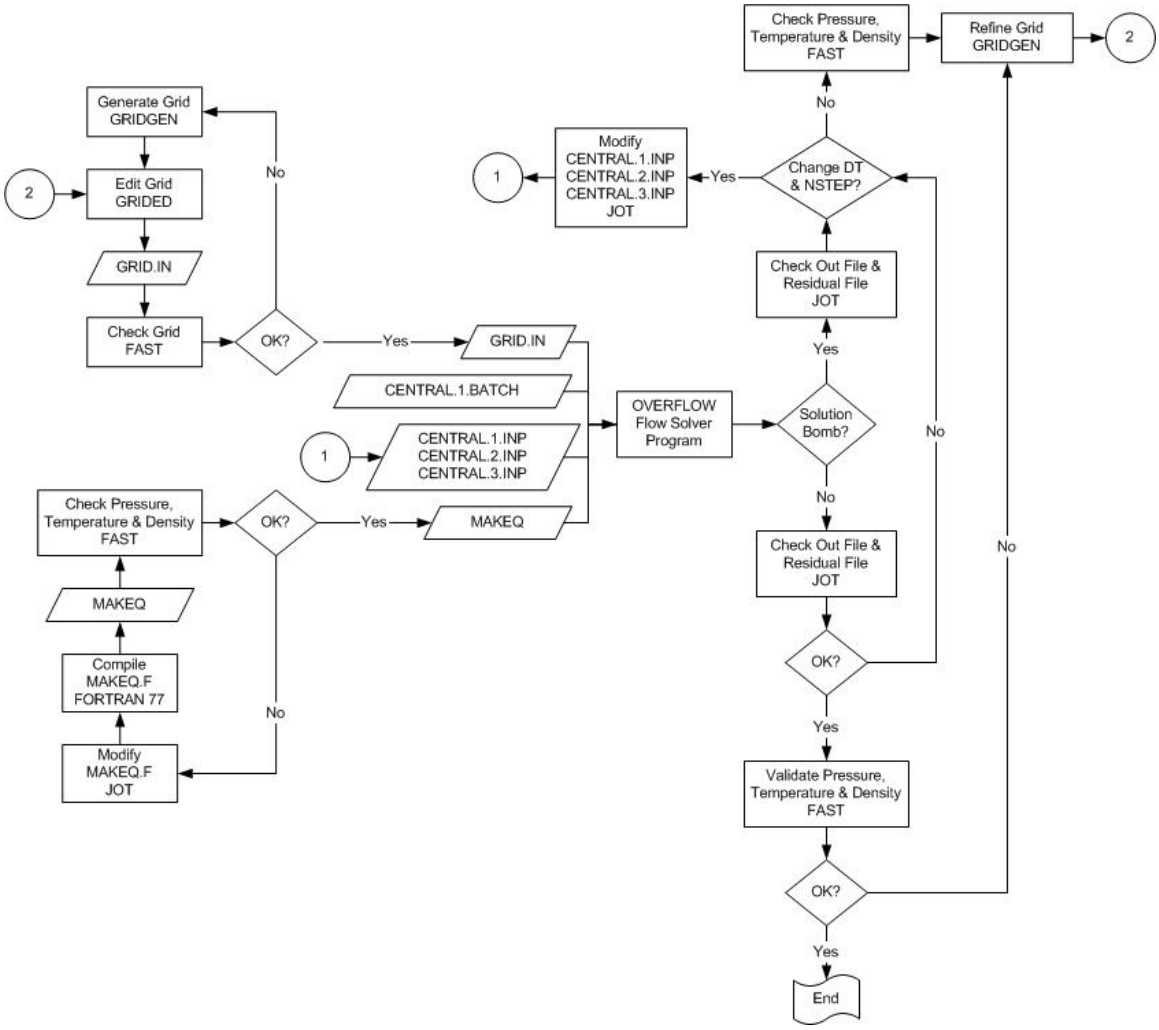

Figure 25. CDF Procedures Flow Chart

THIS PAGE INTENTIONALLY LEFT BLANK

V. CFD RESULTS AND ANALYSIS

A. INTRODUCTION

This chapter discusses and analyzes the CFD results generated by the flow solver for the cylindrical and scalloped combustor geometries described earlier. Interestingly, it was founded that the maximum temperature regions for cylindrical combustors and smaller diameter scalloped combustor were primarily due to shock focusing efforts as expected. But the maximum temperature regions of the larger diameter scalloped combustors appeared to be due to the high vorticity regions with some contributions of shock focusing efforts.

B. TEMPERATURE

1. Duration of Maximum Temperature Regions

An annular region of high temperature was typically formed at about 0.1 to 0.2 inches after the initiator and between the outer diameters of the initiator and the combustor. Figure 26 shows the maximum temperature of one of the high temperature regions and its duration for the various combustors.

It was observed that for the cylindrical combustors, the high temperature region would increase as the diameter of main combustor varied from 2.25 to 2.75 inches, but then decreased slightly for a 3 inches diameter. Generally, the maximum temperature distributions had an initial sharp rise, followed by a plateau region and then a second gradual rise as the shock wave propagated towards the end of the main combustor except for the 2.25 inches diameter scalloped combustor. The 2.25 inches diameter scalloped combustor had a larger second rise than the first. The high temperature regions for the second temperature rise were focused at the center of each scallop of the combustor wall geometry as shown in Figure 62 of Appendix J. The first and second temperature rises were due an initial weaker shock reflection, followed by a secondary stronger shock reflection.

A normal shock wave would propagate at Mach 2.8 in the initiator, diffract into the combustor and propagate at Mach 2.5 there after. Based on the initial gas temperature

and normal shock properties, the temperature across the normal shock propagating at Mach 2.5 was 616°K. Figure 26 shows that the durations for the maximum temperature regions defined as those above 616°K, were approximately 50, 80, 160 and 40 micro-seconds for the 2.25, 2.5, 2.75 and 3 inch diameter cylindrical combustors respectively. The temperature duration would reach its optimal at 2.75 inches and decline drastically at 3 inches and thereafter due to the increasing expansion condition.

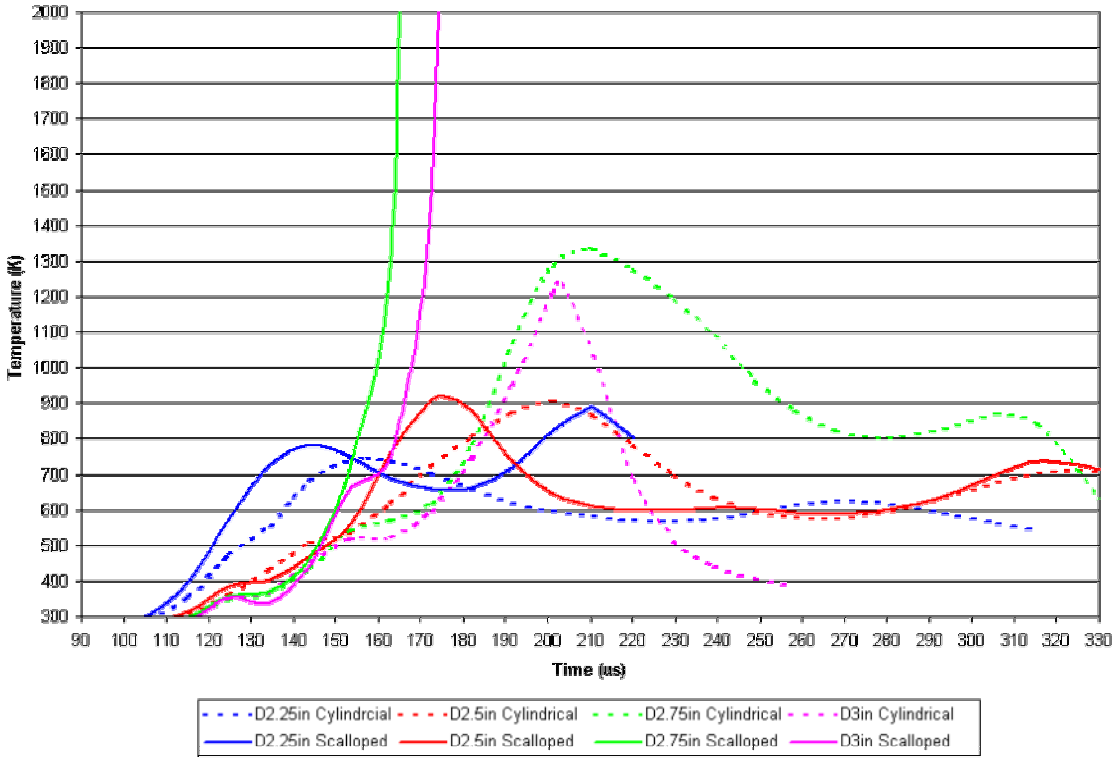

Figure 26. Maximum Temperature Vs Duration Plot of Various Combustors

The scalloped combustors produce maximum temperature durations of approximately 120 and 40 micro-seconds for the 2.25 and 2.5 inches diameter geometries respectively. The maximum temperature duration for both the unmodified and modified scalloped combustors for the 2.75 and 3 inches diameters could not be accurately accounted for as their temperatures rapidly rise beyond 4,000°K preventing their CFD solutions from converging due to the inaccuracy of the perfect gas law at those conditions.

The Arrhenius rate law of equation (13) shows the relationship of reaction rate with temperature rise. The maximum temperature regions coupled with their duration rapidly accelerates the rate of chemical reaction of a combustible mixture. Therefore, the 2.75 and 3 inches scalloped combustors would have considerable potential in initiating the less sensitive hydrocarbon fuel/air mixture in the combustor through a Mach 5.5 shock wave from the hydrocarbon fuel/air initiator.

Generally, the maximum temperature regions of the scalloped combustors are approximately 1.5 to 5.5% marginally higher than the cylindrical combustor for the 2.25 and 2.5 inches diameter. But the maximum temperature ratios between the scalloped and cylinder combustors are 2.4 and more than 3.2 for the 2.75 and 3 inches diameter respectively. Thus only the 2.75 and 3 inches diameter cylindrical and scalloped combustors are selected for subsequent comparisons.

2. Temperature Variation in the Main Combustor

The temperature plots of the 3 inches diameter cylindrical and scalloped combustors are compared in Figures 27 and 28. The temperature variation of the high temperature regions was reasonably uniform for the cylinder combustor whereas the extremely high temperature regions were only found primarily near the scallop edges of the scalloped combustors.

Figure 29 shows that the temperature distributions of the high temperature regions along the circumferential index (L index) of the grid would oscillate circumferentially for both the 2.75 and 3 inches diameter cylindrical combustors. Whereas for the 2.75 and 3 inches diameter scalloped combustors, extremely high temperature spikes (some more than 4,000°K) were created near the scallop edges. The high temperature spikes are not exactly consistent at each scallop edge due to slight dimensional variation of each scallop. The majority of the temperature distributions are similar in magnitude to the cylindrical combustor results for both scalloped combustors. Appendix J shows the remaining temperature plots of the other combustors.

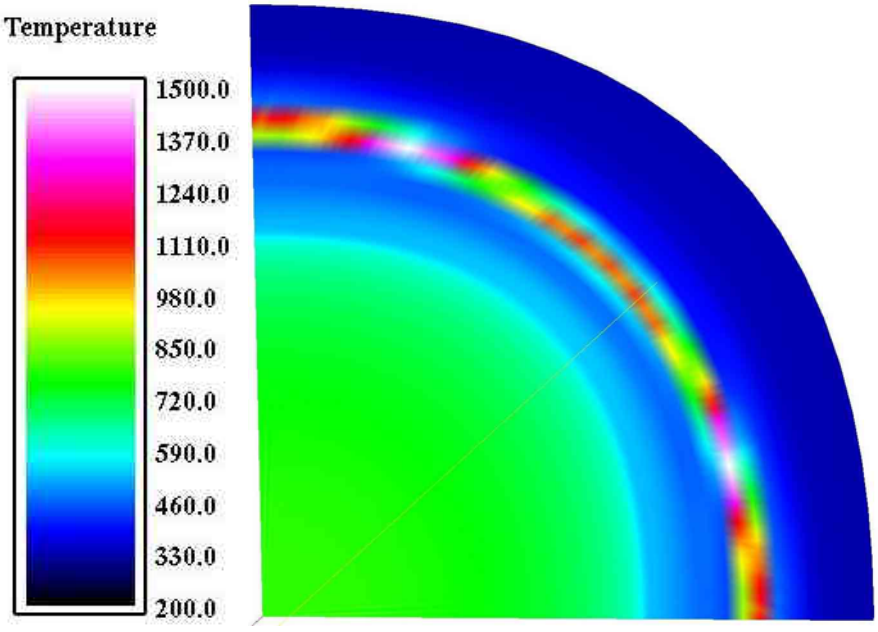

Figure 27. Temperature Plot of 3 inches Diameter Cylindrical Combustor.

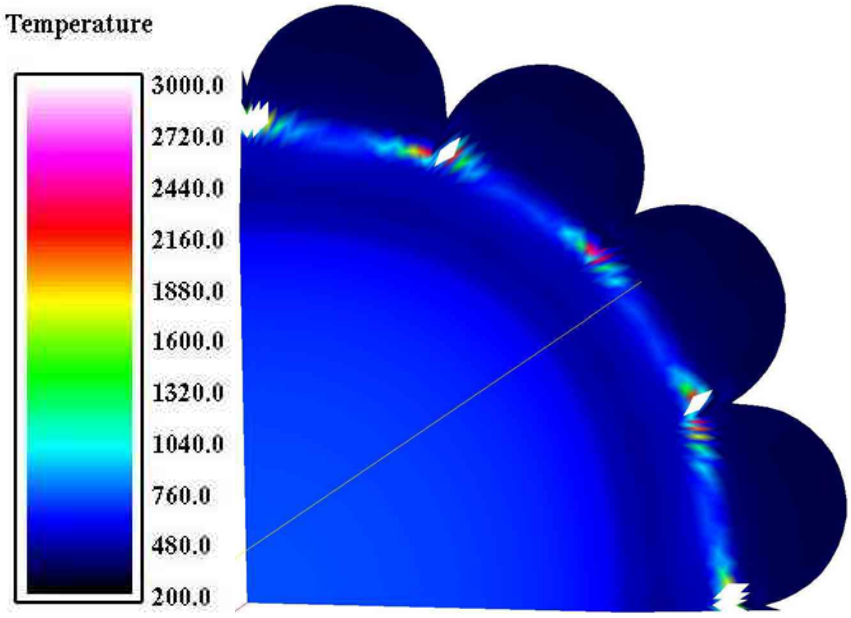

Figure 28. Temperature Plot of 3 inches Diameter Scalloped Combustor.

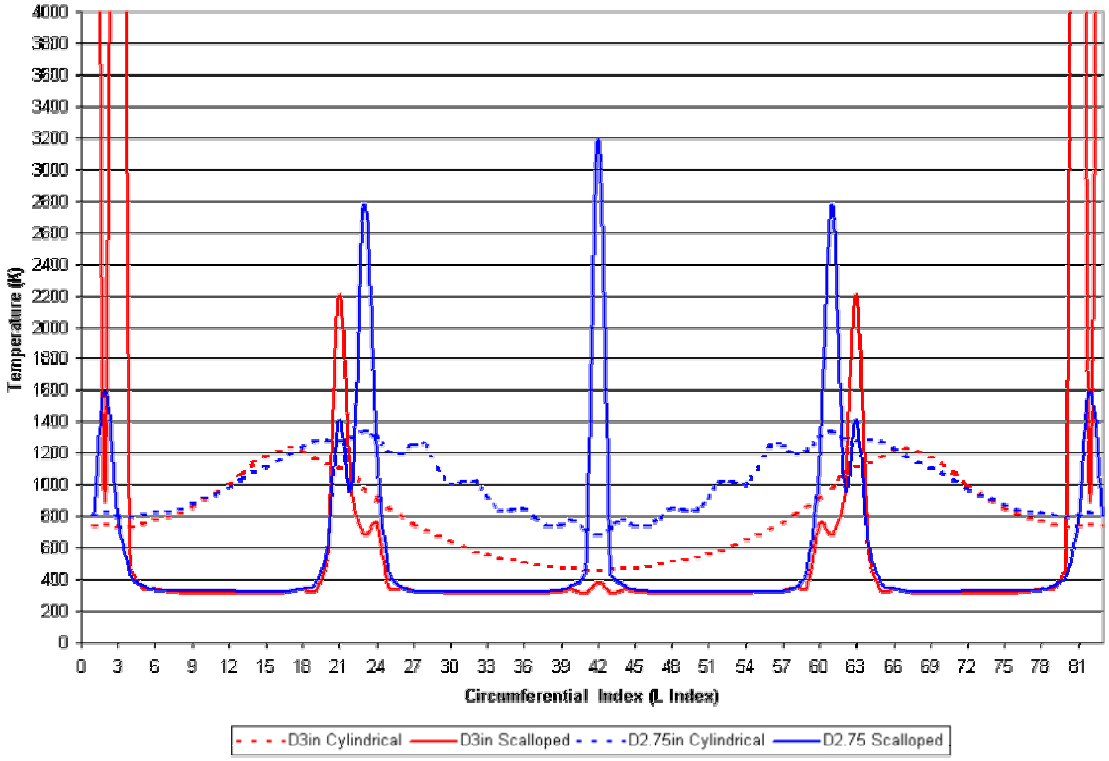

Figure 29. Temperature Variation of High Temperature Regions for 2.75 and 3 inches Diameter Cylindrical and Scalloped Combustors.

3. Axial Temperature and Pressure Contour Plots

The axial temperature and pressure contour plots of the 3 inches diameter cylindrical and scalloped combustors are compared in Figures 30 and 31 at 203.15 and 182.16 micro seconds after the initiation of the run respectively. Appendix I showed the remaining temperature and pressure contour plots of the other combustors. Although not directly shown, after the shock wave from the initiator expanded into the combustor, a portion of the flow diffracts 180° and forms a normal shock wave, which propagates towards the entrance of the combustor.

The pressure gradients of the reflected pressure waves were similar due to their constant diameter for the cylindrical combustors, but the reflected shock waves from the combustor walls were not ideal since the incident shock waves from the initiator were highly curves and not sufficiently planar at 2.25 and 2.5 inches diameter. The maximum reflected shock benefit occurred for the 2.75 inches diameter combustor. At a combustor

diameter of 3 inches and larger, this magnitude started to decrease as the reflected pressure region increasingly diffused axially to the rear and front ends of the combustor. The pressure contours of the reflected pressure region for the scalloped combustors produced interesting results along the scallop edges; which represented the internal diameter of the combustor and the remainder took place at the most outer tangents of the scalloped wall.

The governing mechanism creating the high temperature regions appeared to be primarily shock reflection from the combustor wall and not vorticity generation for the cylindrical combustors and the smaller 2.25 and 2.5 inches diameter scalloped combustors. The extremely high temperature regions of the 2.75 and 3 inches diameter scalloped combustors were primarily generated by high vorticity regions, not shock focusing directly. This phenomenon is further elaborated later in this chapter.

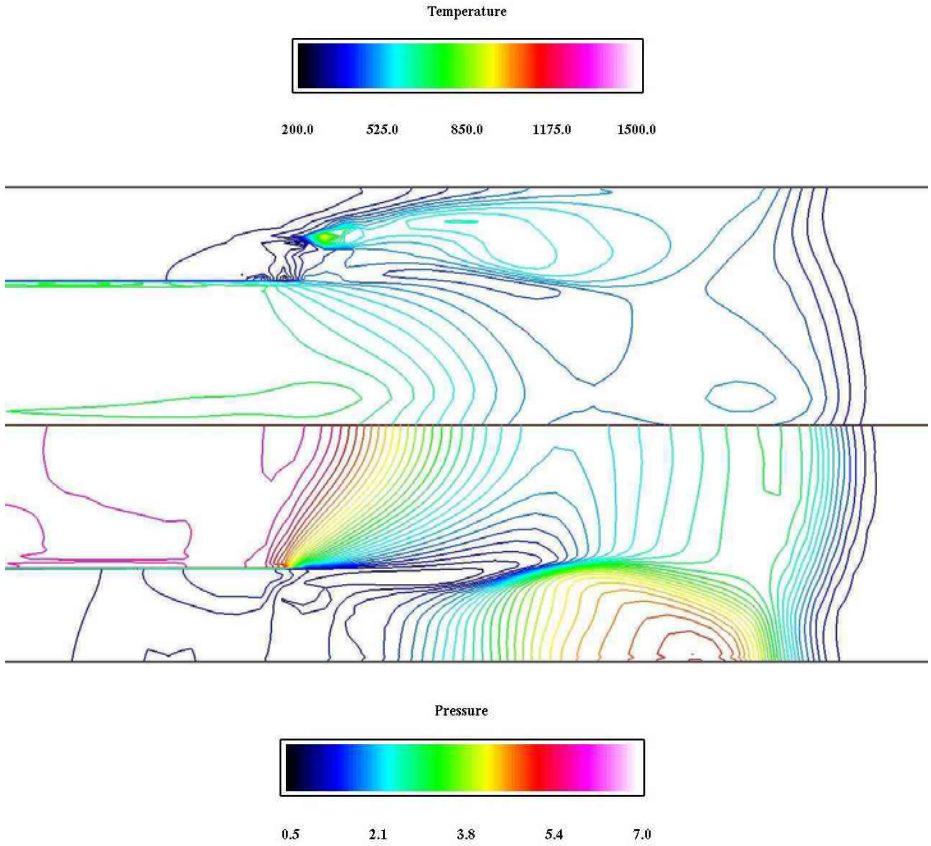

Figure 30. Temperature and Pressure Contour Plot of 3 inches Diameter Cylindrical Combustor.

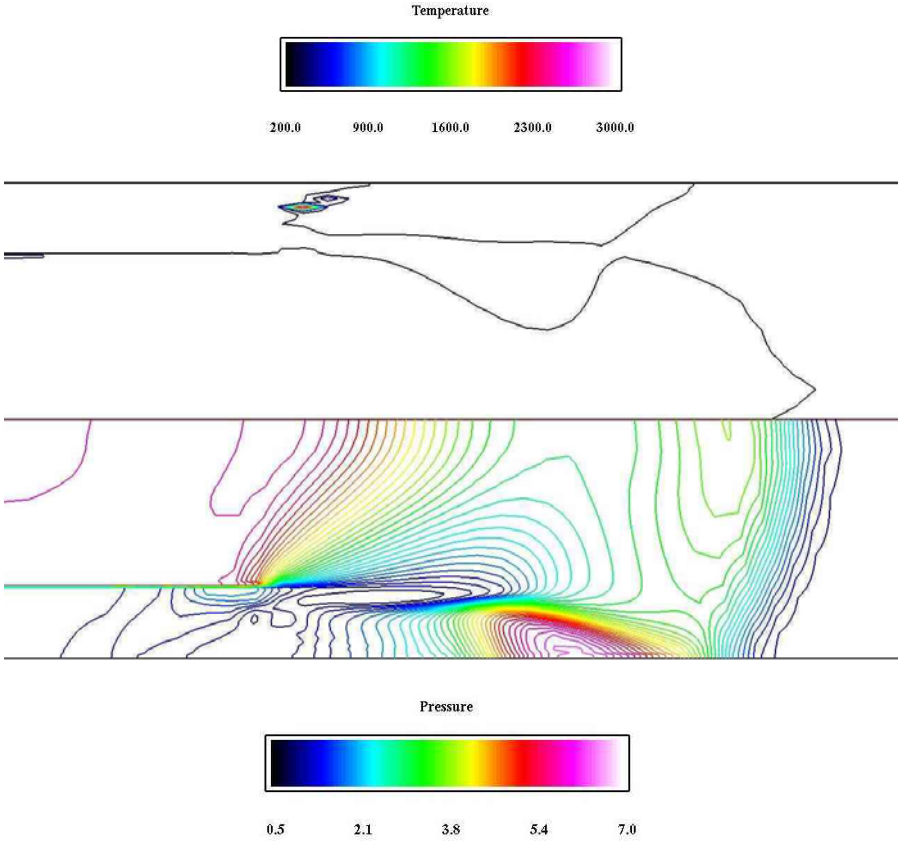

Figure 31. Temperature and Pressure Contour Plot of 3 inches Diameter Scalloped Combustor.

C. DURATION OF MAXIMUM REFLECTED PRESSURE REGIONS

Figure 32 shows the maximum pressure of the reflected pressure region and its duration of the various combustors. Depending on the diameter and geometry of combustors, the maximum reflected pressure distributions would have an initial sharp rise to about 4.9 to 6 atmospheric pressure and gradually decline to 2.5 to 3.4 atmospheres towards the end of the shock wave propagation. Generally, the scalloped combustors had slightly higher maximum reflected pressure than the cylindrical combustors as shown in Figure 32.

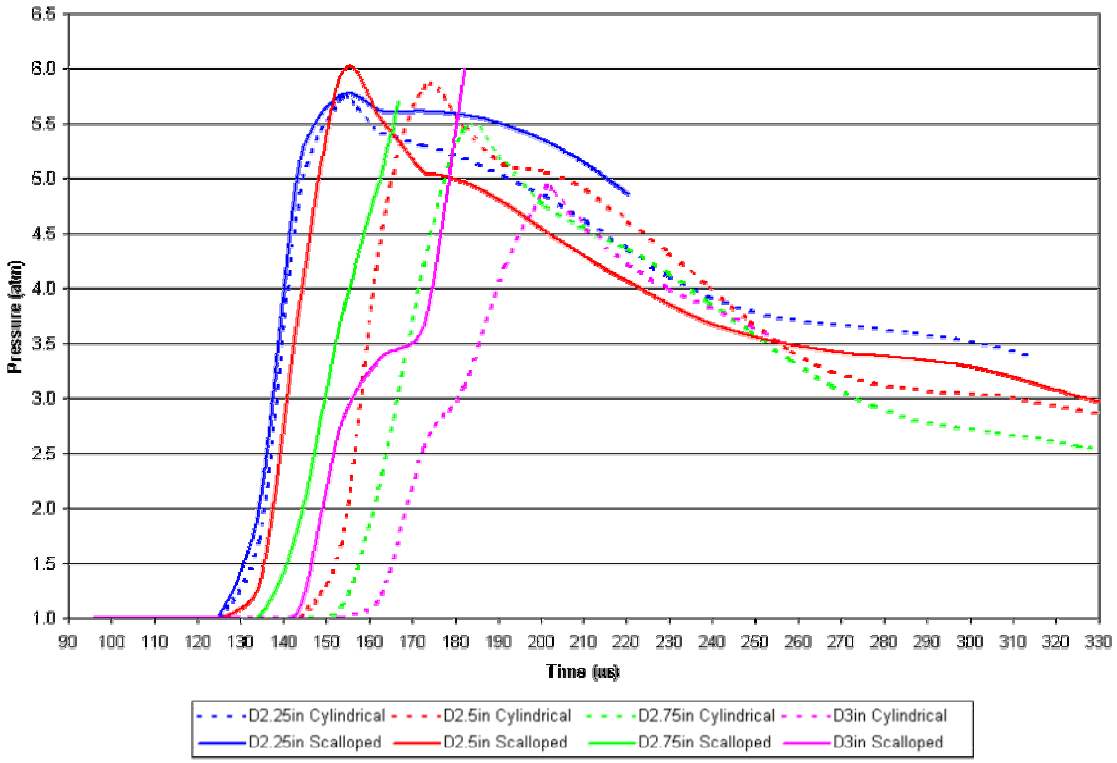

Figure 32. Maximum Reflected Pressure Vs Duration Plot of Various Combustors.

Figure 33 shows the pressure variation at the high temperature regions along the circumferential index (L index) of the grid for the 2.75 and 3 inches diameter cylindrical and scalloped combustors. Generally the pressures of the scalloped combustors are higher than the cylindrical combustors, but not significantly. The pressure distributions tend to oscillate circumferentially as well; which is similar to their temperature distribution but add a phase shift for the cylindrical combustors. The erratic pressure distributions were associated to their corresponding temperature fluctuations due to complexity of the scalloped geometry.

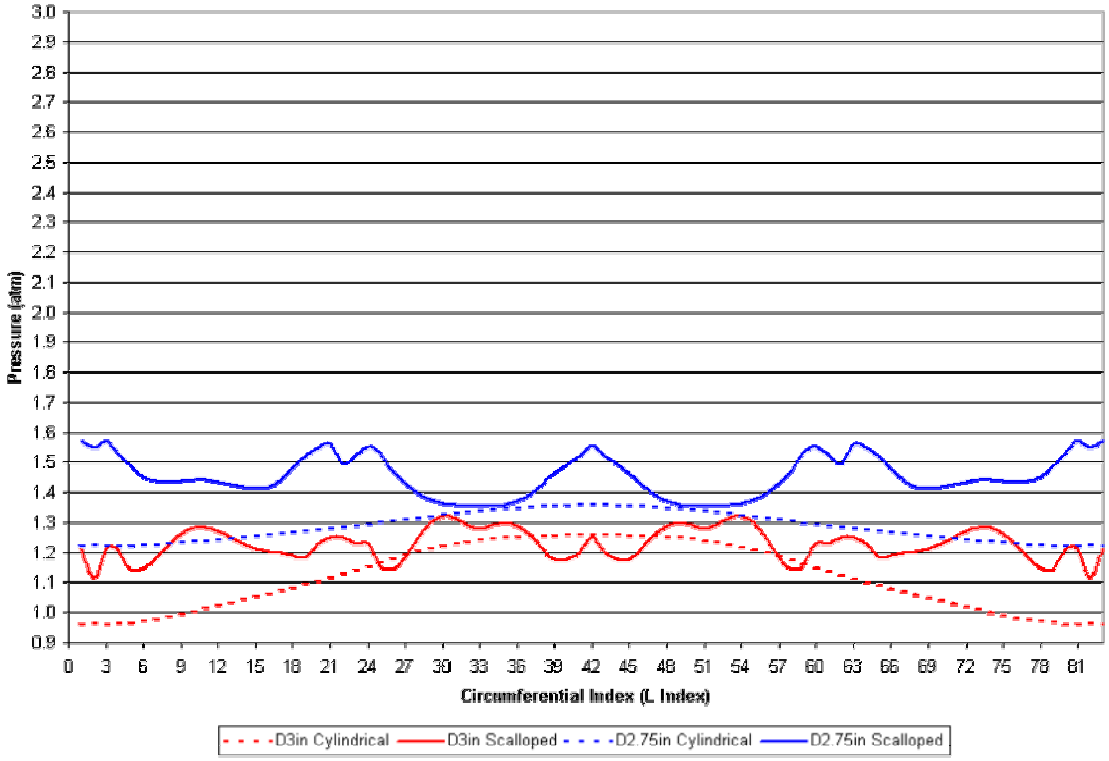

Figure 33. Reflected Pressure Variation Vs Time Plot for 2.75 and 3 inches Diameter Cylindrical and Scalloped Combustors.

D. MACH NUMBER

Figures 34 and 35 show the Mach number vector plots of the 3 inches diameter cylindrical and scalloped combustors. Appendix K shows the Mach number plots of the other combustors. Both cylindrical and scalloped combustors have the supersonic Mach number vectors, expanded outwardly from the initiator, and the sub-sonic Mach number vectors, reflected from the wall of the combustor, opposing each other.

The directions of both opposing Mach number vectors shown in Figure 34 varied circumferentially, revealing large counter-rotating structures for the 3 inches diameter cylindrical combustor. Figure 35 shows that the Mach number vectors crossed multiple times near the scallop edges for the 3 inches diameter scalloped combustor. In fact, there are three opposing Mach number vectors near the scallop edges from the initiator, the left and the right scallops instead of two. Thus the high vorticity generated in that region as described later in this chapter was responsible for causing high viscous frictional heat generation.

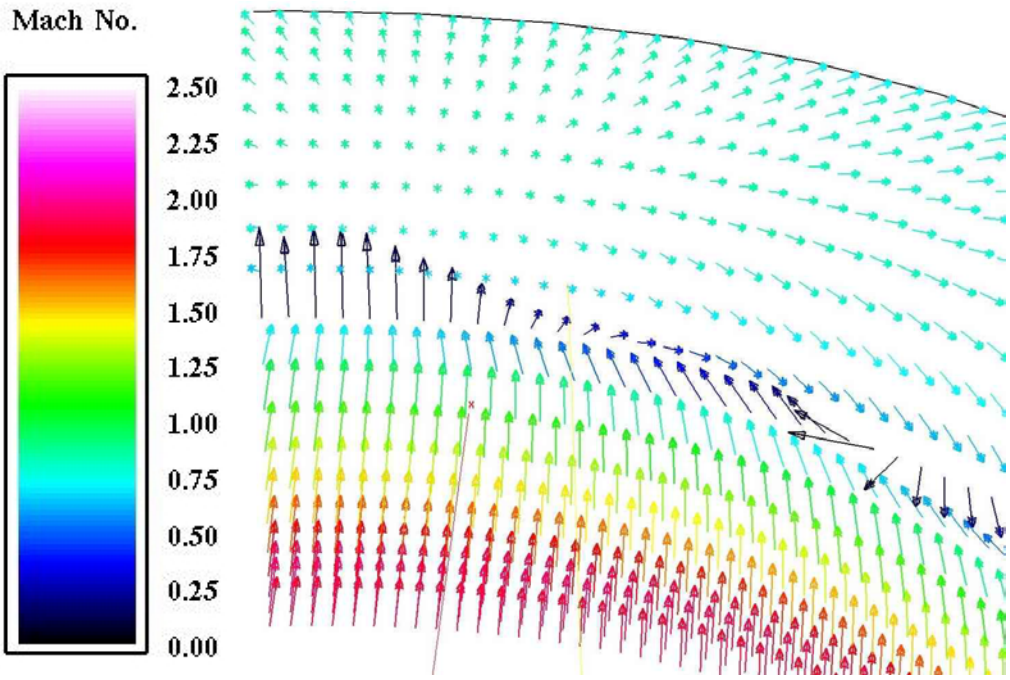

Figure 34. Mach No. Vector Plot of 3 inches Diameter Cylindrical Combustor

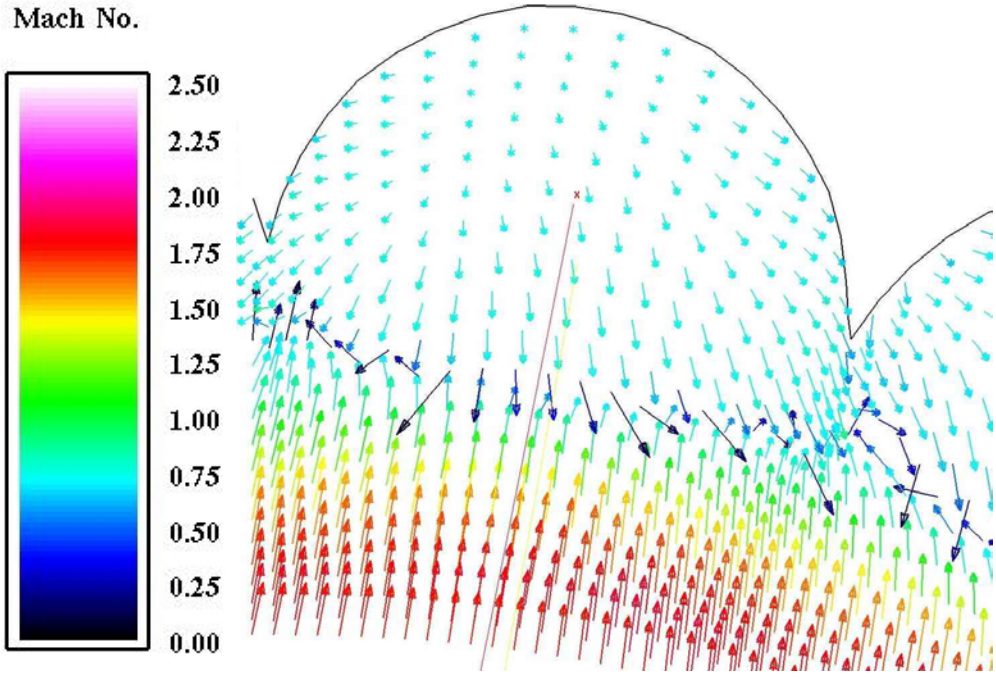

Figure 35. Mach No. Vector Plot of 3 inches Diameter Scalloped Combustor

E. VORTICITY MAGNITUDE

Figures 36 and 37 show the vorticity magnitude plots of the 3 inches diameter cylindrical and scalloped combustors. The vorticity magnitude of the cylindrical combustor along the ring of the sonic region is uniformly 300 whereas the scalloped combustor was about 1100 near the scallop edges. Thus the vorticity magnitude ratio of the scalloped over the cylindrical combustors was about 3.67. These results indicate that although shock reflection is partially responsible for producing a temperature rise at the high temperature region, the vorticity generation and subsequent dissipation mechanisms are a more dominant mechanism. Appendix L shows the remaining vorticity magnitude plots of the other combustors.

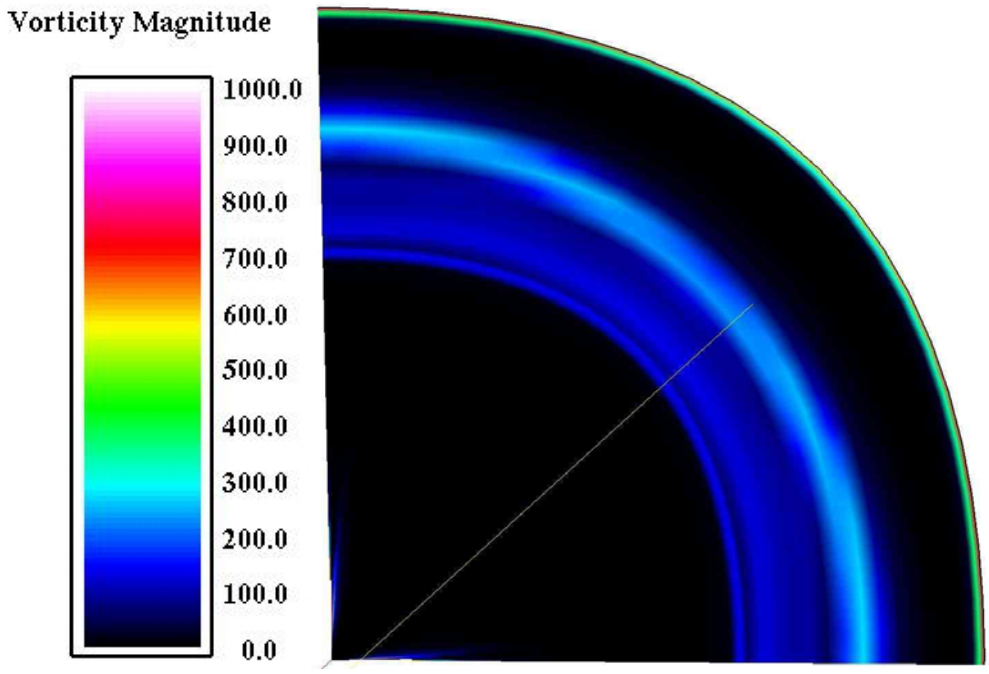

Figure 36. Vorticity Magnitude Plot of 3 inches Diameter Cylindrical Combustor.

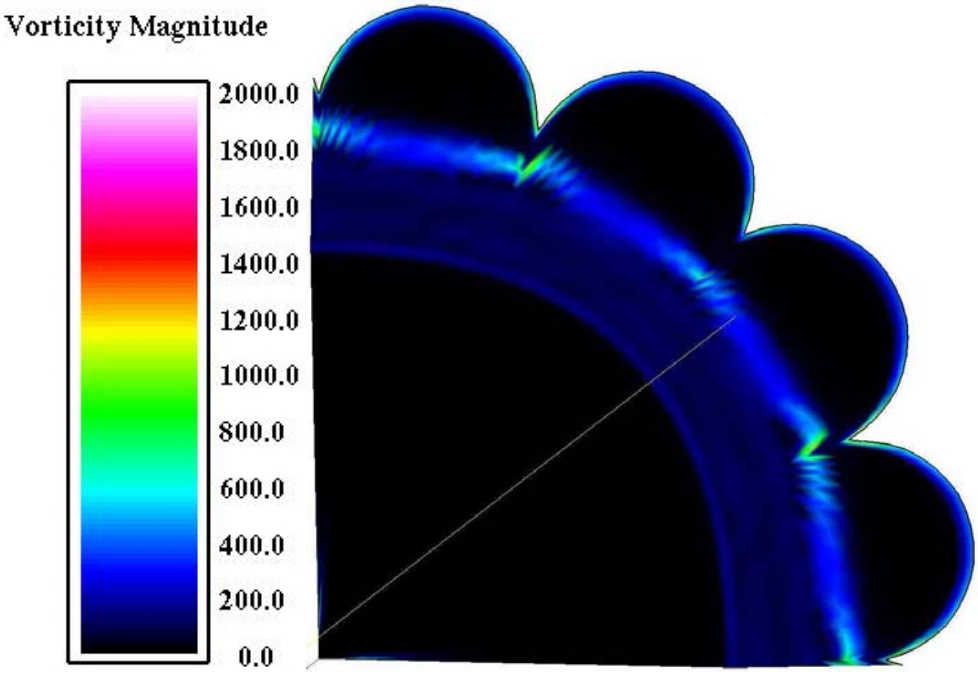

Figure 37. Vorticity Magnitude Plot of 3 inches Diameter Scalloped Combustor.

F. RESULTS SUMMARY

Table 9 shows the summary of results for the 10 combustors evaluated. The maximum temperature generated by the scalloped combustors was only 1.5 to 5.5% higher than the cylindrical combustor for the 2.25 and 2.5 inches diameter due to the effects of shock reflection and reduction in vorticity generation. However, the maximum temperature ratio of the scalloped over the cylindrical combustors were 2.4 and more than 3.2 respectively for the 2.75 and 3 inches diameter due to the large amount of vorticity generated and the supplemental effects of shock reflection/focusing. Although not validated, prolonging the duration of these high temperature regions should be possible so as to further accelerate the chemical reaction of the combustible mixture in those regions. The maximum reflected pressure varied about minimally from a nominal value of 5.61 atmospheres among the combustors.

Table 9. Results Summary of Combustors

Combustor	Time (μsec)	Length After Initiator (inch)	Temperature of Hottest Spot (°K)	Vorticity Magnitude of Hottest Spot	Time (μsec)	Length After Initiator (inch)	Maximum Pressure After Initiator (atm)
2.25in Diameter Cylindrical	159.84	0.1	745	350	150.49	0.9	5.74
2.5in Diameter Cylindrical	197.22	0.2	945	250	169.18	1.3	5.83
2.75in Diameter Cylindrical	205.64	0.2	1,336	300	178.53	1.4	5.45
3in Diameter Cylindrical	199.09	0.2	1,236	300	197.22	1.6	4.92
2.25in Diameter Scalloped	205.64	0.1	885	300	150.49	0.9	5.77
2.5in Diameter Scalloped	171.99	0.2	917	600	150.49	0.9	5.96
2.75in Diameter Scalloped*	163.57	0.2	3,202	1200	163.57	1.0	5.71
3in Diameter Scalloped*	178.79	0.2	>4,000	1100	178.53	1.1	6.01
2.75in Diameter Modified Scalloped*	174.79	0.2	>4000	1750	169.18	1.2	5.88
3in Diameter Modified Scalloped*	167.31	0.2	3,209	1100	167.31	1.0	4.84

Notes:
* CFD solution fails prematurely due to extremely high temperature generated, which defile the perfect gas law algorithm of the OVERFLOW flow solver program.

THIS PAGE INTENTIONALLY LEFT BLANK

VI. CONCLUSION AND RECOMMENDATION

A. CONCLUSION

This thesis evaluated the effects of various geometries on the reflected shock conditions for producing regions of high local temperature and pressure. A total of 10 combustor models were modeled with 4 cylindrical combustor wall geometries and 6 scalloped combustor wall geometries. The effects of shock refection/focusing were studied by fixing the diameter of the initiator at 1.875 inches and varying inner diameter of cylindrical and scalloped combustor at 2.25, 2.5, 2.75 and 3 inches, forming 8 combustor models. Another 2 combustor models with the edges of the 2.75 and 3 inches scalloped combustor wall geometries modified were added.

The results revealed that the reflected pressure and high temperature regions of both the cylindrical and scalloped combustors increase as the combustor diameter increases eventually to a point of diminishing return. The maximum reflected pressure of both the cylindrical and scalloped combustors did not vary much between geometries. The governing mechanism creating the high temperature regions appears to be primarily shock reflection/focusing from the combustor wall geometry coupled with a small amount of vorticity generation for all the cylindrical combustors. This phenomenon is similar for the smaller 2.25 and 2.5 inches diameter scalloped combustors. Whereas the governing mechanisms of creating extremely high temperature regions for the 2.75 and 3 inches diameter scalloped combustors were primarily due to high vorticity generation near the scalloped edges which supplemented the inherent effects of shock reflection/focusing. The maximum temperature ratios between the 2.75 and 3 inches scalloped and cylinder combustors were approximately 2.4 and more than 3.2 respectively due to a large vorticity magnitude ratio of more than 3.67. These magnitudes should be viewed as approximate values since the CFD flow solver program utilizes the ideal gas law and not a real gas model. Therefore, the observed threads should be consistent but reduced in magnitude if a real gas model is utilized.

B. RECOMMENDATIONS

The wall contour of scalloped combustor should be modified to further increase the vorticity magnitude, particularly the angles of the scallop edges, so as to generate higher temperature and duration. A flow solver program capable of handling chemical reaction and hypersonic velocity should be used to model the actual PDE conditions. Experimental work should also be carried out to verify the findings.

APPENDIX A. SUMMARY OF NAMELIST INPUT TO OVERFLOW.

$GLOBAL

CHIMRA	TRUE–expect grid file to be in multiple grid format and PEGSUS-type IBLANK and interpolation information to be in file *INTOUT* or *XINTOUT*. FALSE–expect single grid with no PEGSUS information. [FALSE]
CDISC	TRUE–expect to read a NAMELIST input file *overdisc.con*, containing CDISC inverse design control information. This file will be updated by OVERFLOW. FALSE–do not read or write any CDISC information. [FALSE]
INCORE	TRUE–keep data for all grids in memory. FALSE–store temporary flowfield, grid, and Chimera interpolation information in scratch files. [FALSE]
NSTEPS	Number of steps to advance solution. Use zero for input check. [0]
RESTRT	TRUE–read restart flowfield from file *q.restart*. FALSE–start from initial freestream flowfield. [FALSE]
NSAVE	$\geq$0–Save the overall solution to file *q.save* every how many steps. $<$ 0–Save the solution to file *q.step#* every how many steps. [100]
NFOMO	For overset force/moment integration package (FOMOCO), compute integrated quantities every how many steps. [10]
NQT	Global turbulence model type declaration: 0–algebraic or none. 100–1-equation Baldwin-Barth R_T model. 101–1-equation Spalart-Allmaras R_T model (with trip line specification). 102–1-equation Spalart-Allmaras R_T model (fully turbulent). 202–2-equation k-ω model. 203–2-equation SST model. [0]
NQC	Variable γ model type declaration (number of species): 0–Constant γ, 1-gas variable γ, or 2-gas variable γ mixing based on stagnation enthalpy. $\geq$2–Multiple gas variable γ based on solution of NQC species continuity equations. [0]
MULTIG	Flag to enable/disable multigrid acceleration. [FALSE]
FMG	Flag to enable/disable "full multigrid" (grid sequencing) precedure. Only for use with multigrid. [FALSE]
NGLVL	Number of multigrid levels to use. [3]
FMGCYC(level#)	Number of steps to take on coarse grid levels during full multigrid procedure. (Here index 1 is the coarsest level, 2 the next finer, etc.) [300 for all coarse levels]
DTPHYS	Nondimensionalized physical timestep for time-accurate simulations. Nondimensionalization is based on grid length and freestream velocity. [0.]
NITNWT	Number of Newton/dual subiterations per timestep, or 0 for no subiteration. [0]
ORDNWT	(Not used. Number of orders of convergence per timestep for Newton/dual subiteration.) [0.]
FSONWT	1.0–first-order in time Newton/dual subiteration. 2.0–second-order in time Newton/dual subiteration. Intermediate values allowed. [2.0]

$FLOINP

ALPHA	Angle-of-attack (α), deg. [0.0]
BETA	Sideslip angle (β), deg. [0.0]
FSMACH	Freestream Mach number (M_∞). [0.0]
GAMINF	Freestream ratio of specific heats (γ_∞). [1.4]
REY	Reynolds number (Re) (based on freestream velocity and grid length unit). [0.0]
PR	Prandtl number (Pr). [0.72]
PRT	Turbulent Prandtl number (Pr_t). [0.9]
TINF	Freestream temperature (T_∞), deg. Rankine. [518.7]
RETINF	Freestream turbulence level $(\mu_t/\mu_l)_\infty$ for 1- or 2-equation turbulence models. [0.1]
XKINF	Freestream turbulent kinetic energy $(k_\infty/\mathcal{V}_\infty^2)$ for k-ω and SST turbulence models. [0.0001]
FROUDE	Froude number (gravity term) (Fr) (based on freestream velocity and grid length unit). [0.0]
GVEC(3)	Unit up-vector for gravity term. (Note that this vector is taken verbatim–it is *not* modified internally by the angle-of-attack, since other orientation angles (such as bank angle) are not known.) [0,0,1]
TARGCL	TRUE–Enable the C_L-driver option. [FALSE]
CLTARG	Value of C_L which the code will try to match. [0.]
CLALPH	Initial value of d(CL)/d(ALPHA) used to estimate the necessary change in ALPHA. This is only used for the first correction, after which the CL and ALPHA changes from the previous correction are used. [0.1]
NTARG	Number of steps (or cycles) between ALPHA corrections, with the following exceptions: (1) Corrections are not done during grid sequencing (initial coarse grid cycles) as when FMG=TRUE; (2) Corrections are not done on the first or last (fine grid) steps; (3) coarse grid cycles are not counted towards NTARG. [200]

$VARGAM

IGAM Options for specifying calculation of γ when *not* solving species continuity equations (i.e., $NQC < 2$):
0–Use a constant γ value of GAMINF.
1–Single gas with variation of γ with temperature computed using ALT0-4, AUT0-4.
2–Two gases, variation of γ with temperature computed using ALT0-4, AUT0-4; all gas 1 below HT1, all gas 2 above HT2, linear mix in between. [0]

HT1 Total enthalpy ratio $h_0^*/h_{0\infty}^*$ below which the mixture is all gas 1. [10.]

HT2 Total enthalpy ratio $h_0^*/h_{0\infty}^*$ above which the mixture is all gas 2. [10.]

SCINF(gas#) Freestream species mass fraction $c_{i\infty}$. [1 for gas 1, 0 for all others]

SMW(gas#) Species molecular weight MW, or normalized molecular weight MW/MW_∞ (if preferred). [1.]

ALT0(gas#) Lower temperature range polynomial coefficient a_0 ($540°R \leq T \leq 1800°R$). [$\gamma_\infty/(\gamma_\infty - 1)$]

ALT1(gas#) Lower temperature range polynomial coefficient a_1 ($540°R \leq T \leq 1800°R$). [0.]

ALT2(gas#) Lower temperature range polynomial coefficient a_2 ($540°R \leq T \leq 1800°R$). [0.]

ALT3(gas#) Lower temperature range polynomial coefficient a_3 ($540°R \leq T \leq 1800°R$). [0.]

ALT4(gas#) Lower temperature range polynomial coefficient a_4 ($540°R \leq T \leq 1800°R$). [0.]

AUT0(gas#) Upper temperature range polynomial coefficient a_0 ($1800°R \leq T \leq 9000°R$). [$\gamma_\infty/(\gamma_\infty - 1)$]

AUT1(gas#) Upper temperature range polynomial coefficient a_1 ($1800°R \leq T \leq 9000°R$). [0.]

AUT2(gas#) Upper temperature range polynomial coefficient a_2 ($1800°R \leq T \leq 9000°R$). [0.]

AUT3(gas#) Upper temperature range polynomial coefficient a_3 ($1800°R \leq T \leq 9000°R$). [0.]

AUT4(gas#) Upper temperature range polynomial coefficient a_4 ($1800°R \leq T \leq 9000°R$). [0.]

$GRDNAM

NAME Grid name (for input identification purposes only, not used within the code). [" "]

$NITERS

ITER $>$ 0–Number of flow solver (sub)iterations per step (number of iterations before continuing to the next grid). Each iteration of the flow solver implies ITERT iterations of the turbulence model and ITERC iterations of the species continuity equations.
0–Do not advance the flow solution; take ITERT iterations of the turbulence model, ITERC iterations of the species continuity equations. Use ITER = ITERT = ITERC = 0 to skip this grid. [1]

$METPRM

IRHS 0–central difference Euler terms.
2–Yee's symmetric TVD scheme.
3–Liou AUSM$^+$-ap upwind scheme.
4–Roe upwind scheme. [0]

ILHS 0–ARC3D 3-factor block tridiagonal scheme.
1–F3D two-factor scheme.
2–ARC3D 3-factor diagonal scheme.
3–LU-SGS algorithm.
4–D3ADI algorithm with Huang subiteration. [2]

ILHSIT Number of subiterations for D3ADI scheme. [1]

IDISS 1–F3D dissipation scheme (2nd and 4th order on both RHS and LHS for ILHS=2, 2nd order only on LHS for ILHS=1).
2–ARC3D dissipation scheme (2nd and 4th order on both RHS and LHS for ILHS=2, F3D 2nd order on LHS for ILHS=1).
3–TLNS3D dissipation scheme (as with IDISS=2, but smooth ρh_0 instead of ρe_0).
4–Matrix dissipation scheme (see additional parameters VEPSL, VEPSN and ROEAVG in $SMOACU). [3]

BIMIN 1.–Disable low-Mach number preconditioning.
$< 1.$–Enable low-Mach number preconditioning.
$-1.$–Enable low-Mach number preconditioning; reset BIMIN to $3 \times M_\infty^2$. [1.]

MULTIG Local flag to enable/disable multigrid acceleration. [Default is value of MULTIG from $GLOBAL.]

SMOOP Smoothing coefficient for interpolation (prolongation) of coarse grid solutions onto the next finer level (FMG=TRUE only). [0.]

SMOOC Smoothing coefficient for interpolation of multigrid correction onto the next finer level. [0.]

SMOOR Smoothing coefficient for multigrid residual smoothing before restricting to the next coarser level. [0.]

CORSVI Enable/disable computation of viscous terms on coarse grid levels. [TRUE]

$TIMACU

ITIME 0–time accurate.
1–local timestep scaling (with 0.005 fudge factor).
2–local timestep scaling (with 0 fudge factor).
3–Constant CFL number (based on CFLMAX value). [1]
ITIME=3 uses the sum of the (max) eigenvalue in each coordinate direction to determine the local CFL number. All other uses of CFLMIN/CFLMAX use the maximum eigenvalue to determine the CFL number.

IRELAX 0–no over-relaxation.
1–N-relaxation scheme enabled (Ref. 19). [0]

DT Timestep parameter. For time-accurate runs (ITIME=0), DT is nondimensionalized by grid length and freestream speed-of-sound. [0.5]

TFOSO 1.0–first-order time accuracy (Euler implicit scheme).
2.0–second-order time accuracy (trapeziodal implicit scheme).
Other values allowed; 0.5, 1.9 OK. [1.0]

CFLMIN Minimum CFL number cutoff. [0.0]

CFLMAX Maximum CFL number cutoff. [0.0 (none)]

$SMOACU

ISPEC Single value to specify ISPECJ, ISPECK, ISPECL. Does not override ISPECJ, ISPECK, ISPECL. [2]

ISPECJ −1–sum spectral radii in J,K,L for dissipation scaling in J.
1–constant coefficient dissipation in J.
2–spectral radius in J for dissipation scaling in J.
3–weighted spectral radius in J (à la TLNS3D) for dissipation scaling in J. [ISPEC]

ISPECK −1–sum spectral radii in J,K,L for dissipation scaling in K.
1–constant coefficient dissipation in K.
2–spectral radius in K for dissipation scaling in K.
3–weighted spectral radius in K (à la TLNS3D) for dissipation scaling in K. [ISPEC]

ISPECL −1–sum spectral radii in J,K,L for dissipation scaling in L.
1–constant coefficient dissipation in L.
2–spectral radius in L for dissipation scaling in L.
3–weighted spectral radius in L (à la TLNS3D) for dissipation scaling in L. [ISPEC]

SMOO 0.0–spectral radius is computed normally, i.e. as $(|U| + kc)$, where $k = \sqrt{\xi_x^2 + \xi_y^2 + \xi_z^2}$, etc.
1.0–sound speed c is replaced by $\sqrt{\mathcal{V}^2/M_\infty^2}$ in spectral radius terms.
Intermediate values are allowed. [1.0]

DIS2 Single value to specify DIS2J, DIS2K, DIS2L. Does not override DIS2J, DIS2K, DIS2L. [2.0]

DIS2J 2nd-order smoothing coefficient in J (IDISS=2,3 only). [DIS2]

DIS2K 2nd-order smoothing coefficient in K (IDISS=2,3 only). [DIS2]

DIS2L 2nd-order smoothing coefficient in L (IDISS=2,3 only). [DIS2]

DIS4 Single value to specify DIS4J, DIS4K, DIS4L. Does not override DIS4J, DIS4K, DIS4L. [0.04]

DIS4J 4th-order smoothing coefficient in J (IDISS=2,3 only). [DIS4]

DIS4K 4th-order smoothing coefficient in K (IDISS=2,3 only). [DIS4]

DIS4L 4th-order smoothing coefficient in L (IDISS=2,3 only). [DIS4]

EPSE Central difference smoothing coefficient (IDISS=1 only). [0.05]

EPSSGS LU-SGS left-hand side spectral radius epsilon term (ILHS=3 only). [0.02]

DELTA Upwind scheme (MUSCL) limiter fix parameter (IRHS=3,4 only). [1.]
< 0.–Turn off limiter.
0.–Koren limiter.
1.–Koren limiter with CFL3D parameter $\epsilon = \delta \left(\frac{10}{JD-1}\right)^3$.
(Other values allowed.)

FSO 1.0–first-order for flux splitting/upwind options.
2.0–second-order.
3.0–third-order (currently implemented only for Roe and AUSM$^+$-ap upwinding).
4.0–fourth-order (implemented only for central differencing).
Intermediate values allowed. [2.0 for IRHS=0,2, 3.0 for IRHS=3,4]

VEPSL Matrix dissipation (minimum) limit on linear eigenvalues. [0.]

VEPSN Matrix dissipation (minimum) limit on nonlinear eigenvalues. [0.]

ROEAVG Matrix dissipation flag for using Roe averaging for half-grid point flow quantities. [FALSE]

$VISINP

VISC	TRUE–include all viscous terms including cross terms. This overrides VISCJ, VISCK, VISCL and VISCX. FALSE–include only specified or automatically enabled viscous terms. [FALSE]
VISCJ	TRUE–include viscous thin layer terms in J. FALSE–viscous terms in J enabled (only) if there are J-direction viscous walls. [FALSE]
VISCK	TRUE–include viscous thin layer terms in K. FALSE–viscous terms in K enabled (only) if there are K-direction viscous walls. [FALSE]
VISCL	TRUE–include viscous thin layer terms in L. FALSE–viscous terms in L enabled (only) if there are L-direction viscous walls. [FALSE]
VISCX	TRUE–include viscous cross terms between coordinate directions which have thin layer terms enabled. FALSE–no viscous cross terms. [FALSE]
NTURB	Number of turbulent wall regions to be specified (optional). [0]
ITTYP(region#)	Type of turbulent modeling (see Table 3.2).
ITDIR(region#)	Coordinate direction of turbulent model (away from wall or shear layer). 1, 2, 3, −1, −2, −3 represent J, K, L, −J, −K, −L, respectively.
JTLS(region#)	Starting J index.
JTLE(region#)	Ending J index.
KTLS(region#)	Starting K index.
KTLE(region#)	Ending K index.
LTLS(region#)	Starting L index.
LTLE(region#)	Ending L index.
TLPAR1(region#)	Turbulence model parameter (use depends on turbulence model type).
ITERT	Number of turbulence model (sub)iterations per flow solver iteration (ITER), or number of turbulence model (sub)iterations if ITER=0. [1]
ITLHIT	Number of subiterations for DDADI scheme. [1]
CFLT	Turbulence model timestep is CFLT times the flow solver timestep. [1.]

$BCINP

NBC	Number of boundary condition regions to be specified (optional). [0]
IBTYP(region#)	Type of boundary condition (see Table 3.3).
IBDIR(region#)	Coordinate direction of boundary condition (away from boundary surface). 1, 2, 3, −1, −2, −3 represent J, K, L, −J, −K, −L, respectively.
JBCS(region#)	Starting J index.
JBCE(region#)	Ending J index.
KBCS(region#)	Starting K index.
KBCE(region#)	Ending K index.
LBCS(region#)	Starting L index.
LBCE(region#)	Ending L index.
BCPAR1(region#)	Boundary condition parameter (use depends on boundary condition type).
BCFILE(region#)	Filename for reading boundary data (type 42).

$SCEINP

ITERC	Number of species continuity (sub)iterations per flow solver iteration (ITER), or number of species continuity (sub)iterations if ITER=0. [1]
CFLC	Species convection timestep is CFLC times the flow solver timestep. [1.]
IUPC	0–2nd-order central differencing for species continuity convection terms. 1–2nd-order upwind differencing for species continuity convection terms. [1]
DIS2C	2nd-order smoothing coefficient for species continuity ($IUPC = 0$ only). [2.0]
DIS4C	4th-order smoothing coefficient for species continuity ($IUPC = 0$ only). [0.04]

APPENDIX B. TURBULENCE REGION TYPES

Type	*Description*
1	Baldwin-Lomax boundary layer model (with variable Degani-Schiff cutoff)
11	Baldwin-Lomax shear layer model (with variable C_{wk})
102	1- or 2-equation laminar region (zero production)
103	Spalart-Allmaras boundary layer trip line

Type	*Description*
1	Inviscid adiabatic wall (pressure extrapolation)
2	Inviscid adiabatic wall (normal momentum eqn)
3	Inviscid constant temperature wall (pressure extrapolation)
4	Inviscid constant temperature wall (normal momentum eqn)
5	Viscous adiabatic wall (pressure extrapolation)
6	Viscous adiabatic wall (normal momentum eqn)
7	Viscous constant temperature wall (pressure extrapolation)
8	Viscous constant temperature wall (normal momentum eqn)
10	Periodic condition (apply to either 1 or last plane)
11	Symmetry in X (apply to 1 and/or last separately)
12	Symmetry in Y (apply to 1 and/or last separately)
13	Symmetry in Z (apply to 1 and/or last separately)
14	Axis (J around)
15	Axis (K around)
16	Axis (L around)
17	Symmetry with no reflection plane
18	Periodic flow/nonperiodic grid (apply to either 1 or last plane)
21	2D condition in Y (3 planes supplied, ± 1 in Y) (apply to 1 or last plane)
22	Axisymmetric condition in Y, rotate about X (3 planes supplied, $\pm 1^\circ$ rotation) (apply to 1 or last plane)
30	Outflow (extrapolation)
31	Characteristic condition based on Riemann invariants
32	Supersonic/subsonic inflow/outflow
33	Specified pressure outflow
35	Outflow (1st-order extrapolation)
40	Impose freestream
41	Nozzle inflow (p_0, T_0 constant, mass flow extrapolated)
42	Prescribed Q (read once from file)
43	Prescribed Q with slow-start (read from file)
44	Actuator disk (IDIR is flow direction)
45	Prescribed Q (read from file)/inflow-outflow condition
46	Prescribed Q with slow start (read from file)/inflow-outflow condition
47	Freestream/characteristic condition
48	Simple jet mass flow condition
49	Default (no change)

THIS PAGE INTENTIONALLY LEFT BLANK

APPENDIX C. GRID MESH OF COMBUSTORS

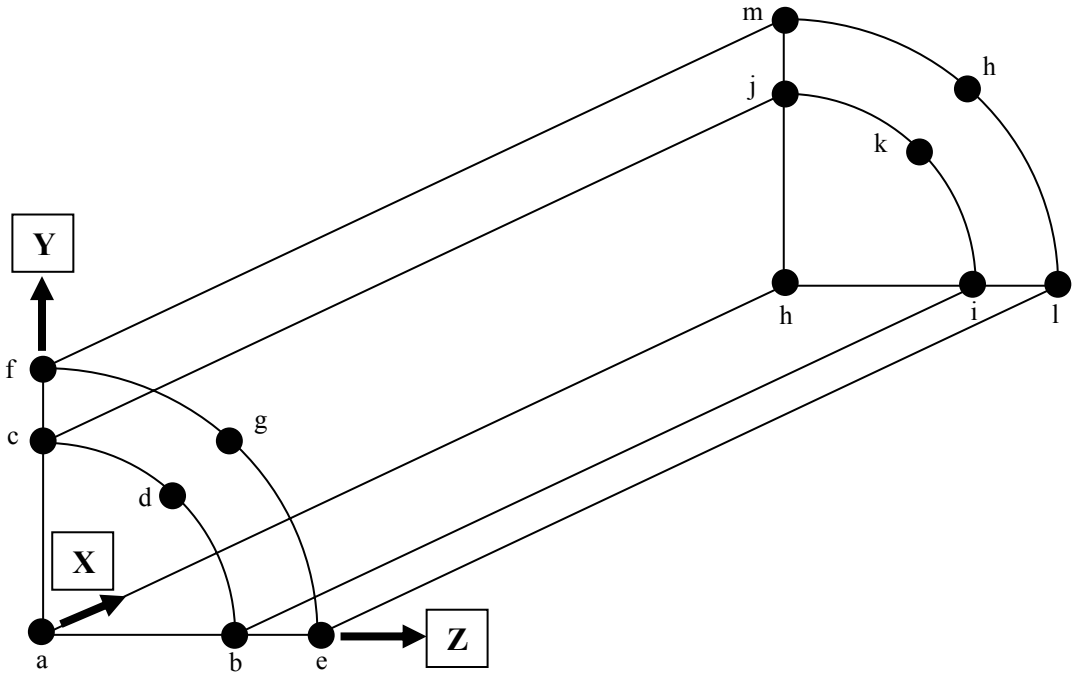

Figure 38. Grid Construction Model of Cylindrical Combustor.

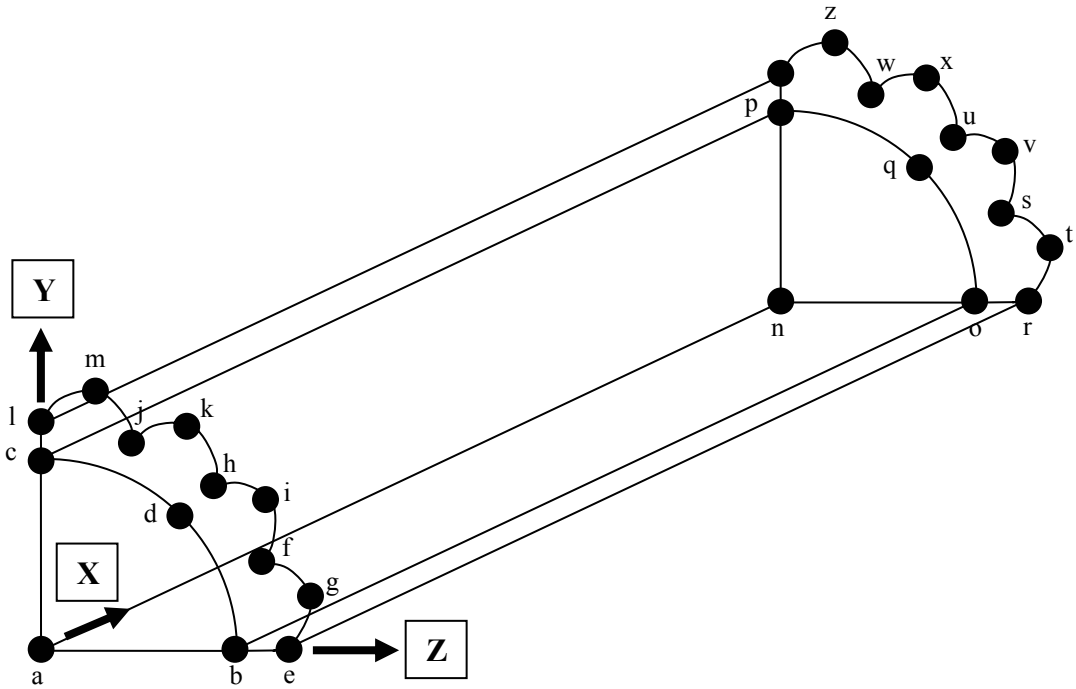

Figure 39. Grid Construction Model of Scallop Combustor.

Table 10. Coordinates of Grid Points of Combustors.

	a	b	c	d	e	f	g	h	i	j	k	l	m	n	o	p	q	r	s	t	u	v	w	x	y	z
2.25in Diameter Cylindrical Combustor																										
X	000000	000000	000000	000000	000000	000000	000000	1 foot	1 foot	1 foot	1 foot	1 foot	1 foot	1 foot	-	-	-	-	-	-	-	-	-	-	-	-
Y	000000	000000	078125	078125	000000	093750	093750	000000	000000	078125	078125	000000	093750	093750	-	-	-	-	-	-	-	-	-	-	-	-
Z	000000	078125	000000	078125	093750	000000	093750	000000	078125	000000	078125	093750	000000	093750	-	-	-	-	-	-	-	-	-	-	-	-
2.50in Diameter Cylindrical Combustor																										
X	000000	000000	000000	000000	000000	000000	000000	1 foot	1 foot	1 foot	1 foot	1 foot	1 foot	1 foot	-	-	-	-	-	-	-	-	-	-	-	-
Y	000000	000000	078125	078125	000000	104167	104167	000000	000000	078125	078125	000000	104167	104167	-	-	-	-	-	-	-	-	-	-	-	-
Z	000000	078125	000000	078125	104167	000000	104167	000000	078125	000000	078125	104167	000000	104167	-	-	-	-	-	-	-	-	-	-	-	-
2.75in Diameter Cylindrical Combustor																										
X	000000	000000	000000	000000	000000	000000	000000	1 foot	1 foot	1 foot	1 foot	1 foot	1 foot	1 foot	-	-	-	-	-	-	-	-	-	-	-	-
Y	000000	000000	078125	078125	000000	114583	114583	000000	000000	078125	078125	000000	114583	114583	-	-	-	-	-	-	-	-	-	-	-	-
Z	000000	078125	000000	078125	114583	000000	114583	000000	078125	000000	078125	114583	000000	114583	-	-	-	-	-	-	-	-	-	-	-	-
3.00in Diameter Cylindrical Combustor																										
X	000000	000000	000000	000000	000000	000000	000000	1 foot	1 foot	1 foot	1 foot	1 foot	1 foot	1 foot	-	-	-	-	-	-	-	-	-	-	-	-
Y	000000	000000	078125	078125	000000	125000	125000	000000	000000	078125	078125	000000	125000	125000	-	-	-	-	-	-	-	-	-	-	-	-
Z	000000	078125	000000	078125	125000	000000	125000	000000	078125	000000	078125	125000	000000	125000	-	-	-	-	-	-	-	-	-	-	-	-
2.25in Diameter Scallop Combustor																										
X	000000	000000	000000	000000	000000	000000	000000	000000	000000	000000	000000	000000	000000	1 foot	1 foot	1 foot	1 foot	1 foot	1 foot	1 foot	1 foot	1 foot	1 foot	1 foot	1 foot	1 foot
Y	000000	000000	078125	078125	000000	031000	018777	059000	055000	075000	082000	080453	094401	000000	000000	078125	078125	000000	031000	018777	059000	055000	075000	082000	080453	094401
Z	000000	078125	000000	078125	080453	075000	094401	059000	082000	031000	055000	000000	018777	000000	078125	000000	078125	080453	075000	094401	059000	082000	031000	055000	000000	018777
2.50in Diameter Scallop Combustor																										
X	000000	000000	000000	000000	000000	000000	000000	000000	000000	000000	000000	000000	000000	1 foot	1 foot	1 foot	1 foot	1 foot	1 foot	1 foot	1 foot	1 foot	1 foot	1 foot	1 foot	1 foot
Y	000000	000000	078125	078125	000000	034120	020810	066000	061000	082373	094000	089160	104617	000000	000000	078125	078125	000000	034120	020810	066000	061000	082373	094000	089160	104617
Z	000000	078125	000000	078125	089160	082373	104617	066000	094000	034120	061000	000000	020810	000000	078125	000000	078125	089160	082373	104617	066000	094000	034120	061000	000000	020810
2.75in Diameter Scallop Combustor																										
X	000000	000000	000000	000000	000000	000000	000000	000000	000000	000000	000000	000000	000000	1 foot	1 foot	1 foot	1 foot	1 foot	1 foot	1 foot	1 foot	1 foot	1 foot	1 foot	1 foot	1 foot
Y	000000	000000	078125	078125	000000	037452	022842	073000	070000	090418	120000	097867	114834	000000	000000	078125	078125	000000	037452	022842	073000	070000	090418	120000	097867	114834
Z	000000	078125	000000	078125	097867	090418	114834	073000	120000	037452	070000	000000	022842	000000	078125	000000	078125	097867	090418	114834	073000	120000	037452	070000	000000	022842
3.00in Diameter Scallop Combustor																										
X	000000	000000	000000	000000	000000	000000	000000	000000	000000	000000	000000	000000	000000	1 foot	1 foot	1 foot	1 foot	1 foot	1 foot	1 foot	1 foot	1 foot	1 foot	1 foot	1 foot	1 foot
Y	000000	000000	078125	078125	000000	040784	024874	080000	075000	098462	110000	106575	125050	000000	000000	078125	078125	000000	040784	024874	080000	075000	098462	110000	106575	125050
Z	000000	078125	000000	078125	106575	098462	125050	080000	110000	040784	075000	000000	024874	000000	078125	000000	078125	106575	098462	125050	080000	110000	040784	075000	000000	024874

Note:
All the above dimensions are in feet divided by 100,000 unless specified.

Table 11. Grid Mesh Construction of Cylindrical Combustors.

Face	Domain	Connector	Type of Segment	No. of Grid Points	Distribution Function	Distribution Factor 1, ΔS1	Distribution Factor 2, ΔS1
2.25in / 2.50in / 3.00in Diameter Cylindrical Combustor							
A	A	a-a	Line	81	Default	Default	Default
		a-b	Line	25	Hyperbolic Tangent	0.8E-2	0.1E-2
		a-c	Line	25	Hyperbolic Tangent	0.1E-2	0.1E-2
		b-c-d	General Conic Section	81	Default	Default	Default
	B	b-c-d	General Conic Section	81	Default	Default	Default
		b-e	Line	See Notes	Hyperbolic Tangent	0.1E-2	0.1E-2
		c-l	Line	See Notes	Hyperbolic Tangent	0.1E-2	0.1E-2
		e-f-g	General Conic Section	81	Default	Default	Default
B	C	h-h	Line	81	Default	Default	Default
		h-i	Line	25	Hyperbolic Tangent	0.8E-2	0.1E-2
		h-j	Line	25	Hyperbolic Tangent	0.1E-2	0.1E-2
		i-j-k	General Conic Section	81	Default	Default	Default
	D	i-j-k	General Conic Section	81	Default	Default	Default
		i-l	Line	See Notes	Hyperbolic Tangent	0.1E-2	0.1E-2
		j-m	Line	See Notes	Hyperbolic Tangent	0.1E-2	0.1E-2
		l-m-n	General Conic Section	81	Default	Default	Default
C	E	a-a	Line	81	Default	Default	Default
		h-h	Line	81	Default	Default	Default
		a-h	Line	121	Default	Default	Default
		a-h	Line	121	Default	Default	Default
D	F	a-b	Line	25	Hyperbolic Tangent	0.8E-2	0.1E-2
		h-i	Line	25	Hyperbolic Tangent	0.8E-2	0.1E-2
		a-h	Line	121	Default	Default	Default
		b-i	Line	121	Default	Default	Default
	G	b-e	Line	25	Hyperbolic Tangent	0.8E-2	0.1E-2
		i-l	Line	25	Hyperbolic Tangent	0.8E-2	0.1E-2
		b-i	Line	121	Default	Default	Default
		e-l	Line	121	Default	Default	Default
E	H	a-c	Line	25	Hyperbolic Tangent	0.8E-2	0.1E-2
		h-j	Line	25	Hyperbolic Tangent	0.8E-2	0.1E-2
		a-h	Line	121	Default	Default	Default
		c-j	Line	121	Default	Default	Default
	I	c-f	Line	25	Hyperbolic Tangent	0.8E-2	0.1E-2
		j-m	Line	25	Hyperbolic Tangent	0.8E-2	0.1E-2
		c-j	Line	121	Default	Default	Default
		f-m	Line	121	Default	Default	Default
F	J	e-f-g	General Conic Section	81	Default	Default	Default
		l-m-n	General Conic Section	81	Default	Default	Default
		e-l	Line	121	Default	Default	Default
		f-m	Line	121	Default	Default	Default

Notes:
No. of grid points for 2.25in diameter cylindrical combustor is 11.
No. of grid points for 2.50in diameter cylindrical combustor is 13.
No. of grid points for 2.75in diameter cylindrical combustor is 16.
No. of grid points for 3.00in diameter cylindrical combustor is 21.

Table 12. Grid Mesh Construction of Scallop Combustors.

Face	Domain	Connector	Type of Segment	No. of Grid Points	Distribution Function	Distribution Factor 1, ΔS1	Distribution Factor 2, ΔS1
2.25in / 2.50in / 3.00in Diameter Scallop Combustor							
A	A	a-a	Line	81	Default	Default	Default
		a-b	Line	25	Hyperbolic Tangent	0.8E-2	0.1E-2
		a-c	Line	25	Hyperbolic Tangent	0.1E-2	0.1E-2
		b-c-d	General Conic Section	81	Default	Default	Default
	B	b-c-d	General Conic Section	81	Default	Default	Default
		b-e	Line	See Notes	Hyperbolic Tangent	0.1E-2	0.1E-2
		c-l	Line	See Notes	Hyperbolic Tangent	0.1E-2	0.1E-2
		e-f-g	3 Point Circular Arc	21	Default	Default	Default
		f-h-i	3 Point Circular Arc	21	Default	Default	Default
		h-j-k	3 Point Circular Arc	21	Default	Default	Default
		j-l-m	3 Point Circular Arc	21	Default	Default	Default
B	C	n-n	Line	81	Default	Default	Default
		n-o	Line	25	Hyperbolic Tangent	0.8E-2	0.1E-2
		n-p	Line	25	Hyperbolic Tangent	0.1E-2	0.1E-2
		o-p-q	General Conic Section	81	Default	Default	Default
	D	o-p-q	General Conic Section	81	Default	Default	Default
		o-r	Line	See Notes	Hyperbolic Tangent	0.1E-2	0.1E-2
		p-y	Line	See Notes	Hyperbolic Tangent	0.1E-2	0.1E-2
		r-s-t	3 Point Circular Arc	21	Default	Default	Default
		s-u-v	3 Point Circular Arc	21	Default	Default	Default
		u-w-x	3 Point Circular Arc	21	Default	Default	Default
		w-y-z	3 Point Circular Arc	21	Default	Default	Default
C	E	a-a	Line	81	Default	Default	Default
		n-n	Line	81	Default	Default	Default
		a-n	Line	121	Default	Default	Default
		a-n	Line	121	Default	Default	Default
D	F	a-b	Line	25	Hyperbolic Tangent	0.8E-2	0.1E-2
		n-o	Line	25	Hyperbolic Tangent	0.8E-2	0.1E-2
		a-n	Line	121	Default	Default	Default
		b-o	Line	121	Default	Default	Default
	G	b-e	Line	See Notes	Hyperbolic Tangent	0.8E-2	0.1E-2
		o-r	Line	See Notes	Hyperbolic Tangent	0.8E-2	0.1E-2
		b-o	Line	121	Default	Default	Default
		e-o	Line	121	Default	Default	Default
E	H	a-c	Line	25	Hyperbolic Tangent	0.8E-2	0.1E-2
		n-p	Line	25	Hyperbolic Tangent	0.8E-2	0.1E-2
		a-n	Line	121	Default	Default	Default
		c-p	Line	121	Default	Default	Default
	I	c-l	Line	See Notes	Hyperbolic Tangent	0.8E-2	0.1E-2
		p-y	Line	See Notes	Hyperbolic Tangent	0.8E-2	0.1E-2
		c-p	Line	121	Default	Default	Default
		l-y	Line	121	Default	Default	Default
F	J	e-f-g	3 Point Circular Arc	21	Default	Default	Default
		f-h-i	3 Point Circular Arc	21	Default	Default	Default
		h-j-k	3 Point Circular Arc	21	Default	Default	Default
		j-l-m	3 Point Circular Arc	21	Default	Default	Default
		r-s-t	3 Point Circular Arc	21	Default	Default	Default
		s-u-v	3 Point Circular Arc	21	Default	Default	Default
		u-w-x	3 Point Circular Arc	21	Default	Default	Default
		w-y-z	3 Point Circular Arc	21	Default	Default	Default
		e-r	Line	121	Default	Default	Default
		l-y	Line	121	Default	Default	Default

Notes:
No. of grid points for 2.25in diameter scallop combustor is 11.
No. of grid points for 2.50in diameter scallop combustor is 13.
No. of grid points for 2.75in diameter scallop combustor is 16.
No. of grid points for 3.00in diameter scallop combustor is 21.

APPENDIX D. BOUNDARY CONDITIONS OF COMBUSTORS.

Table 13. Boundary Conditions of Cylindrical and Scallop Combustors

No.	Location	Boundary Condition Type	Boundary Condition Coordinate Direction	Starting J Index	Ending J Index	Starting K Index	Ending K Index	Starting L Index	Ending L Index
1	Core Axis	Axis, L Around (16)	Positive K (2)	1 (1)	121 (-1)	1 (1)	1 (1)	1 (1)	83* (-1)
2	Initiator Front Plane Wall	Inviscid Adiabatic Wall, Pressure Extrapolation (1)	Positive J (1)	1 (1)	1 (1)	1 (1)	25 (25)	1 (1)	83* (-1)
3	Combustor Front Plane	Outflow, Extrapolation (30)	Positive J (1)	1 (1)	1 (1)	26 (26)	See Notes (-1)	1 (1)	83* (-1)
4	Combustor Horizontal Plane	Symmetry in Z (13)	Positive L (3)	1 (1)	121 (-1)	1 (1)	See Notes (-1)	1 (1)	1 (-1)
5	Combustor Vertical Plane	Symmetry in Y (12)	Negative L (-3)	1 (1)	121 (-1)	1 (1)	See Notes (-1)	1 (1)	1 (1)
6	Combustor Rear Plane	Outflow, Extrapolation (30)	Positive J (-1)	121 (-1)	121 (-1)	1 (1)	See Notes (-1)	1 (1)	83* (-1)
7	Combustor Inner Diameter Wall	Viscous Adiabatic Wall, Pressure Extrapolation (5)	Negative K (-2)	1 (1)	121 (-1)	See Notes (-1)	See Notes (-1)	1 (1)	83 (-1)
8	Initiator Inner Diameter Wall	Viscous Adiabatic Wall, Pressure Extrapolation (5)	Negative K (-2)	1 (1)	60 (60)	25 (25)	25 (25)	1 (1)	83 (-1)
9	Initiator Outer Diameter Wall	Viscous Adiabatic Wall, Pressure Extrapolation (5)	Positive K (2)	1 (1)	60 (60)	26 (26)	26 (26)	1 (1)	83 (-1)

Notes:
The ending K index for 2.25in diameter cylindrical and scallop combustors is 35.
The ending K index for 2.50in diameter cylindrical and scallop combustors is 37.
The ending K index for 2.75in diameter cylindrical and scallop combustors is 45.
The ending K index for 2.25in diameter cylindrical and scallop combustors is 50.

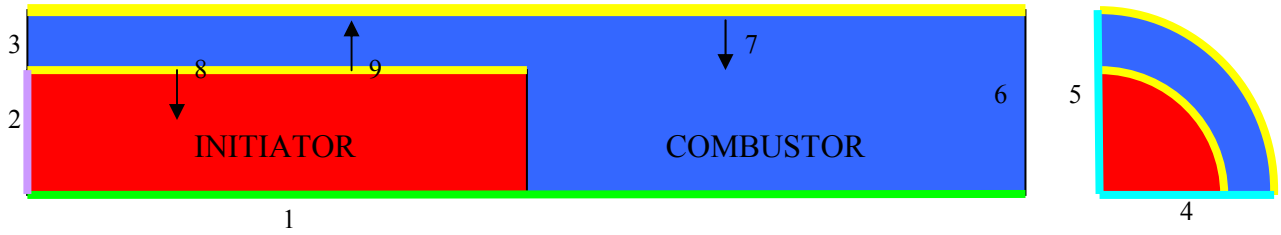

Figure 40. Boundary Conditions of Combustors.

THIS PAGE INTENTIONALLY LEFT BLANK

APPENDIX E. PROCEDURES OF CONVERTING GRID.GRD TO GRID.IN. USING GRIDED.

```
************************************************************
              GRIDED version 3.0d
************************************************************


 Compile time: Fri Mar 26 11:23:07 PST 1999
 Makefile flag: sgi

Enter input PLOT3D grid filename:  grid..grd

 Enter itin (input file type) and itout (output file type)
 1 = 3D unformatted whole,  2 = 3D formatted whole
 3 = 3D unformatted plane,  4 = 3D formatted plane
 5 = 2D unformatted,        6 = 2D formatted
 > 2,1

 Iblanks not detected in grid file.
Current grid dimensions

   N   JMAX   KMAX   LMAX
   1    121     81     37

 Enter operation on multiple grid file from following:

  0 = Exit from this menu and program
  1 = Go to single grid menu
  2 = Append grids by reading new grid file
  3 = Remove grids from current list
  4 = Substitute a grid by reading new single grid
  5 = Add/remove iblanks for all grids
  6 = Swap grid numbers of two grids
  7 = Rearrange sequence of all grids
  9 = Write selected grids to file
1
 Enter number of grids to perform operations on (0 = all)
0
 Enter iop from the following menu

 Operations that do not change the grid dimensions
 -------------------------------------------------
 1 = Exit from this menu and program
 2 = Interchange J and K grid families
 3 = Interchange K and L grid families
 4 = Interchange J and L grid families
 5 = Reverse index direction in J and/or K and/or L
 6 = Scale followed by translate
 7 = Mirror about x=0, y=0 or z=0 plane
 8 = Rotate about x, y, z or any arbitrary axis
 9 = Reset axis/periodic/C-cut/constant-plane bnd. pts.

 Operations that change the grid dimensions
 ------------------------------------------
 11 = Extract a subset
 12 = Add extra planes in J, K or L by extrapolation
 13 = Add extra planes in J or K by reflected symmetry
 14 = Add extra planes to 2D grid to form 3D grid for
     '2D' or 'axisymmetric' option in OVERFLOW
 15 = Duplicate and mirror reflected symmetry grid to form periodic grid in K
 20 = Concatenate another grid to current grid
 21 = Split a grid into 2 grids in J, K, or L direction
 22 = Create a new grid by duplicating a grid -
     further ops will be performed on duplicated grid
 99 = Go to multiple grid menu
 > 5

 Enter jrev,krev,lrev (0=not reverse, 1=reverse)
 > 1,0,0
 WARNING: Options 2,3,4,5a,5b,5c,7 have been performed an odd number of times.
 Grid indices have changed from right-handed to left-handed or vice versa.

Do you wish to perform further operations (1=yes,0=no) > 1
 Enter iop from the following menu

 Operations that do not change the grid dimensions
 -------------------------------------------------
 1 = Exit from this menu and program
 2 = Interchange J and K grid families
 3 = Interchange K and L grid families
 4 = Interchange J and L grid families
 5 = Reverse index direction in J and/or K and/or L
 6 = Scale followed by translate
 7 = Mirror about x=0, y=0 or z=0 plane
 8 = Rotate about x, y, z or any arbitrary axis
 9 = Reset axis/periodic/C-cut/constant-plane bnd. pts.

 Operations that change the grid dimensions
 ------------------------------------------
 11 = Extract a subset
 12 = Add extra planes in J, K or L by extrapolation
 13 = Add extra planes in J or K by reflected symmetry
 14 = Add extra planes to 2D grid to form 3D grid for
     '2D' or 'axisymmetric' option in OVERFLOW
 15 = Duplicate and mirror reflected symmetry grid to form periodic grid in K
 20 = Concatenate another grid to current grid
 21 = Split a grid into 2 grids in J, K, or L direction
 22 = Create a new grid by duplicating a grid -
     further ops will be performed on duplicated grid
 99 = Go to multiple grid menu
 > 2


Do you wish to perform further operations (1=yes,0=no) > 1
 Enter iop from the following menu

 Operations that do not change the grid dimensions
 -------------------------------------------------
 1 = Exit from this menu and program
 2 = Interchange J and K grid families
 3 = Interchange K and L grid families
 4 = Interchange J and L grid families
 5 = Reverse index direction in J and/or K and/or L
 6 = Scale followed by translate
 7 = Mirror about x=0, y=0 or z=0 plane
 8 = Rotate about x, y, z or any arbitrary axis
 9 = Reset axis/periodic/C-cut/constant-plane bnd. pts.

 Operations that change the grid dimensions
 ------------------------------------------
 11 = Extract a subset
 12 = Add extra planes in J, K or L by extrapolation
 13 = Add extra planes in J or K by reflected symmetry
 14 = Add extra planes to 2D grid to form 3D grid for
     '2D' or 'axisymmetric' option in OVERFLOW
 15 = Duplicate and mirror reflected symmetry grid to form periodic grid in K
 20 = Concatenate another grid to current grid
 21 = Split a grid into 2 grids in J, K, or L direction
 22 = Create a new grid by duplicating a grid -
     further ops will be performed on duplicated grid
 99 = Go to multiple grid menu
 > 13

 Enter jsyma,jsymb,ksyma,ksymb (0=no change, 1=add)
 > 1,0,0,0
 Enter isymm (1=x,2=y,3=z)
 > 3

Do you wish to perform further operations (1=yes,0=no) > 1
 Enter iop from the following menu

 Operations that do not change the grid dimensions
 -------------------------------------------------
 1 = Exit from this menu and program
 2 = Interchange J and K grid families
 3 = Interchange K and L grid families
 4 = Interchange J and L grid families
 5 = Reverse index direction in J and/or K and/or L
 6 = Scale followed by translate
 7 = Mirror about x=0, y=0 or z=0 plane
 8 = Rotate about x, y, z or any arbitrary axis
 9 = Reset axis/periodic/C-cut/constant-plane bnd. pts.

 Operations that change the grid dimensions
 ------------------------------------------
 11 = Extract a subset
 12 = Add extra planes in J, K or L by extrapolation
 13 = Add extra planes in J or K by reflected symmetry
 14 = Add extra planes to 2D grid to form 3D grid for
     '2D' or 'axisymmetric' option in OVERFLOW
 15 = Duplicate and mirror reflected symmetry grid to form periodic grid in K
 20 = Concatenate another grid to current grid
 21 = Split a grid into 2 grids in J, K, or L direction
 22 = Create a new grid by duplicating a grid -
     further ops will be performed on duplicated grid
 99 = Go to multiple grid menu
 > 5
```

```
Enter jrev,krev,lrev (0=not reverse, 1=reverse)
 > 1,0,0
 WARNING: Options 2,3,4,5a,5b,5c,7 have been performed an odd number of times.
 Grid indices have changed from right-handed to left-handed or vice versa.

Do you wish to perform further operations (1=yes,0=no) > 1
 Enter iop from the following menu

 Operations that do not change the grid dimensions
 -------------------------------------------------
 1 = Exit from this menu and program
 2 = Interchange J and K grid families
 3 = Interchange K and L grid families
 4 = Interchange J and L grid families
 5 = Reverse index direction in J and/or K and/or L
 6 = Scale followed by translate
 7 = Mirror about x=0, y=0 or z=0 plane
 8 = Rotate about x, y, z or any arbitrary axis
 9 = Reset axis/periodic/C-cut/constant-plane bnd. pts.

 Operations that change the grid dimensions
 ------------------------------------------
 11 = Extract a subset
 12 = Add extra planes in J, K or L by extrapolation
 13 = Add extra planes in J or K by reflected symmetry
 14 = Add extra planes to 2D grid to form 3D grid for
     '2D' or 'axisymmetric' option in OVERFLOW
 15 = Duplicate and mirror reflected symmetry grid to form periodic grid in K
 20 = Concatenate another grid to current grid
 21 = Split a grid into 2 grids in J, K, or L direction
 22 = Create a new grid by duplicating a grid -
      further ops will be performed on duplicated grid
 99 = Go to multiple grid menu
 > 13

 Enter jsyma,jsymb,ksyma,ksymb (0=no change, 1=add)
 > 1,0,0,0
 Enter isymm (1=x,2=y,3=z)
 > 2
 WARNING: Options 2,3,4,5a,5b,5c,7 have been performed an odd number of times.
 Grid indices have changed from right-handed to left-handed or vice versa.

Do you wish to perform further operations (1=yes,0=no) > 1
 Enter iop from the following menu

 Operations that do not change the grid dimensions
 -------------------------------------------------
 1 = Exit from this menu and program
 2 = Interchange J and K grid families
 3 = Interchange K and L grid families
 4 = Interchange J and L grid families
 5 = Reverse index direction in J and/or K and/or L
 6 = Scale followed by translate
 7 = Mirror about x=0, y=0 or z=0 plane
 8 = Rotate about x, y, z or any arbitrary axis
 9 = Reset axis/periodic/C-cut/constant-plane bnd. pts.

 Operations that change the grid dimensions
 ------------------------------------------
 11 = Extract a subset
 12 = Add extra planes in J, K or L by extrapolation
 13 = Add extra planes in J or K by reflected symmetry
 14 = Add extra planes to 2D grid to form 3D grid for
     '2D' or 'axisymmetric' option in OVERFLOW
 15 = Duplicate and mirror reflected symmetry grid to form periodic grid in K
 20 = Concatenate another grid to current grid
 21 = Split a grid into 2 grids in J, K, or L direction
 22 = Create a new grid by duplicating a grid -
      further ops will be performed on duplicated grid
 99 = Go to multiple grid menu
 > 5

 Enter jrev,krev,lrev (0=not reverse, 1=reverse)
 > 1,0,0
```

```
Do you wish to perform further operations (1=yes,0=no) > 1
 Enter iop from the following menu

Operations that do not change the grid dimensions
 -------------------------------------------------
 1 = Exit from this menu and program
 2 = Interchange J and K grid families
 3 = Interchange K and L grid families
 4 = Interchange J and L grid families
 5 = Reverse index direction in J and/or K and/or L
 6 = Scale followed by translate
 7 = Mirror about x=0, y=0 or z=0 plane
 8 = Rotate about x, y, z or any arbitrary axis
 9 = Reset axis/periodic/C-cut/constant-plane bnd. pts.

Operations that change the grid dimensions
 ------------------------------------------
 11 = Extract a subset
 12 = Add extra planes in J, K or L by extrapolation
 13 = Add extra planes in J or K by reflected symmetry
 14 = Add extra planes to 2D grid to form 3D grid for
     '2D' or 'axisymmetric' option in OVERFLOW
 15 = Duplicate and mirror reflected symmetry grid to form periodic grid in K
 20 = Concatenate another grid to current grid
 21 = Split a grid into 2 grids in J, K, or L direction
 22 = Create a new grid by duplicating a grid -
      further ops will be performed on duplicated grid
 99 = Go to multiple grid menu
 > 2

 WARNING: Options 2,3,4,5a,5b,5c,7 have been performed an odd number of times.
 Grid indices have changed from right-handed to left-handed or vice versa.

Do you wish to perform further operations (1=yes,0=no) > 1
 Enter iop from the following menu

 Operations that do not change the grid dimensions
 -------------------------------------------------
 1 = Exit from this menu and program
 2 = Interchange J and K grid families
 3 = Interchange K and L grid families
 4 = Interchange J and L grid families
 5 = Reverse index direction in J and/or K and/or L
 6 = Scale followed by translate
 7 = Mirror about x=0, y=0 or z=0 plane
 8 = Rotate about x, y, z or any arbitrary axis
 9 = Reset axis/periodic/C-cut/constant-plane bnd. pts.

 Operations that change the grid dimensions
 ------------------------------------------
 11 = Extract a subset
 12 = Add extra planes in J, K or L by extrapolation
 13 = Add extra planes in J or K by reflected symmetry
 14 = Add extra planes to 2D grid to form 3D grid for
     '2D' or 'axisymmetric' option in OVERFLOW
 15 = Duplicate and mirror reflected symmetry grid to form periodic grid in K
 20 = Concatenate another grid to current grid
 21 = Split a grid into 2 grids in J, K, or L direction
 22 = Create a new grid by duplicating a grid -
      further ops will be performed on duplicated grid
 99 = Go to multiple grid menu
 > 3


Do you wish to perform further operations (1=yes,0=no) > 0

Enter output PLOT3D grid filename:  grid.in
 Enter 0/1 for single/multiple grid format
0
Output grid dimensions

   N   JMAX   KMAX   LMAX
   1    121     37     83
```

APPENDIX F. OVERFLOW INPUT/OUTPUT FILES.

CENTRAL.1.BATCH

```
f77 -o2 -o makeq makeq.f

makeq

mv q.save q.restart

/export/aahome/garth/overflow1.8w.dir/over1.8w/overflow < central.1.inp > central.1.out
mv q.save q.restart
cp q.restart q.save.10a

/export/aahome/garth/overflow1.8w.dir/over1.8w/overflow < central.3.inp > central.3.out
mv q.save q.restart
cp q.restart q.save.10

/export/aahome/garth/overflow1.8w.dir/over1.8w/overflow < central.3.inp > central.3.out
mv q.save q.restart
cp q.restart q.save.20

/export/aahome/garth/overflow1.8w.dir/over1.8w/overflow < central.3.inp > central.3.out
mv q.save q.restart
cp q.restart q.save.30

/export/aahome/garth/overflow1.8w.dir/over1.8w/overflow < central.3.inp > central.3.out
mv q.save q.restart
cp q.restart q.save.40

/export/aahome/garth/overflow1.8w.dir/over1.8w/overflow < central.3.inp > central.3.out
mv q.save q.restart
cp q.restart q.save.50

/export/aahome/garth/overflow1.8w.dir/over1.8w/overflow < central.3.inp > central.3.out
mv q.save q.restart
cp q.restart q.save.60

/export/aahome/garth/overflow1.8w.dir/over1.8w/overflow < central.3.inp > central.3.out
mv q.save q.restart
cp q.restart q.save.70

/export/aahome/garth/overflow1.8w.dir/over1.8w/overflow < central.3.inp > central.3.out
mv q.save q.restart
cp q.restart q.save.80

/export/aahome/garth/overflow1.8w.dir/over1.8w/overflow < central.3.inp > central.3.out
mv q.save q.restart
cp q.restart q.save.90

/export/aahome/garth/overflow1.8w.dir/over1.8w/overflow < central.3.inp > central.3.out
mv q.save q.restart
cp q.restart q.save.100

/export/aahome/garth/overflow1.8w.dir/over1.8w/overflow < central.2.inp > central.2.out
mv q.save q.restart
cp q.restart q.save.101

/export/aahome/garth/overflow1.8w.dir/over1.8w/overflow < central.2.inp > central.2.out
mv q.save q.restart
cp q.restart q.save.102

/export/aahome/garth/overflow1.8w.dir/over1.8w/overflow < central.2.inp > central.2.out
mv q.save q.restart
cp q.restart q.save.103

/export/aahome/garth/overflow1.8w.dir/over1.8w/overflow < central.2.inp > central.2.out
```

```
mv q.save q.restart
cp q.restart q.save.104

/export/aahome/garth/overflow1.8w.dir/over1.8w/overflow < central.2.inp > central.2.out
mv q.save q.restart
cp q.restart q.save.105

/export/aahome/garth/overflow1.8w.dir/over1.8w/overflow < central.2.inp > central.2.out
mv q.save q.restart
cp q.restart q.save.106

/export/aahome/garth/overflow1.8w.dir/over1.8w/overflow < central.2.inp > central.2.out
mv q.save q.restart
cp q.restart q.save.107

/export/aahome/garth/overflow1.8w.dir/over1.8w/overflow < central.2.inp > central.2.out
mv q.save q.restart
cp q.restart q.save.108

/export/aahome/garth/overflow1.8w.dir/over1.8w/overflow < central.2.inp > central.2.out
mv q.save q.restart
cp q.restart q.save.109

/export/aahome/garth/overflow1.8w.dir/over1.8w/overflow < central.2.inp > central.2.out
mv q.save q.restart
cp q.restart q.save.110

/export/aahome/garth/overflow1.8w.dir/over1.8w/overflow < central.2.inp > central.2.out
mv q.save q.restart
cp q.restart q.save.111

/export/aahome/garth/overflow1.8w.dir/over1.8w/overflow < central.2.inp > central.2.out
mv q.save q.restart
cp q.restart q.save.112

/export/aahome/garth/overflow1.8w.dir/over1.8w/overflow < central.2.inp > central.2.out
mv q.save q.restart
cp q.restart q.save.113

/export/aahome/garth/overflow1.8w.dir/over1.8w/overflow < central.2.inp > central.2.out
mv q.save q.restart
cp q.restart q.save.XXX
```

MAKEQ.F

```
      PARAMETER ( jdim=121,kdim=42,ldim=83 )
C
C
      real q(jdim,kdim,ldim,6)
      real dum(10)
C
C
      gamma    = 1.4
C
C
       do 10 j=1,jdim
       do 10 k=1,kdim
       do 10 l=1,ldim
              if(j .le. 30*jdim/121 .and. k .le. 25*kdim/42) then
                rinf = 6.0
         pinf = 20.0
                u    = 0.0
                v    = 0.0
                w    = 0.0
              else
                rinf = 1.0
                pinf = 1.0
                u    = 0.0
                v    = 0.0
                w    = 0.0
              endif
          q(j,k,l,1)  = rinf
          q(j,k,l,2)  = rinf*u
          q(j,k,l,3)  = rinf*v
          q(j,k,l,4)  = rinf*w
          q(j,k,l,5)  = pinf/gamma/(gamma-1.0)+0.5*( q(j,k,l,2)**2+
     &                q(j,k,l,3)**2+q(j,k,l,4)**2 )/q(j,k,l,1)
          q(j,k,l,6)  = gamma
 10    continue
c
       jmax = jdim
       kmax = kdim
       lmax = ldim
       open(unit=3,file='q.save',form='unformatted')
       write(3) jmax,kmax,lmax,6,0
       write(3) (dum(n),n=1,10)
       write(3) ((((q(j,k,l,n),j=1,jmax),k=1,kmax),l=1,lmax),n=1,6)
       close(3)
100   continue
c
      stop
      end
```

CENTRAL.1.INP

```
$GLOBAL
   NSTEPS = 10,  RESTRT = .T., NSAVE = 10, NITNWT = 10,
   $END
$FLOINP
   FSMACH = 0.5, REY = 9.E6, TINF= 460.0,
   $END
$VARGAM $END

$GRDNAM
   NAME = 'Sod shock tube grid',
   $END
$NITERS $END
$METPRM
   IDISS = 4,
   $END
$TIMACU
   ITIME = 0,  DT = 0.0001,
   $END
$SMOACU $END
$VISINP
   VISCK = .T., VISCJ = .T.,
   $END
$BCINP
   NBC = 9
   IBTYP = 16,  1, 30, 13, 12, 30,  5,  5,  5,
   IBDIR =  2,  1,  1,  3, -3, -1, -2, -2,  2,
   JBCS  =  1,  1,  1,  1,  1, -1,  1,  1,  1,
   JBCE  = -1,  1,  1, -1, -1, -1, -1, 60, 60,
   KBCS  =  1,  1, 26,  1,  1,  1, -1, 25, 26,
   KBCE  =  1, 25, -1, -1, -1, -1, -1, 25, 26,
   LBCS  =  1,  1,  1,  1, -1,  1,  1,  1,  1,
   LBCE  = -1, -1, -1,  1, -1, -1, -1, -1, -1,
   $END
$SCEINP $END
```

CENTRAL.2.INP

```
$GLOBAL
   NSTEPS = 1,  RESTRT = .T., NSAVE = 1, NITNWT = 10,
   $END
$FLOINP
   FSMACH = 0.5, REY = 9.E6, TINF= 460.0,
   $END
$VARGAM $END

$GRDNAM
   NAME = 'Sod shock tube grid',
   $END
$NITERS $END
$METPRM
   IDISS = 4,
   $END
$TIMACU
   ITIME = 0,  DT = 0.001,
   $END
$SMOACU $END
$VISINP
   VISCK = .T., VISCJ = .T.,
   $END
$BCINP
   NBC = 9
   IBTYP = 16,  1, 30, 13, 12, 30,  5,  5,  5,
   IBDIR =  2,  1,  1,  3, -3, -1, -2, -2,  2,
   JBCS  =  1,  1,  1,  1,  1, -1,  1,  1,  1,
   JBCE  = -1,  1,  1, -1, -1, -1, -1, 60, 60,
   KBCS  =  1,  1, 26,  1,  1,  1, -1, 25, 26,
   KBCE  =  1, 25, -1, -1, -1, -1, -1, 25, 26,
   LBCS  =  1,  1,  1,  1, -1,  1,  1,  1,  1,
   LBCE  = -1, -1, -1,  1, -1, -1, -1, -1, -1,
   $END
$SCEINP $END
```

CENTRAL.3.INP

```
$GLOBAL
   NSTEPS = 10,  RESTRT = .T., NSAVE = 1, NITNWT = 10,
   $END
$FLOINP
   FSMACH = 0.5, REY = 9.E6, TINF= 460.0,
   $END
$VARGAM $END

$GRDNAM
   NAME = 'Sod shock tube grid',
   $END
$NITERS $END
$METPRM
   IDISS = 4,
   $END
$TIMACU
   ITIME = 0,  DT = 0.001,
   $END
$SMOACU $END
$VISINP
   VISCK = .T., VISCJ = .T.,
   $END
$BCINP
   NBC = 9
   IBTYP = 16,  1, 30, 13, 12, 30,  5,  5,  5,
   IBDIR =  2,  1,  1,  3, -3, -1, -2, -2,  2,
   JBCS  =  1,  1,  1,  1,  1, -1,  1,  1,  1,
   JBCE  = -1,  1,  1, -1, -1, -1, -1, 60, 60,
   KBCS  =  1,  1, 26,  1,  1,  1, -1, 25, 26,
   KBCE  =  1, 25, -1, -1, -1, -1, -1, 25, 26,
   LBCS  =  1,  1,  1,  1, -1,  1,  1,  1,  1,
   LBCE  = -1, -1, -1,  1, -1, -1, -1, -1, -1,
   $END
$SCEINP $END
```

PEXT1.F

```
C
C   Extract x vs. Cp from PLOT3D grid and Q files, and write out in
C   XYPLOT format.
C   SET FOR MULTI GRIDS
C
      PARAMETER (MI=201,MJ=80,MK=123,MG=1)
      DIMENSION XYZ(MI,MJ,MK,3),Q(MI,MJ,MK,5),ibl(mi,mj,mk)
      DIMENSION JKL(MG,3)
      CHARACTER*80 FILEX, FILEQ, FILEO
      dimension xp(5*MI),pp(5*MI)
C
      DATA GAMMA/1.4/
      data xscale/1.0/
C
      pi     = 4.0*atan( 1.0 )
C
C   Get x and q files.
C
      WRITE(*,1)
    1 FORMAT(' Enter PLOT3D grid filename:  ',$)
      READ(*,2) FILEX
    2 FORMAT(A)
      OPEN(UNIT=1,FILE=FILEX,STATUS='OLD',FORM='UNFORMATTED')
      WRITE(*,4)
    4 FORMAT(' Enter PLOT3D    Q filename:  ',$)
      READ(*,2) FILEQ
      OPEN(UNIT=2,FILE=FILEQ,STATUS='OLD',FORM='UNFORMATTED')
C
C   Get range of (i,j,k) for each grid.
C
      write(*,12)
   12 format(' Enter number of cuts ',$)
      read(*,*) ncuts
      do 1000 nc=1,ncuts
        WRITE(*,14)
   14   FORMAT(' Enter XYPLOT   Cp filename:  ',$)
        READ(*,2) FILEO
              print *,'output file = ',FILEO
        OPEN(UNIT=3,FILE=FILEO,STATUS='UNKNOWN',FORM='FORMATTED')
        write(*,13)
   13   format(' Enter number of grids that are in this cut ',$)
        read(*,*) ncg
              ii    = 0
        do 500 nn = 1,ncg
          WRITE(*,11)
   11     FORMAT(' Enter  grid,IS,IE, JS,JE, KS,KE:  ',$)
        READ(*,*) NG,IS,IE,JS,JE,KS,KE
C
C   Read q and grid file.
C
        NGRIDS = 1
CRWT          READ(1) NGRIDS
        READ(1) (JKL(N,1),JKL(N,2),JKL(N,3),N=1,NGRIDS)
CRWT          READ(2) NGRIDS
        READ(2) (JKL(N,1),JKL(N,2),JKL(N,3),N=1,NGRIDS)
        do 400 na=1,ngrids
          if( na.eq.ng ) then
            print *,'na,ng ',na,ng
            NI    = JKL(na,1)
            NJ    = JKL(na,2)
            NK    = JKL(na,3)
            IF (NI.GT.MI .OR. NJ.GT.MJ .OR. NK.GT.MK) THEN
              WRITE(*,3)
    3         FORMAT('Grid is too big, exceeds internal dimensions.')
              GOTO 100
            ENDIF
            READ(1) ((((XYZ(I,J,K,NX),I=1,NI),J=1,NJ),K=1,NK),NX=1,3)
            READ(2) FSMACH,ALPHA,RE,TIME
```

```
          print *,' MACH NUMBER IS ',fsmach
          print *,' TIME IS ',time
          READ(2) ((((Q(I,J,K,NX),I=1,NI),J=1,NJ),K=1,NK),NX=1,5)
C
C   Compute and write out x vs. Cp.
C
          GM1    = GAMMA-1.
          RHOINF = 1.
          CINF   = 1.
          PINF   = 1./GAMMA
          V2INF  = 0.5*(FSMACH/CINF)**2
          QINF   = RHOINF*V2INF
                 CN     = 0.0
c
          DO 20 K = KS,KE
          DO 20 J = JS,JE
          DO 20 I = IS,IE
                   ii    = ii+1
            RHO    = Q(I,J,K,1)
            U      = Q(I,J,K,2)/RHO
            V      = Q(I,J,K,3)/RHO
            W      = Q(I,J,K,4)/RHO
            E0     = Q(I,J,K,5)/RHO
            V2     = 0.5*(U**2 + V**2 + W**2)
            EI     = E0 - V2
            P      = GM1*RHO*EI
            X      = XYZ(I,J,K,1)/xscale
                           T              = P/(RHO)

            xp(ii) = x
            pp(ii) = p
                           write(3,*)x,rho,u,p,T
                           imax   = ii
c
  20       CONTINUE
          else
            read(1)
            read(2)
            read(2)
          endif
  400    continue
         rewind(1)
         rewind(2)
  500  continue
C
 1000 CONTINUE
C     do 999 ii = 1,imax
C               write(3,*) xp(ii),pp(ii)
C               print *,'ii,xp,pp ',ii,xp(ii),pp(ii)
C999  continue
       CLOSE(UNIT=3)
C
  100 CONTINUE
      STOP
      END
```

CENTRAL.OUT

```
      OVERFLOW  --  OVERLAPPED GRID FLOW SOLVER
         VERSION 1.8w   12 December 2002

   Compiled for SINGLE PRECISION:  using __REAL
   Compile time: Thu Feb 13 15:00:12 PST 2003

Code was compiled with the following:
F77     = f77
F77FLAGS= -mips4 -64 -O3 -trapuv -OPT:Olimit=0:IEEE_arithmetic=3:roundoff=3
CC      = cc
CFLAGS  = -mips4 -64 -O3 -trapuv
CPP     = /lib/cpp
CPPFLAGS= -DMIPS4

Current time: Wed Nov 19 21:23:31 2003

GLOBAL PARAMETERS                    ($GLOBAL)
  CHIMERA STYLE INPUT?                (CHIMRA) = F
  RUN INCORE?                        (INCORE) = F
  RUNNING CDISC INVERSE DESIGN?       (CDISC ) = F
  NUMBER OF STEPS                    (NSTEPS) =    10
  READ RESTART FILE?                  (RESTRT) = T
  SAVE RESTART FILE EVERY             (NSAVE )      10 STEPS
  COMPUTE FORCE/MOMENT COEFS EVERY    (NFOMO )      10 STEPS
  TURBULENCE MODEL TYPE               (NQT)    =    0
  NUMBER OF SPECIES                   (NQC)    =    0
  USE MULTIGRID?                     (MULTIG) = F
  USE FULL MULTIGRID?                 (FMG)    = F
  NO. OF GRID LEVELS (IF MULTIG=.T.)    (NGLVL)  =    3
  NO. OF FMG CYCLES (IF FMG=.T.)       (FMGCYC) =    0    0
  PHYSICAL TIMESTEP (NON-DIM BY V_INF)   (DTPHYS) =  0.00000E+00
  MAX NUMBER OF NEWTON/DUAL SUBITERS     (NITNWT) =    10
  NO ORD CONVERGENCE FOR NEWTON/DUAL SUB (ORDNWT) =     0.00000
  FIRST/SECOND ORD NEWTON/DUAL SUB (0-2) (FSONWT) =     2.00000

ALLOCATING MEMORY FOR GRID AND FLOWFIELD ARRAYS:

  REQUESTING   11388762 REAL    WORDS FOR FLOWFIELD ARRAYS (Q,S)
  REQUESTING    6748896 REAL    WORDS FOR GRID ARRAYS (X,Y,Z,METRICS)
  REQUESTING     421806 INTEGER WORDS FOR GRID ARRAY  (IBLANK)
  REQUESTING    1507660 REAL    WORDS FOR TEMPORARY ARRAYS (TMP,TMP2,TMP3)

** NOTE ** Turning off force/moment reporting since input files
         (mixsur.fmp, grid.ibi and grid.ptv) do not exist.

FLOW CONDITIONS                      ($FLOINP)
  ANGLE OF ATTACK (DEG)              (ALPHA ) =    0.00000
  SIDESLIP       (DEG)               (BETA  ) =    0.00000
  FREESTREAM MACH NUMBER             (FSMACH) =    0.50000
  SPECIFIC HEAT RATIO                (GAMINF) =    1.40000
  REYNOLDS NUMBER                     (REY   ) =  0.90000E+07
  PRANDTL NUMBER                     (PR    ) =    0.72000
  TURBULENT PRANDTL NUMBER            (PRT   ) =    0.90000
  FREESTREAM TEMP (DEG R)            (TINF  ) =  460.00000

VARIABLE GAMMA / MULTIPLE SPECIES       ($VARGAM)
  GAMMA CALCULATION METHOD (0-2)     (IGAM  ) =    0
  TOTAL ENTHALPY RATIO FOR ALL GAS 1  (HT1   ) =   10.00000
  TOTAL ENTHALPY RATIO FOR ALL GAS 2  (HT2   ) =   10.00000

INPUTS FOR GRID     1:
  GRID NAME                          ($GRDNAM)
     Sod shock tube grid               (NAME  )
  NUMBER OF TIME STEPS / ITERATIONS    ($NITERS)
     ITERATIONS PER STEP               (ITER  ) =    1

  METHOD CONTROL PARAMETERS            ($METPRM)
     RIGHT-HAND-SIDE OPTION FLAG       (IRHS  ) =    0
```

```
    LEFT-HAND-SIDE OPTION FLAG          (ILHS  ) =     2
    LEFT-HAND-SIDE SUBITERATIONS        (ILHSIT) =     1
    DISSIPATION OPTION FLAG             (IDISS ) =     4
    LOW-MACH PRECONDITIONING PARAMETER  (BIMIN ) =      1.00000
    LOCAL MULTIGRID OPTION              (MULTIG) = F
    PROLONGATION SMOOTHING PARAMETERS   (SMOOPJ) =      0.00000
      (IF MULTIG=.T.)                   (SMOOPK) =      0.00000
                                        (SMOOPL) =      0.00000
    CORRECTION SMOOTHING PARAMETERS     (SMOOCJ) =      0.00000
      (IF MULTIG=.T.)                   (SMOOCK) =      0.00000
                                        (SMOOCL) =      0.00000
    RESIDUAL SMOOTHING PARAMETERS       (SMOORJ) =      0.00000
      (IF MULTIG=.T.)                   (SMOORK) =      0.00000
                                        (SMOORL) =      0.00000
    USE VISCOUS TERMS ON COARSE LEVELS? (CORSVI) = T
    RECOMPUTE MU_T ON FINEST LEVEL?     (RECMUT) = F

TIME STEP/ACCURACY PARAMETERS         ($TIMACU)
    TIME STEP SCALING OPTION FLAG (0-2) (ITIME ) =     0
    RELAXATION FACTOR OPTION FLAG (0-1) (IRELAX) =     0
    TIME STEP                           (DT    ) =  0.10000E-03
    FIRST/SECOND ORDER IN TIME (1-2)    (TFOSO ) =      1.00000
    MINIMUM CFL NUMBER                  (CFLMIN) =      0.00000
    MAXIMUM CFL NUMBER                  (CFLMAX) =      0.00000

SPATIAL SMOOTHING/ACCURACY PARAMETERS ($SMOACU)
    SPECTRAL RAD SMOOTHING (-1,1,2,3)   (ISPECJ) =     2
                                        (ISPECK) =     2
                                        (ISPECL) =     2
    SPECTRAL RAD VS VEL SMOOTHING (0-1) (SMOO  ) =      1.00000
    2ND O SMOOTHING COEFS (ARC3D-TYPE)  (DIS2J ) =      2.00000
                                        (DIS2K ) =      2.00000
                                        (DIS2L ) =      2.00000
    4TH O SMOOTHING COEFS (ARC3D-TYPE)  (DIS4J ) =      0.04000
                                        (DIS4K ) =      0.04000
                                        (DIS4L ) =      0.04000
    CENTRAL DIFF SMOOTHING (F3D-TYPE)   (EPSE  ) =      0.05000
    LU-SGS SPECTRAL RADIUS EPSILON      (EPSSGS) =      0.02000
    ROE LIMITER FIX PARAMETER           (DELTA ) =      1.00000
    CONVECTION SPATIAL DIFF ORDER (1-4) (FSO   ) =      2.00000
    MATRIX DISSIPATION LINEAR LIMIT     (VEPSL ) =      0.00000
    MATRIX DISSIPATION NONLIN LIMIT     (VEPSN ) =      0.00000
    USE ROE AVERAGE IN MATRIX DISSIP?   (ROEAVG) = F

VISCOUS/INVISCID FLAGS                ($VISINP)
    INCLUDE VISCOUS TERMS IN  J?        (VISCJ ) = T
                              K?        (VISCK ) = T
                              L?        (VISCL ) = F
    INCLUDE VISCOUS CROSS TERMS?        (VISCX ) = F

TURBULENT SURFACE SPECS               ($VISINP)
    NUMBER OF TURBULENT SURFACE SPECS   (NTURB ) =  -999

TURBULENCE MODEL PARAMETERS           ($VISINP)
    ITERATIONS PER FLOW SOLVER ITERATION(ITERT ) =     1
    LEFT-HAND-SIDE SUBITERATIONS        (ITLHIT) =     1
    LOCAL TIME STEP CONSTANT            (CFLT  ) =      1.00000

BOUNDARY CONDITION SPECS              ($BCINP )
    NUMBER OF BOUNDARY CONDITION SPECS  (NBC   ) =     9
     (IBTYP) (IBDIR) (JBCS) (JBCE) (KBCS) (KBCE) (LBCS) (LBCE)
        16      2     1     -1     1     1     1     -1
         1      1     1      1     1    25     1     -1
        30      1     1      1    26    -1     1     -1
        13      3     1     -1     1    -1     1      1
        12     -3     1     -1     1    -1    -1     -1
        30     -1    -1     -1     1    -1     1     -1
         5     -2     1     -1    -1    -1     1     -1
         5     -2     1     60    25    25     1     -1
         5      2     1     60    26    26     1     -1
```

```
  SPECIES CONTINUITY EQN PARAMETERS     ($SCEINP)
     ITERATIONS PER FLOW SOLVER ITERATION(ITERC ) =     1
     LOCAL TIME STEP CONSTANT           (CFLC  ) =     1.00000
     UPWIND DIFFERENCING FLAG (0-1)     (IUPC  ) =     1
     2ND O SMOOTHING COEF (ARC3D-TYPE)  (DIS2C ) =     2.00000
     4TH O SMOOTHING COEF (ARC3D-TYPE)  (DIS4C ) =     0.04000

GRID SIZE FOR GRID     1:
  NUMBER OF POINTS IN J  (JD    ) =   121
                K  (KD    ) =   42
                L  (LD    ) =   83

CHECKING TIME STEP SPECIFICATION FOR GRID     1:
  RUNNING TIME-ACCURATE WITH NEWTON SUBITERATIONS
    WITH DT (BASED ON C_INF) =  0.10000E-03

CHECKING BOUNDARY CONDITIONS FOR GRID     1:
   1)  BOUNDARY CONDITION TYPE#    16     DIRECTION     2
    AXIS IN K (L AROUND)
     1.00 ORDER EXTRAPOLATION FOR ZERO SLOPE
    DIR= 2    J-RANGE=    1  121    K-RANGE=    1    1    L-RANGE=    1   83
   2)  BOUNDARY CONDITION TYPE#     1     DIRECTION     1
    INVISCID ADIABATIC SOLID WALL (PRESSURE EXTRAPOLATION)
    DIR= 1    J-RANGE=    1    1    K-RANGE=    1   25    L-RANGE=    1   83
   3)  BOUNDARY CONDITION TYPE#    30     DIRECTION     1
    OUTFLOW (EXTRAPOLATION)
    DIR= 1    J-RANGE=    1    1    K-RANGE=   26   42    L-RANGE=    1   83
   4)  BOUNDARY CONDITION TYPE#    13     DIRECTION     3
    SYMMETRY IN Z, IN L
    DIR= 3    J-RANGE=    1  121    K-RANGE=    1   42    L-RANGE=    1    1
   5)  BOUNDARY CONDITION TYPE#    12     DIRECTION    -3
    SYMMETRY IN Y, IN L
    DIR=-3    J-RANGE=    1  121    K-RANGE=    1   42    L-RANGE=   83   83
   6)  BOUNDARY CONDITION TYPE#    30     DIRECTION    -1
    OUTFLOW (EXTRAPOLATION)
    DIR=-1    J-RANGE=  121  121    K-RANGE=    1   42    L-RANGE=    1   83
   7)  BOUNDARY CONDITION TYPE#     5     DIRECTION    -2
    VISCOUS ADIABATIC SOLID WALL  (PRESSURE EXTRAPOLATION)
    DIR=-2    J-RANGE=    1  121    K-RANGE=   42   42    L-RANGE=    1   83
   8)  BOUNDARY CONDITION TYPE#     5     DIRECTION    -2
    VISCOUS ADIABATIC SOLID WALL  (PRESSURE EXTRAPOLATION)
      NOTE   : CONDITION NOT SPECIFIED AT PLANE 1 OR LAST
    DIR=-2    J-RANGE=    1   60    K-RANGE=   25   25    L-RANGE=    1   83
   9)  BOUNDARY CONDITION TYPE#     5     DIRECTION     2
    VISCOUS ADIABATIC SOLID WALL  (PRESSURE EXTRAPOLATION)
      NOTE   : CONDITION NOT SPECIFIED AT PLANE 1 OR LAST
    DIR= 2    J-RANGE=    1   60    K-RANGE=   26   26    L-RANGE=    1   83

CHECKING VISCOUS AND TURBULENCE MODELING SPECIFICATIONS FOR GRID     1:

  LAMINAR OR BALDWIN-LOMAX 0-EQUATION TURBULENCE MODEL SELECTED

  INCLUDE VISCOUS TERMS IN J-DIRECTION
  INCLUDE VISCOUS TERMS IN K-DIRECTION
  NO     VISCOUS TERMS IN L-DIRECTION

    FOR GRID   1  AT STEP    10   L2NORM =  0.71552276E-05
    FOR GRID   1  AT STEP    10   L2NORM =  0.21428687E-06
    FOR GRID   1  AT STEP    10   L2NORM =  0.50177364E-08
    FOR GRID   1  AT STEP    10   L2NORM =  0.25163888E-09
    FOR GRID   1  AT STEP    10   L2NORM =  0.45577112E-10
    FOR GRID   1  AT STEP    10   L2NORM =  0.32773270E-10
    FOR GRID   1  AT STEP    10   L2NORM =  0.30651485E-10
    FOR GRID   1  AT STEP    10   L2NORM =  0.30269700E-10
    FOR GRID   1  AT STEP    10   L2NORM =  0.30199614E-10
    FOR GRID   1  AT STEP    10   L2NORM =  0.30189667E-10
FLOW SOLVER/TURB MODEL/SPECIES CONVERGENCE RATES:    1.0889    0.0000    0.0000

Current time: Wed Nov 19 21:39:16 2003
```

APPENDIX G. README FILE OF TEST CASE.

This is a shock tube test case for time accuracy.

Problem setup (grid, initial conditions and exact solution) comes
courtesy of Mr. Robert Tramel, Micro Craft, Inc., Tullahoma, TN.

The problem is set up as a 3-dimensional problem (grid is 101x51x5),
with inviscid sidewalls and viscous walls top and bottom. This tests
the ability of the Newton subiteration to drive out factorization errors
in the crossflow directions. Note that each additional Newton
subiteration (beyond 1) takes the same amount of CPU time as one step of
the (original) method. Thus running for 10 subiterations takes 10 times
as long as running without subiterations.

Ten iterations are taken with a timestep (DT) of 0.001 to start the
simulation, then 18 steps are taken with a timestep of 0.01, for a total
(nondimensional) time advance of 0.19. (Time is nondimensinalized using
the freestream speed of sound and one unit of length in the CFD grid.)
The initial smaller timesteps
are needed (at least for central/scalar) to keep the solution from
bombing due to the initial transient.

All runs are done with 2nd-order (3-point backward) time accuracy,
except for initial steps of each run (and when DT is changed). The
previous time level (Q^(n-1)) is NOT stored in the q.save/q.restart file.

Running cases:

Cases can be run using the "runcase" script (and results for a particular
case deleted with "cleancase"). Scripts take a single argument which is
the base name for two input files, (basename).1.inp and
(basename).2.inp. Results are (1) an XYPLOT file of x vs. rho, V and p
in shock.(basename), (2) a residual history in resid.(basename), (3) a Q
file in q.(basename), and (4) a PLOT3D command file in (basename).com
for plotting density contours.

The script "runall" runs a selection of the following cases; "plotall"
generates some comparison plots (using XYPLOT and PLOT3D); and
"cleanall" cleans up these cases.

Input for the following cases is included:

basename	subiter	differencing method
central	no	central, scalar diss, diagonal LHS
central3	3	central, scalar diss, diagonal LHS
central5	5	central, scalar diss, diagonal LHS
central10	10	central, scalar diss, diagonal LHS
matrix	no	central, matrix diss, diagonal LHS
matrix3	3	central, matrix diss, diagonal LHS
matrix5	5	central, matrix diss, diagonal LHS
matrix10	10	central, matrix diss, diagonal LHS
matrix30	30	central, matrix diss, diagonal LHS
roe	no	Roe, diagonal LHS
roe3	3	Roe, diagonal LHS
roe5	5	Roe, diagonal LHS
roe10	10	Roe, diagonal LHS
roe30	30	Roe, diagonal LHS
lu_roe3	3	Roe, LU-SGS LHS
lu_roe10	10	Roe, LU-SGS LHS

Plotting results:

The following PostScript files have already been prepared:

method.ps	Compares central differencing, central with matrix dissipation, and Roe upwinding (cases central3, matrix5, roe10).
central.ps	Compares different numbers of subiterations (cases central, central3, central5).
matrix.ps	Compares different numbers of subiterations (cases matrix3, matrix5, matrix10).
roe.ps	Compares different numbers of subiterations (cases roe5, roe10, roe30).
roe_lhs.ps	Compares Roe upwind with different left-hand sides (cases roe10, lu_roe10).

If you have XYPLOT, results can be compared by typing

```
xyplot -f shock.fmt shock.exact shock.(case1) shock.(case2) ...
```

where (case1), (case2) are to be replaced by the desired basenames.

Density contours in the 3D grid can be plotted using PLOT3D, with the (basename).com command file. This will show the deviation of the solution in the crossflow directions.

Some observations:

o For standard central differencing (scalar 4/2 dissipation), 3 subiterations is adequate to remove factorization errors (as determined by looking at the line plots of density, velocity and pressure, and by looking at contour plots of density in K=26 and L=3 planes).

o Similarly, central differencing plus matrix dissipation takes 5 subiterations (with slight changes past this), and Roe upwinding takes 10 subiterations.

o At 10 subiterations, the (diagonalized) central left-hand side (ILHS=2) appears to have less crossflow distortion than the LU-SGS scheme (ILHS=3). Specifically, the contours near the viscous walls are much straighter.

o Looking at the residual files, convergence of the Newton subiterations slows down greatly after the first 3 iterations, indicating not much benefit from additional subiterations (for the larger timestep part of the run). However, for the first 10 steps with the smaller DT, additional subiterations continues to help convergence. This indicates that the timestep of 0.01 may simply be too large for maximum benefit of the Newton subiteration procedure. An examination of accuracy vs. timestep is in order.

Reference for the physical problem:

G.A. Sod, "A Survey of Several Finite Difference Methods for Systems of Non-Linear Hyperbolic Conservation Laws," JCP, Vol. 27, 1978, pp. 1-31.

Reference for additional comparisons of schemes:

R.W. Tramel and R.H. Nichols, "A Highly Efficient Numerical Method for Overset-Mesh Moving-Body Problems," AIAA-97-????.

APPENDIX H. GRID MESH OF COMBUSTORS USING FAST.

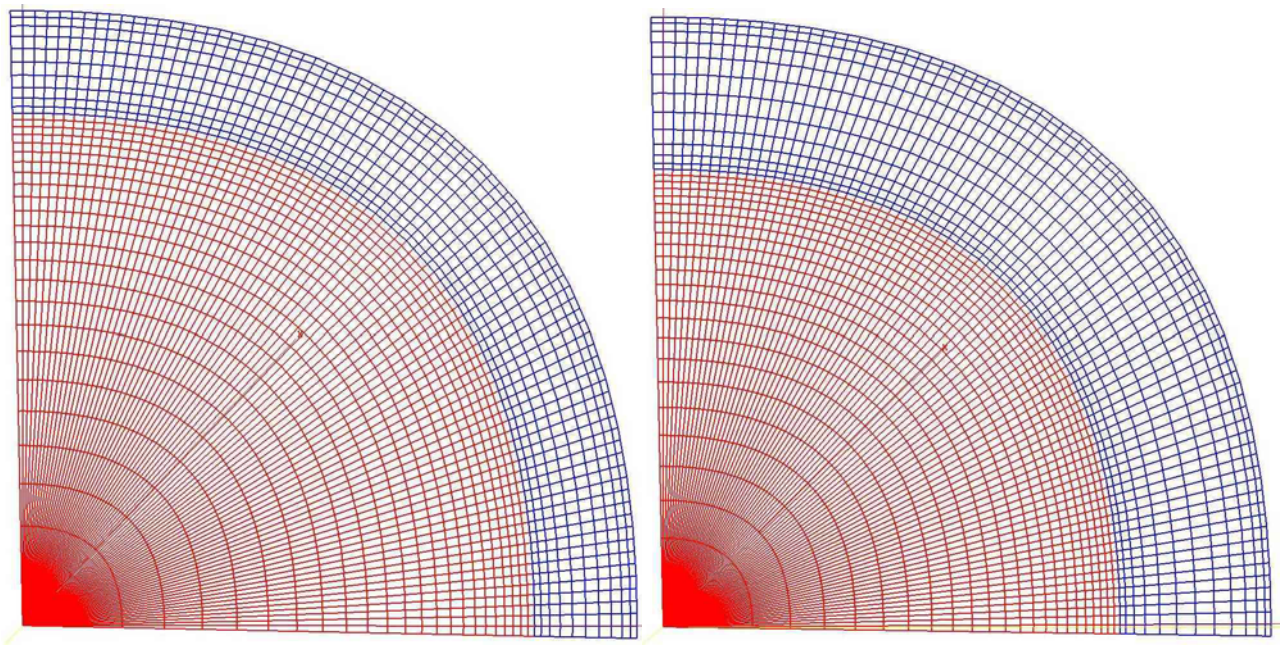

Figure 41. Grid Mesh of 2.25 inches Diameter Cylindrical Combustor (Left)
Figure 42. Grid Mesh of 2.5inches Diameter Cylindrical Combustor (Right)

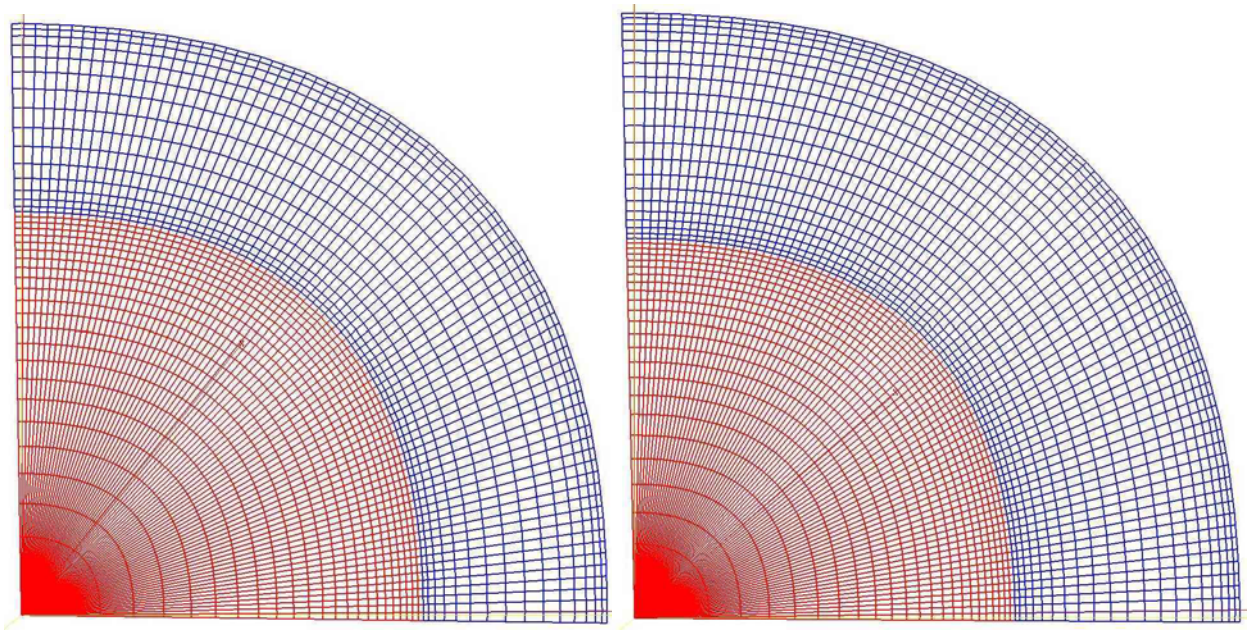

Figure 43. Grid Mesh of 2.75 inches Diameter Cylindrical Combustor (Left).
Figure 44. Grid Mesh of 3 inches Diameter Cylindrical Combustor (Right).

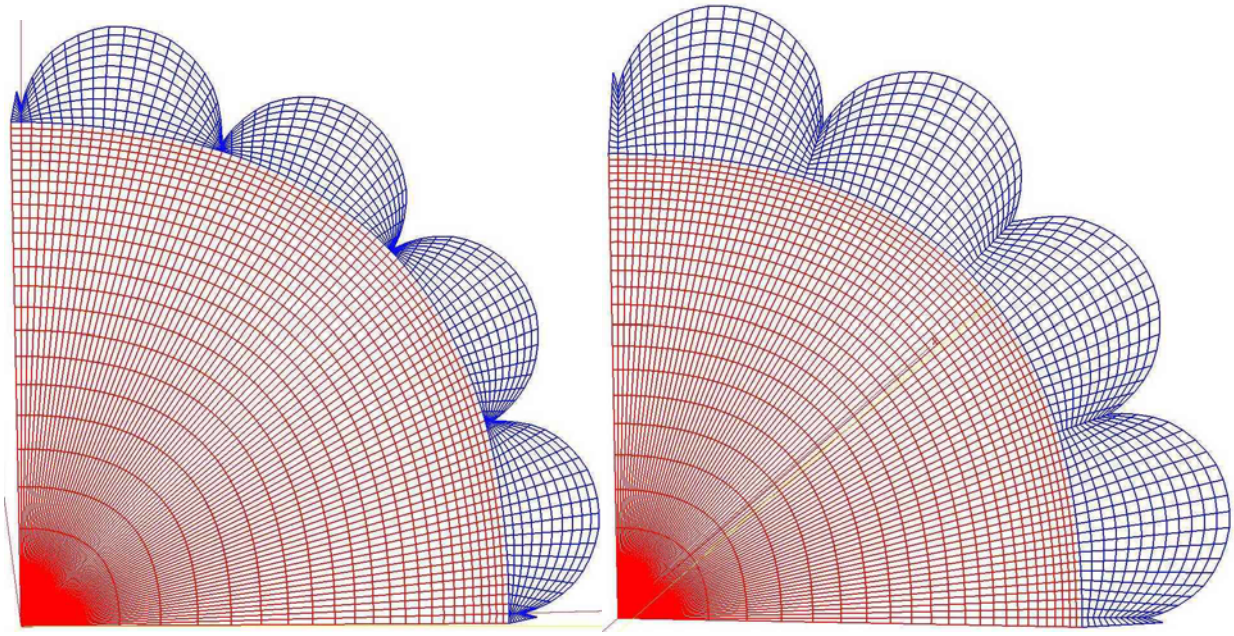

Figure 45. Grid Mesh of 2.25 inches Diameter Scalloped Combustor (Left).
Figure 46. Grid Mesh of 2.5inches Diameter Scalloped Combustor (Right).

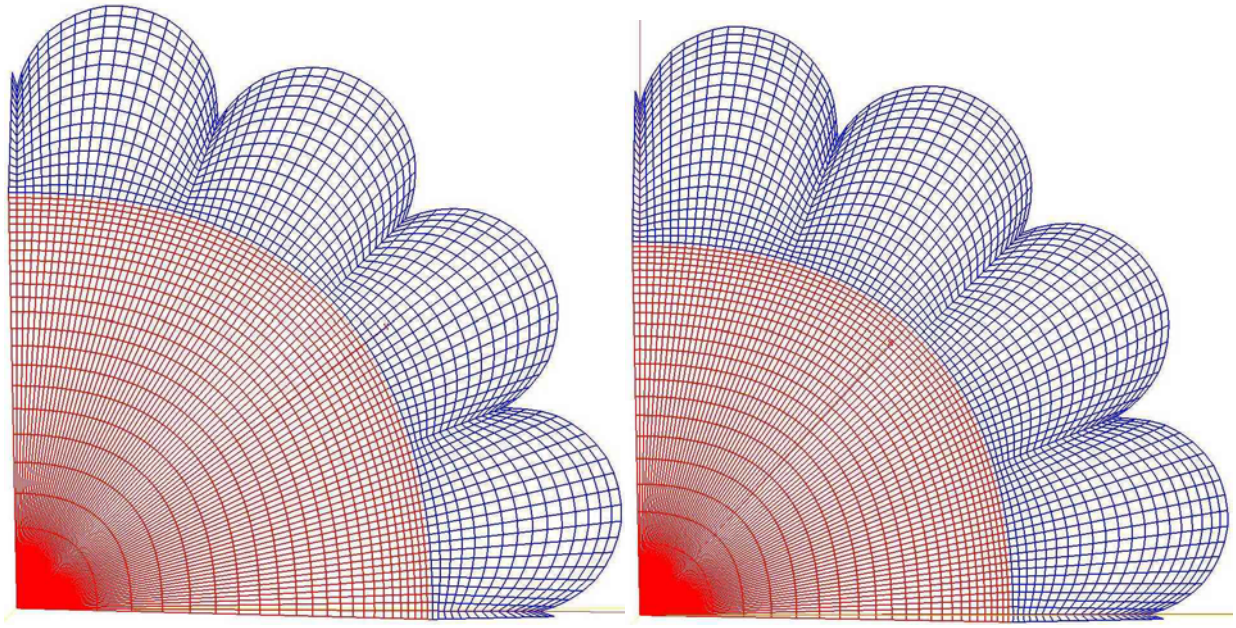

Figure 47. Grid Mesh of 2.75 inches Diameter Scalloped Combustor.
Figure 48. Grid Mesh of 3 inches Diameter Scalloped Combustor.

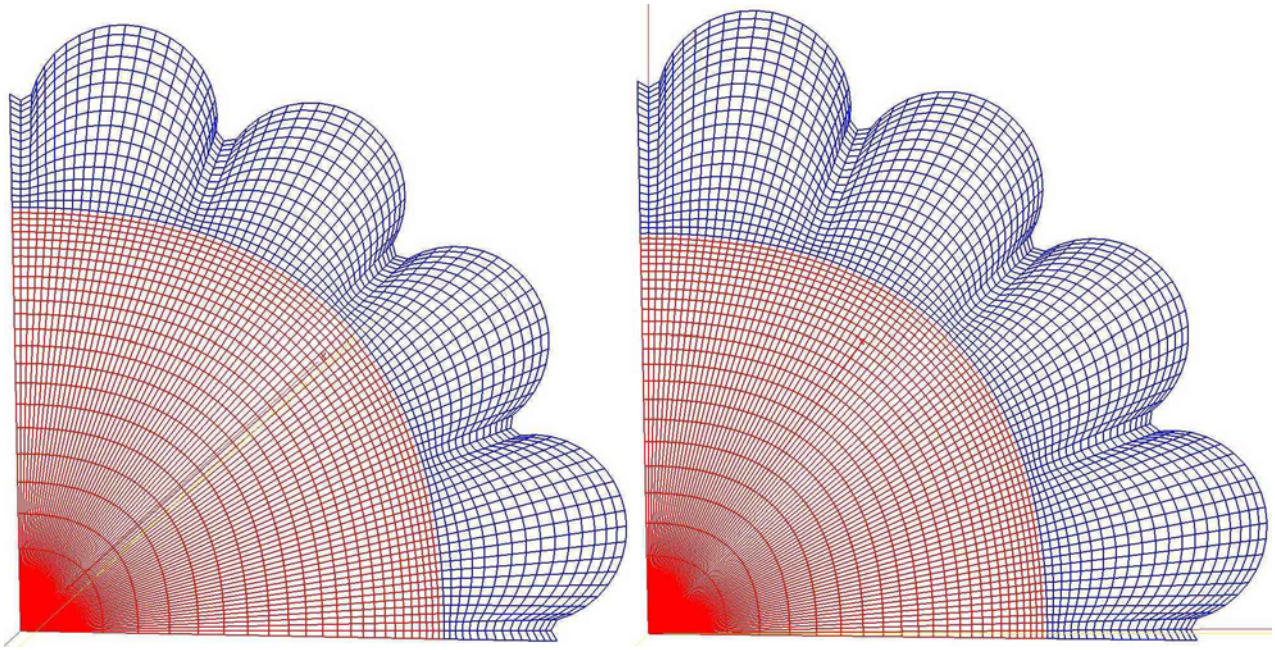

Figure 49. Grid Mesh of 2.75 inches Diameter Modified Scalloped Combustor (Left).
Figure 50. Grid Mesh of 3 inches Diameter Modified Scalloped Combustor (Right).

THIS PAGE INTENTIONALLY LEFT BLANK

APPENDIX I. TEMPERATURE AND PRESSURE CONTOUR PLOTS OF COMBUSTORS.

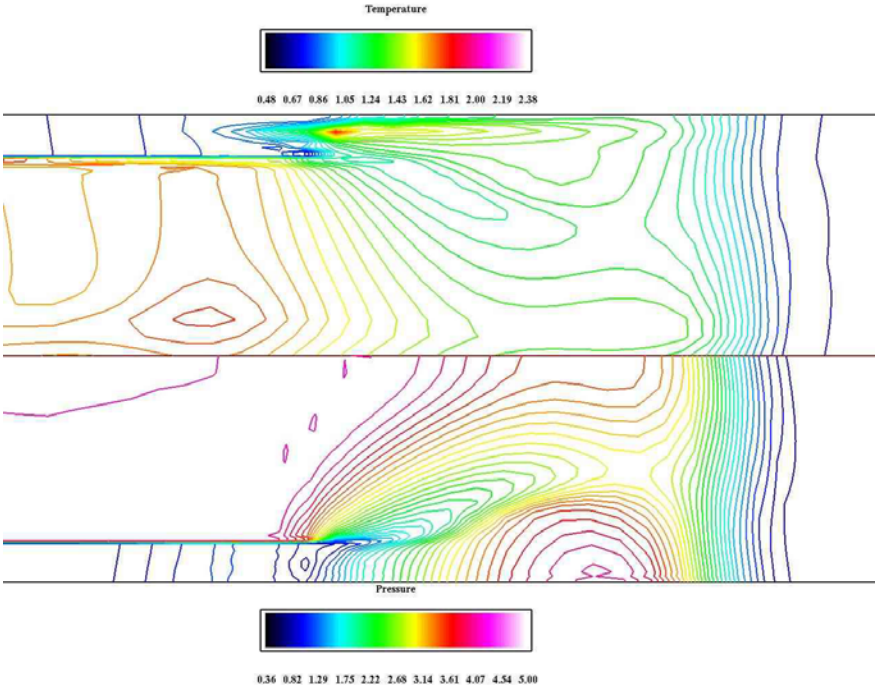

Figure 51. Temperature and Pressure Contour Plot of 2.25 inches Diameter Cylindrical Combustor.

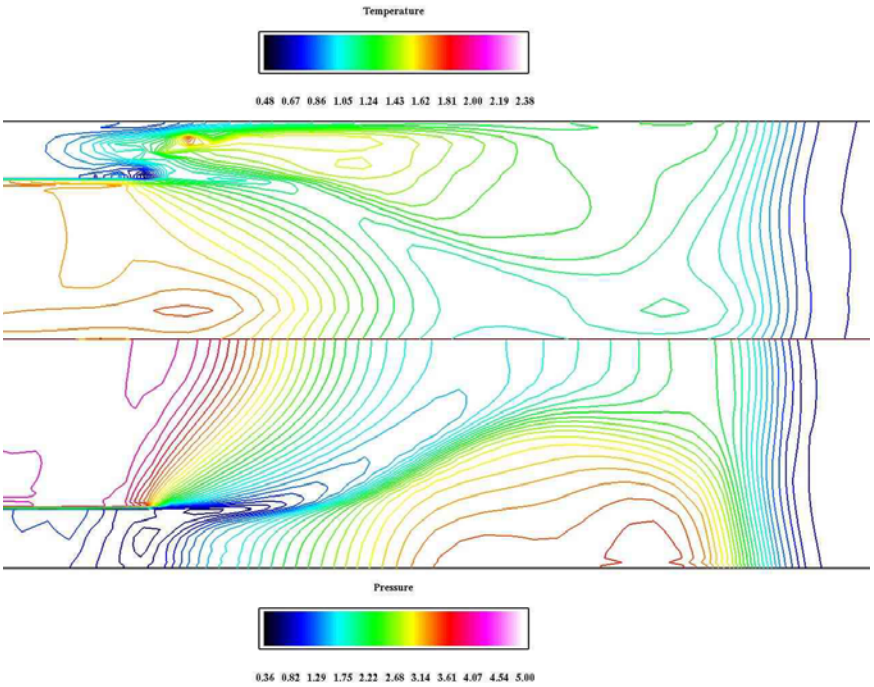

Figure 52. Temperature and Pressure Contour Plot of 2.5inches Diameter Cylindrical Combustor.

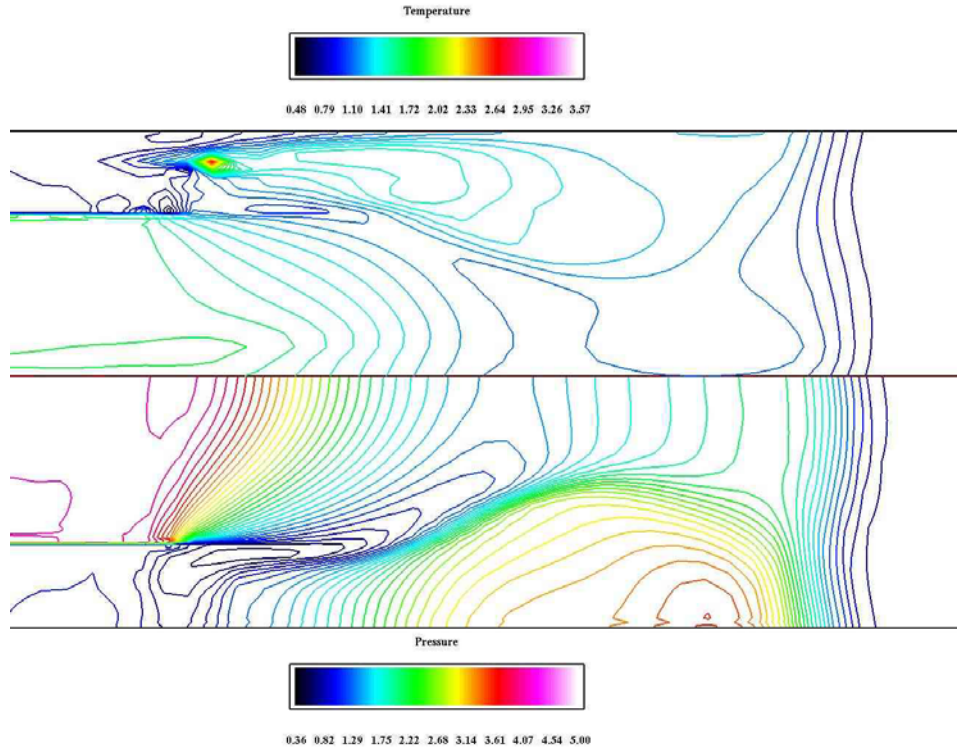

Figure 53. Temperature and Pressure Contour Plot of 2.75 inches Diameter Cylindrical Combustor.

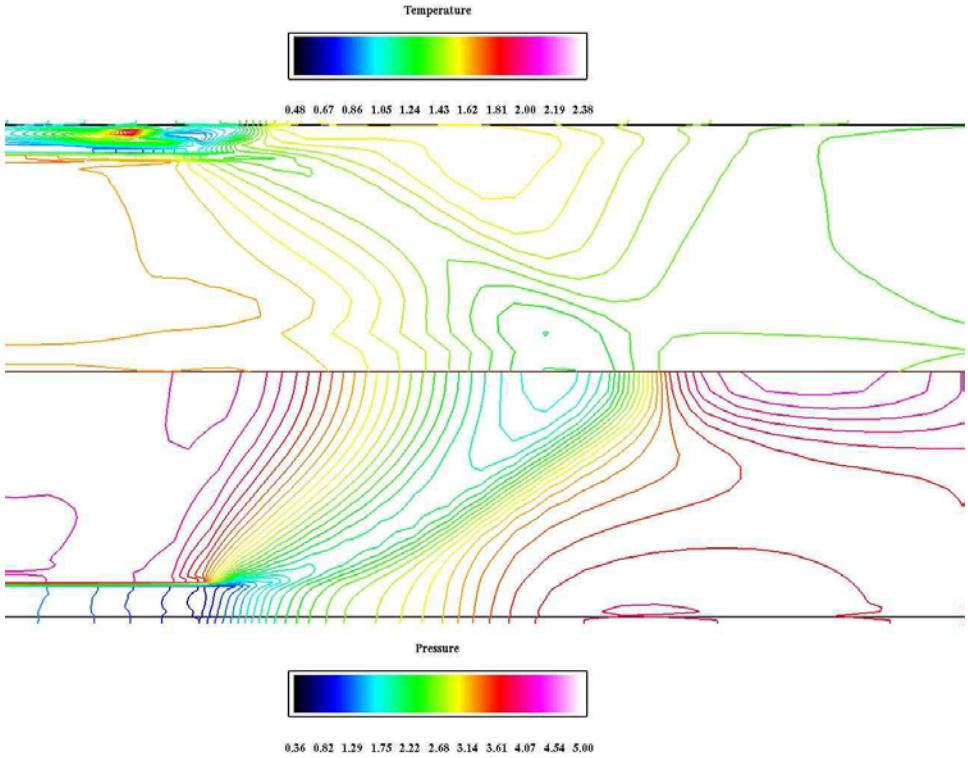

Figure 54. Temperature and Pressure Contour Plot of 2.25 inches Diameter Scalloped Combustor.

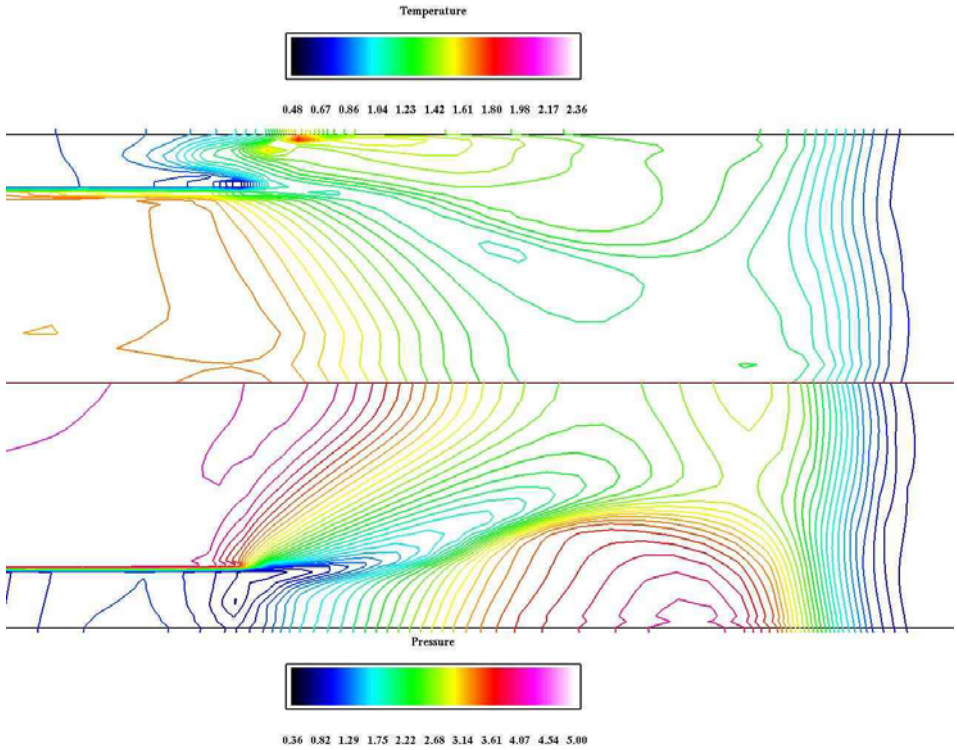

Figure 55. Temperature and Pressure Contour Plot of 2.5 inches Diameter Scalloped Combustor.

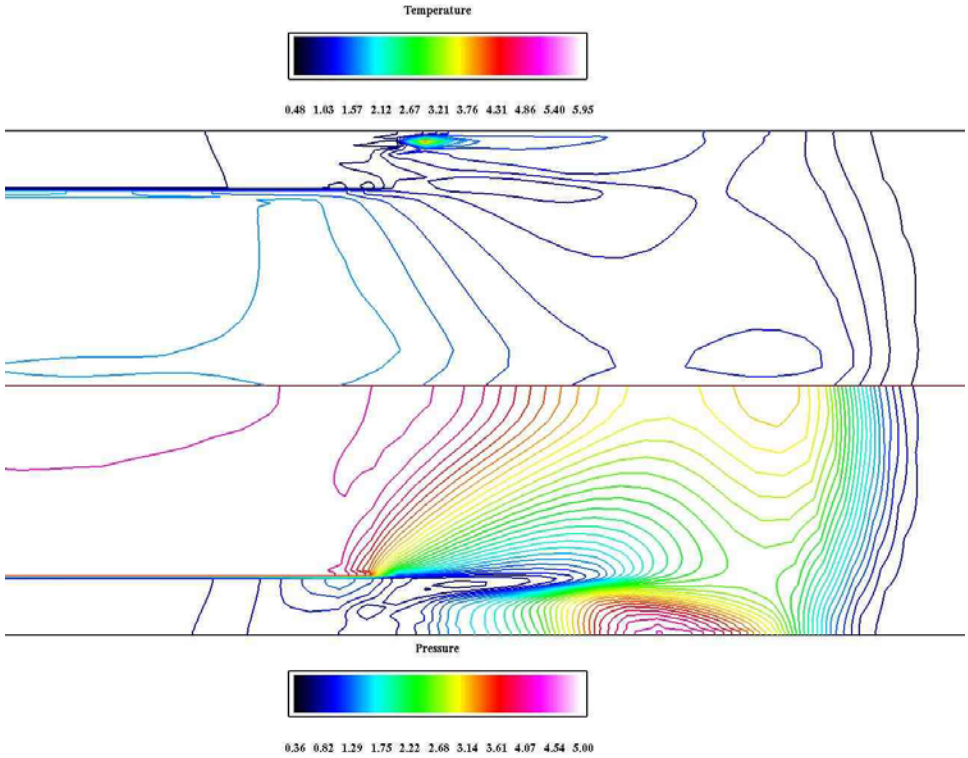

Figure 56. Temperature and Pressure Contour Plot of 2.75 inches Diameter Scalloped Combustor.

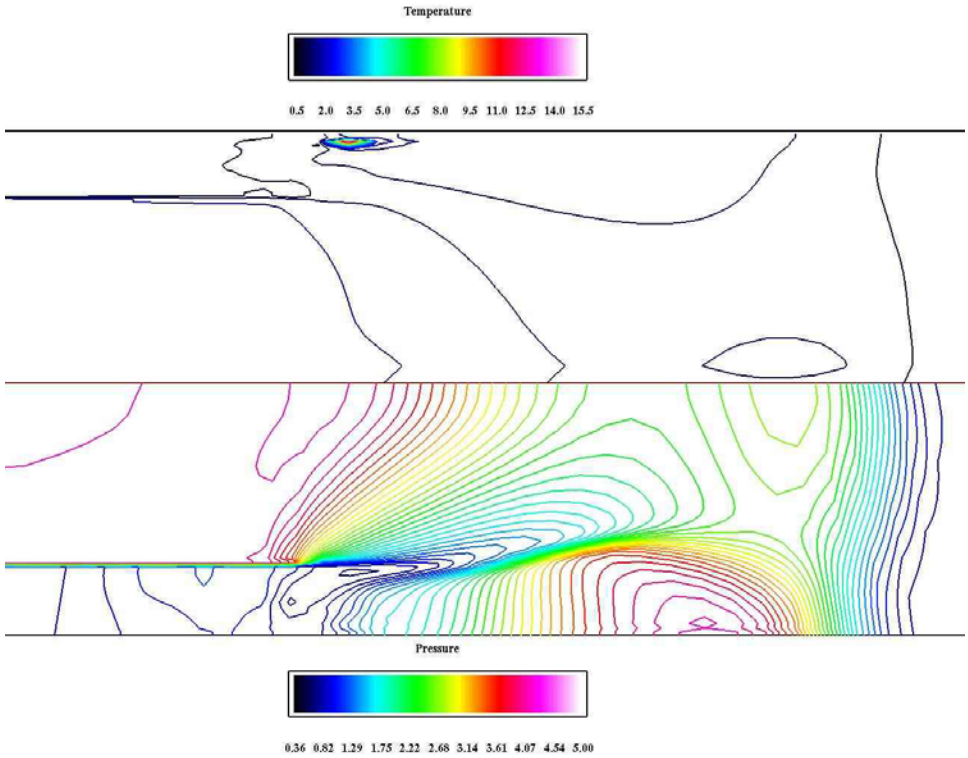

Figure 57. Temperature and Pressure Contour Plot of 2.75 inches Diameter Modified Scalloped Combustor.

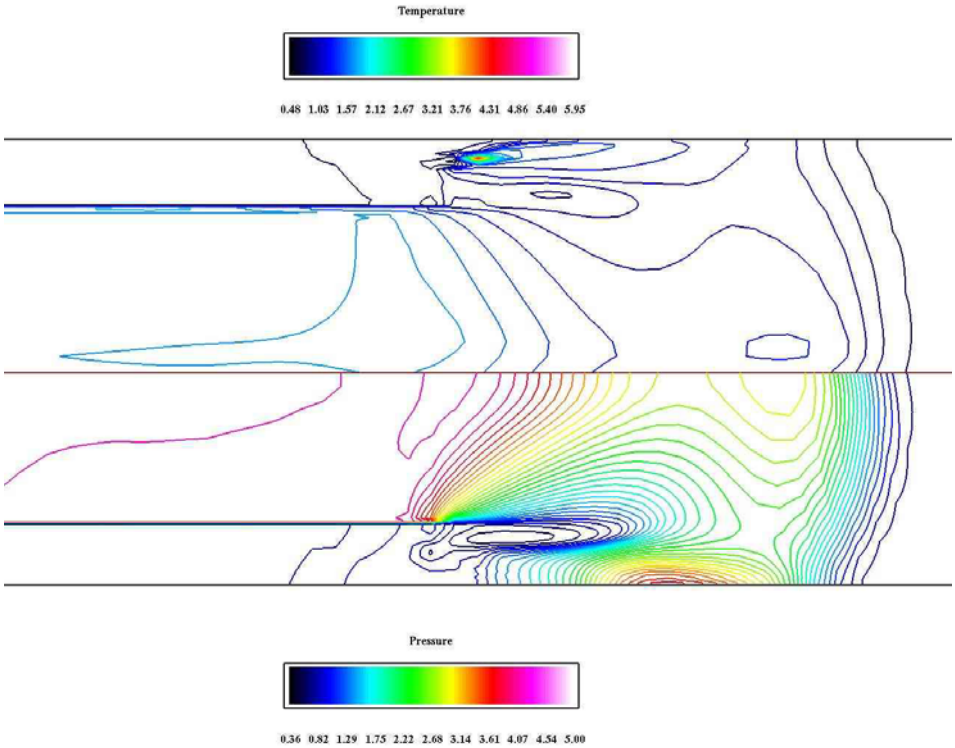

Figure 58. Temperature and Pressure Contour Plot of 3 inches Diameter Modified Scalloped Combustor.

APPENDIX J. TEMPERATURE PLOTS OF COMBUSTORS.

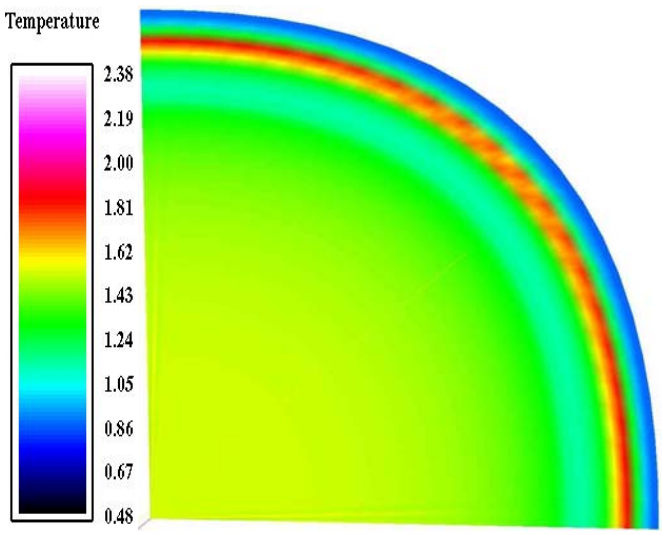

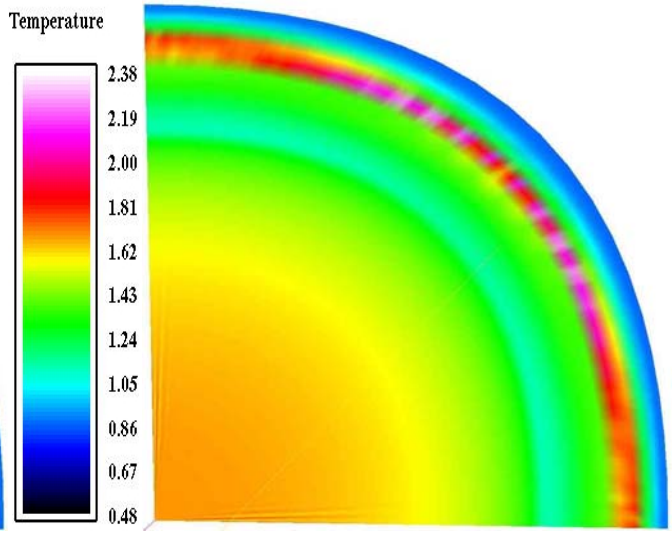

Figure 59. Temperature Plot of 2.25 inches Diameter Cylindrical Combustor (Left).
Figure 60. Temperature Plot of 2.5 inches Diameter Cylindrical Combustor (Right).

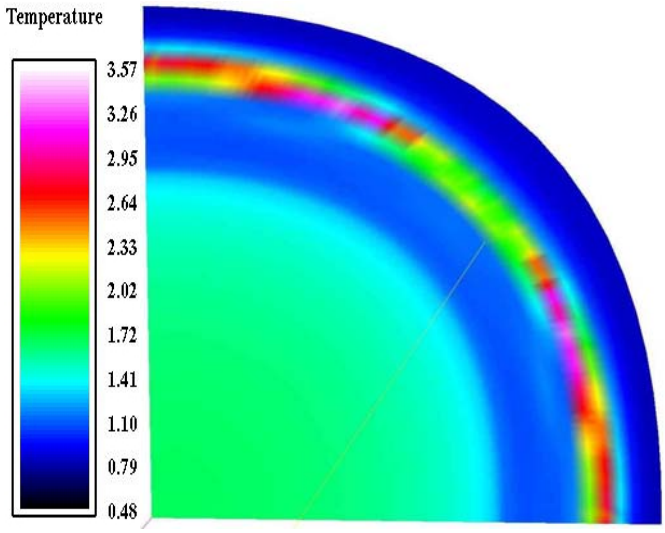

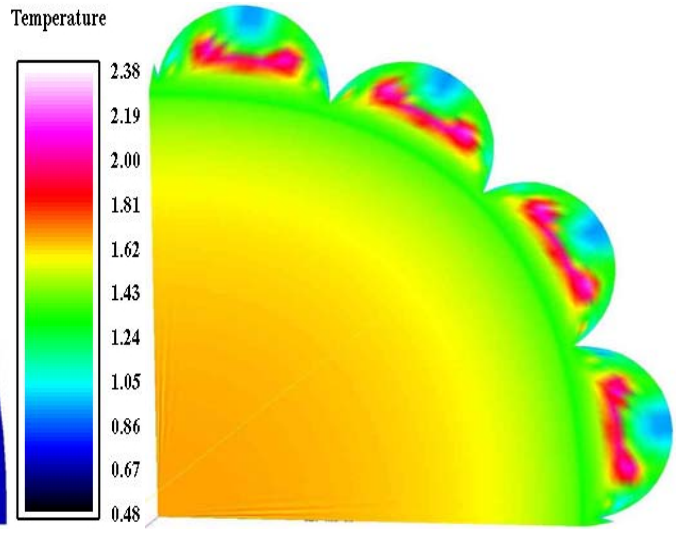

Figure 61. Temperature Plot of 2.75 inches Diameter Cylindrical Combustor (Left).
Figure 62. Temperature Plot of 2.25 inches Diameter Scalloped Combustor (Right).

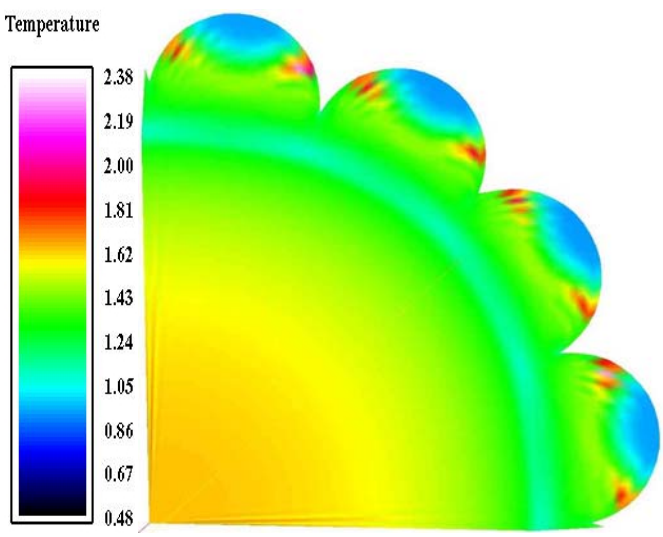

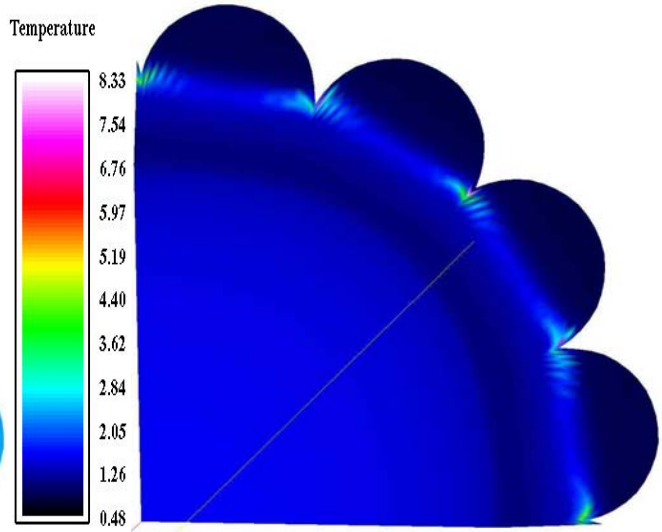

Figure 63. Temperature Plot of 2.5 inches Diameter Scalloped Combustor (Left).
Figure 64. Temperature Plot of 2.75 inches Diameter Scalloped Combustor (Right).

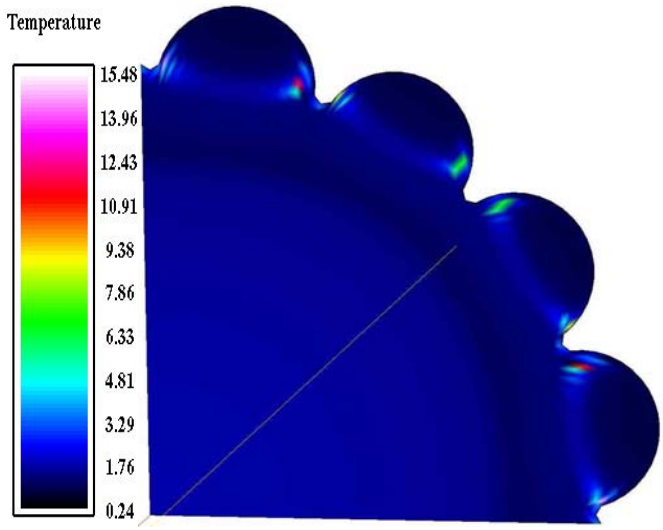

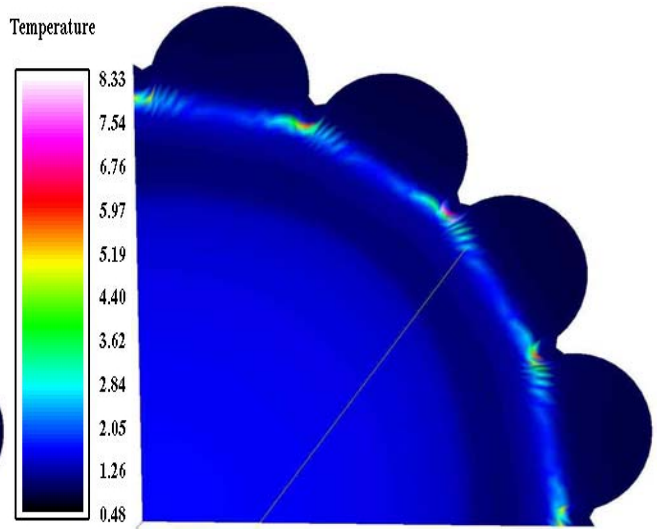

Figure 65. Temperature Plot of 2.75 inches Diameter Modified Scalloped Combustor (Left).
Figure 66. Temperature Plot of 3 inches Diameter Modified Scalloped Combustor (Right).

APPENDIX K. MACH NO. PLOTS OF COMBUSTORS.

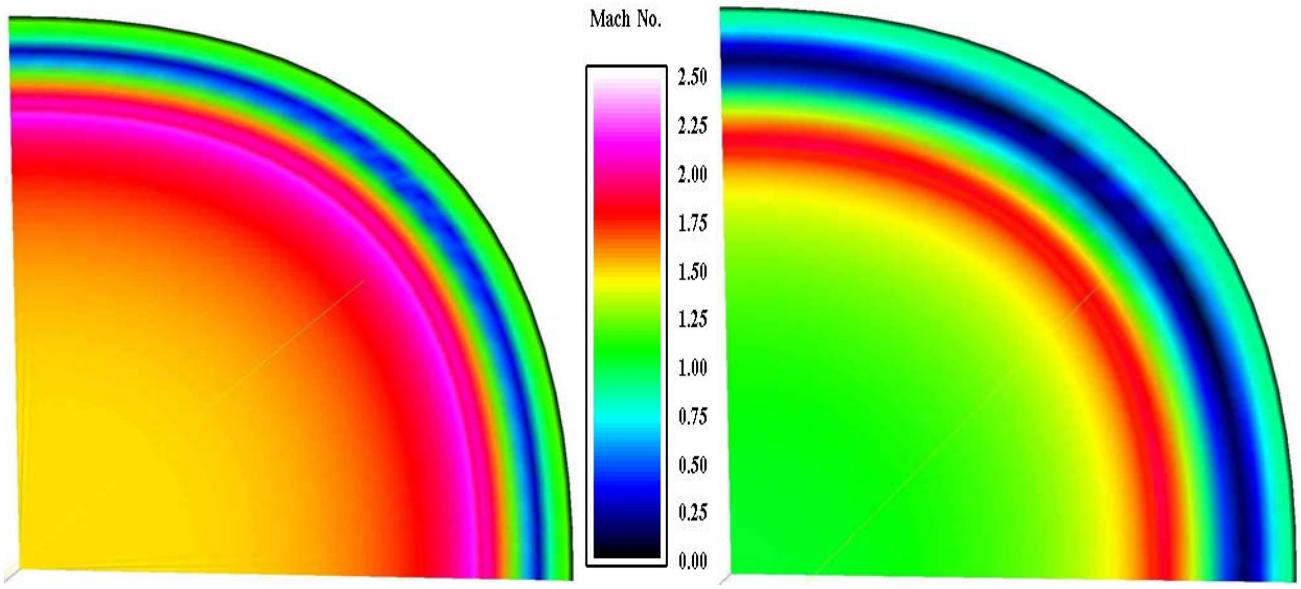

Figure 67. Mach No. Plot of 2.25 inches Diameter Cylindrical Combustor (Left).
Figure 68. Mach No. Plot of 2.5 inches Diameter Cylindrical Combustor (Right).

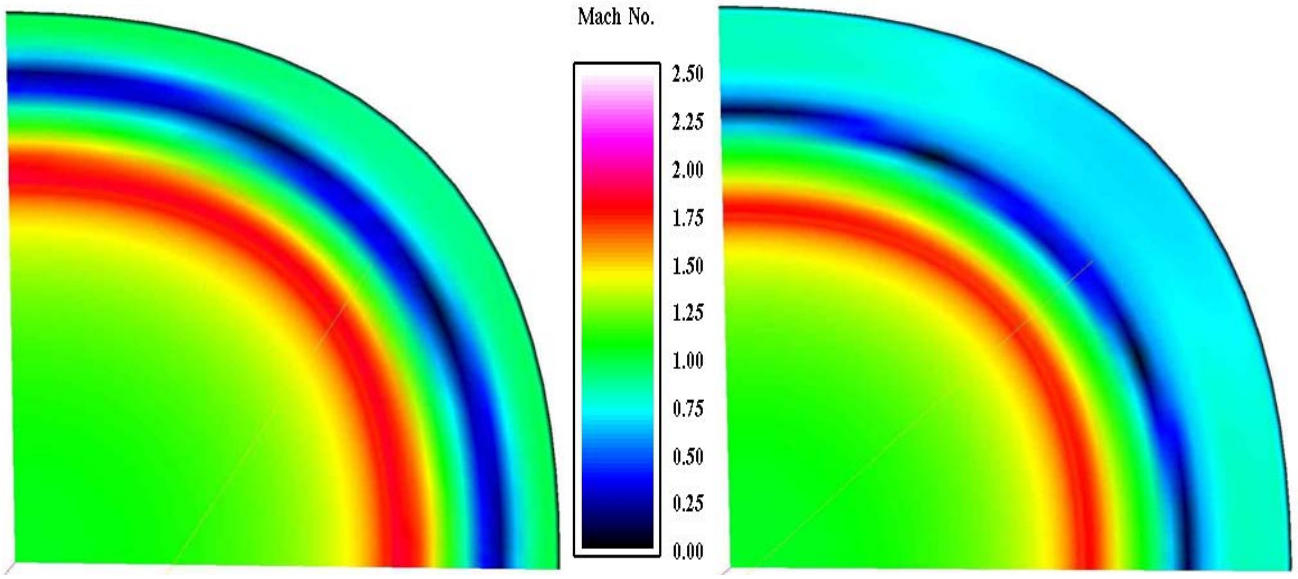

Figure 69. Mach No. Plot of 2.75 inches Diameter Cylindrical Combustor (Left).
Figure 70. Mach No. Plot of 3 inches Diameter Cylindrical Combustor (Right).

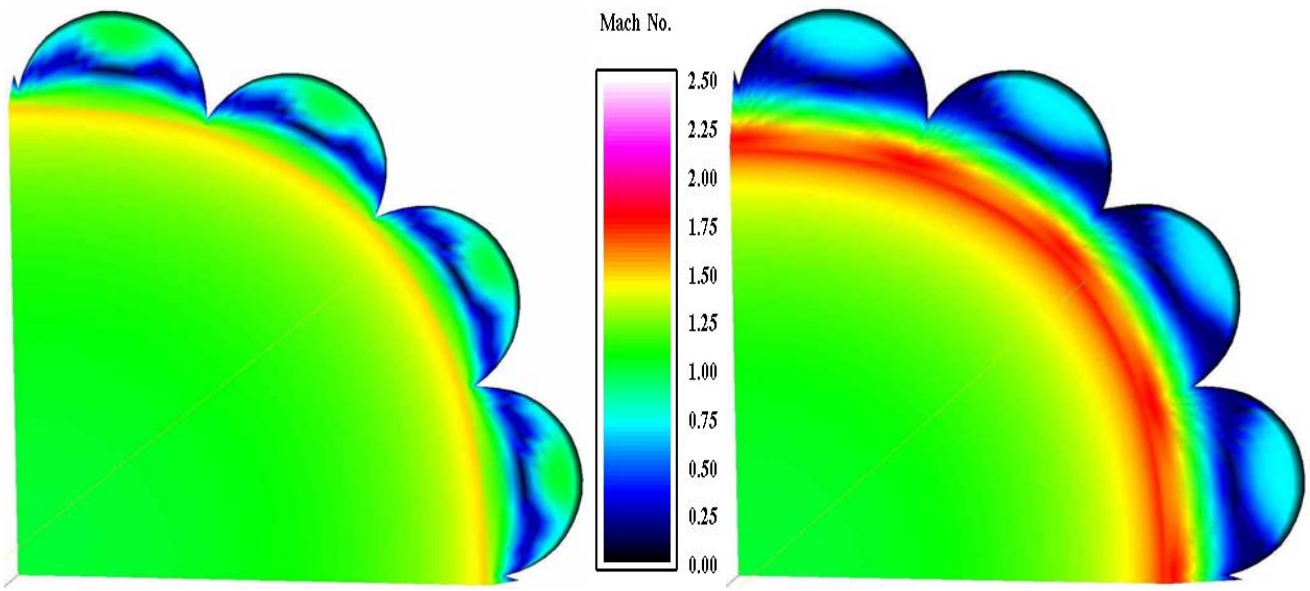

Figure 71. Mach No. Plot of 2.25 inches Diameter Scalloped Combustor (Left).
Figure 72. Mach No. Plot of 2.5 inches Diameter Scalloped Combustor (Right).

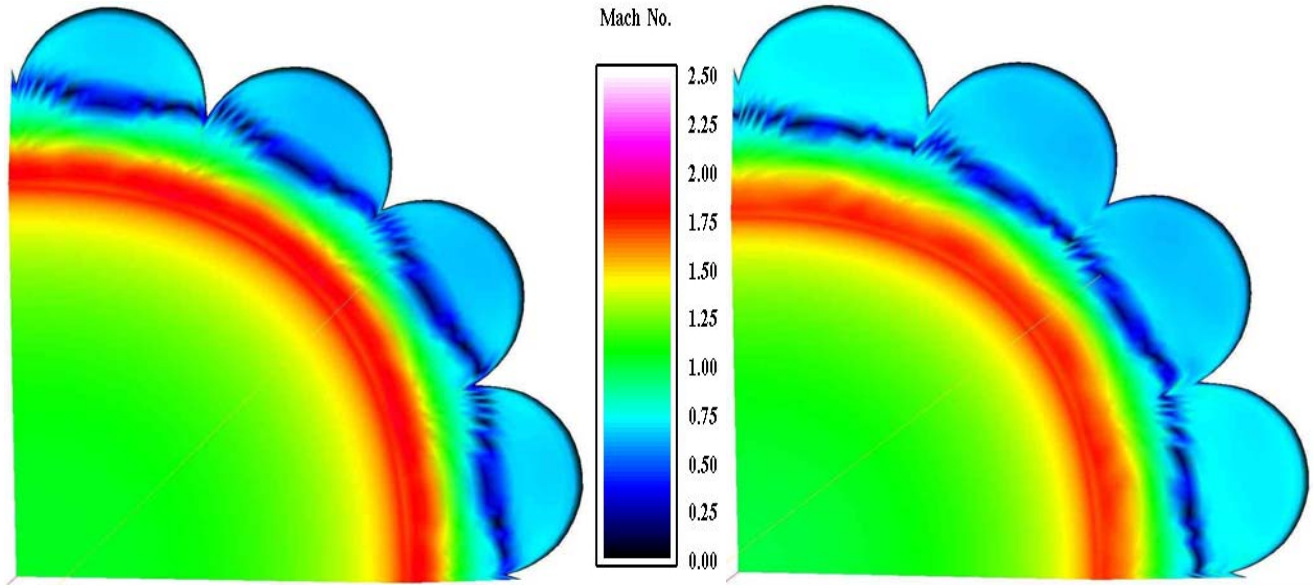

Figure 73. Mach No. Plot of 2.75 inches Diameter Scalloped Combustor (Left).
Figure 74. Mach No. Plot of 3 inches Diameter Scalloped Combustor (Right).

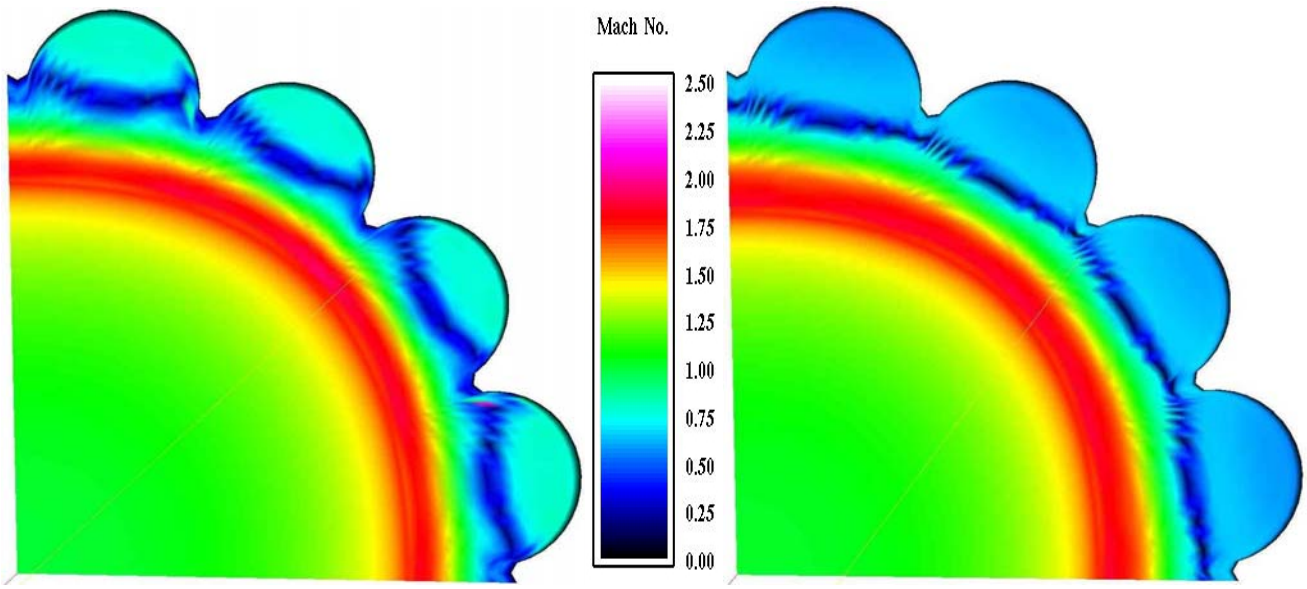

Figure 75. Mach No. Plot of 2.75 inches Diameter Modified Scalloped Combustor (Left).
Figure 76. Mach No. Plot of 3 inches Diameter Modified Scalloped Combustor (Right).

THIS PAGE INTENTIONALLY LEFT BLANK

APPENDIX L. VORTICITY MAGNITUDE PLOTS OF COMBUSTORS.

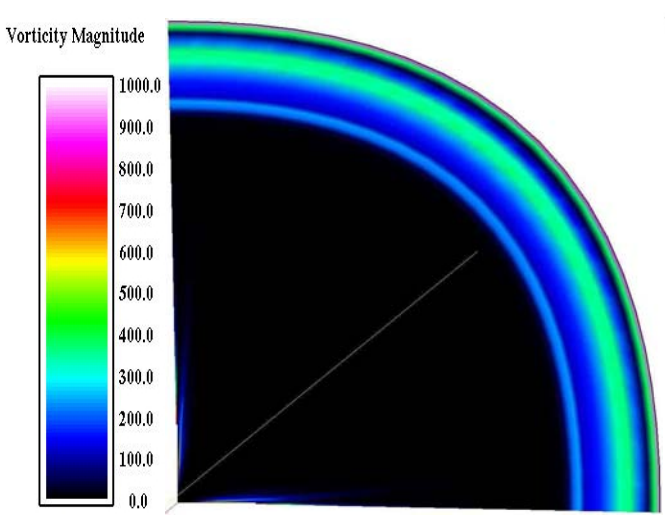

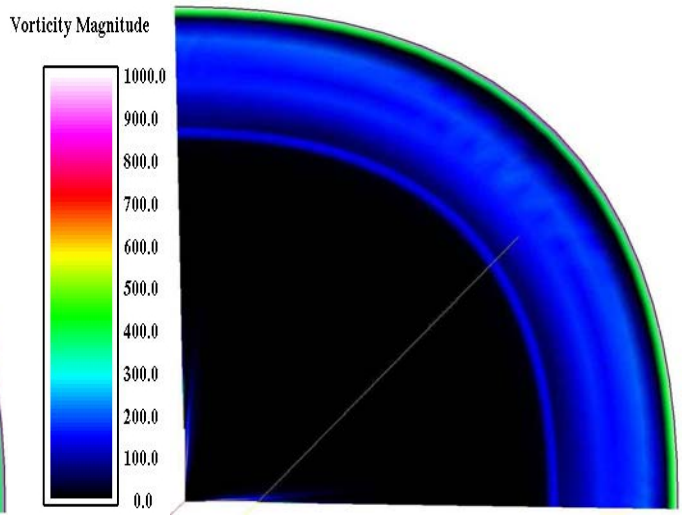

Figure 77. Vorticity Magnitude Plot of 2.25 inches Diameter Cylindrical Combustor (Left).
Figure 78. Vorticity Magnitude Plot of 2.5 inches Diameter Cylindrical Combustor (Right).

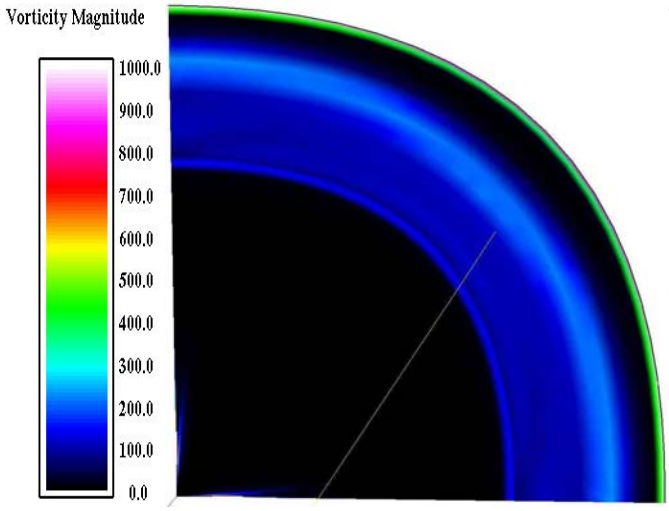

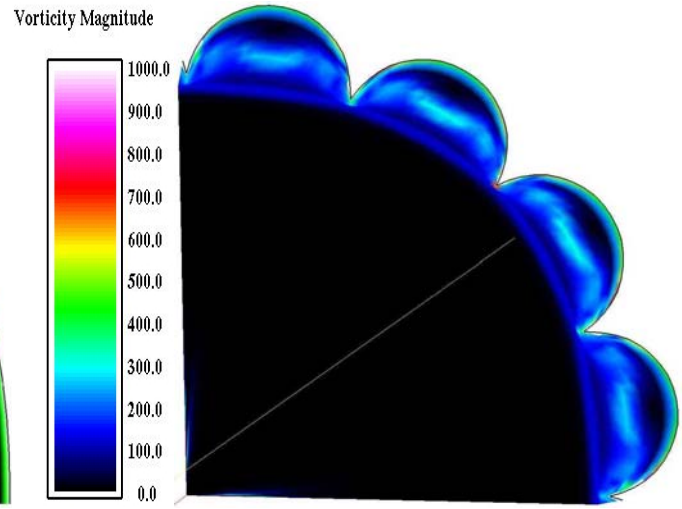

Figure 79. Vorticity Magnitude Plot of 2.75 inches Diameter Cylindrical Combustor (Left).
Figure 80. Vorticity Magnitude Plot of 2.25 inches Diameter Scalloped Combustor (Right).

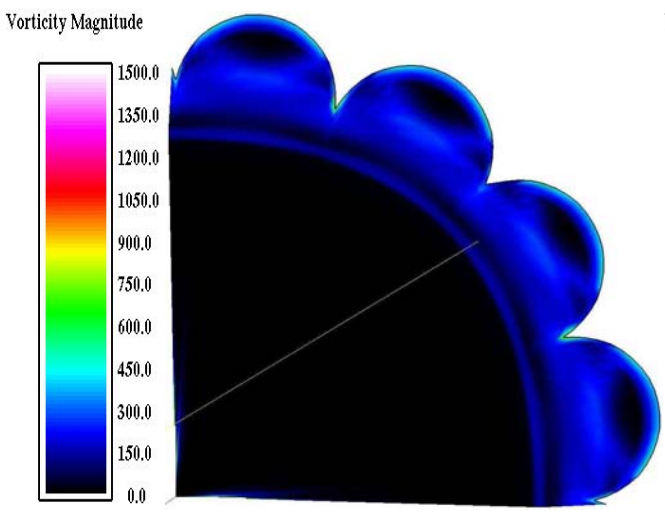

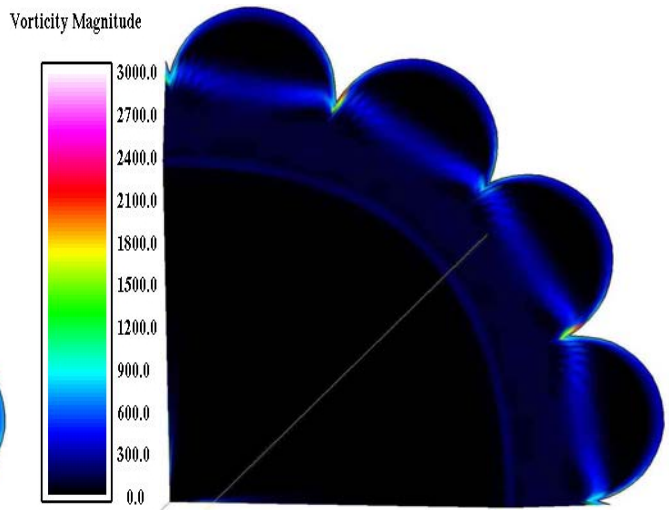

Figure 81. Vorticity Magnitude Plot of 2.5 inches Diameter Scalloped Combustor (Left).
Figure 82. Vorticity Magnitude Plot of 2.75 inches Diameter Scalloped Combustor (Right).

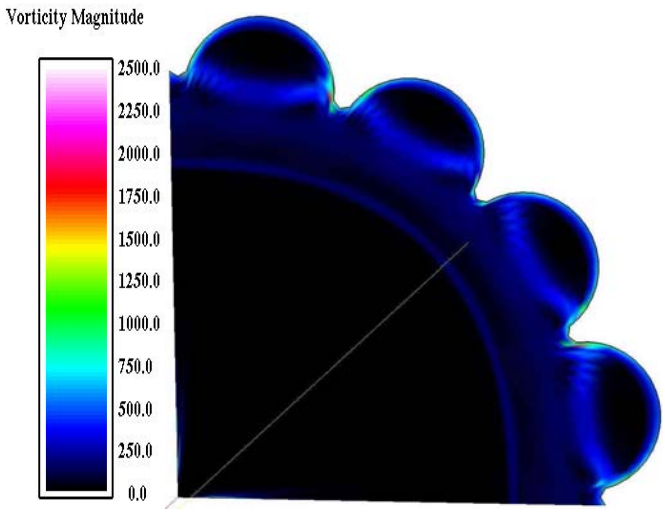

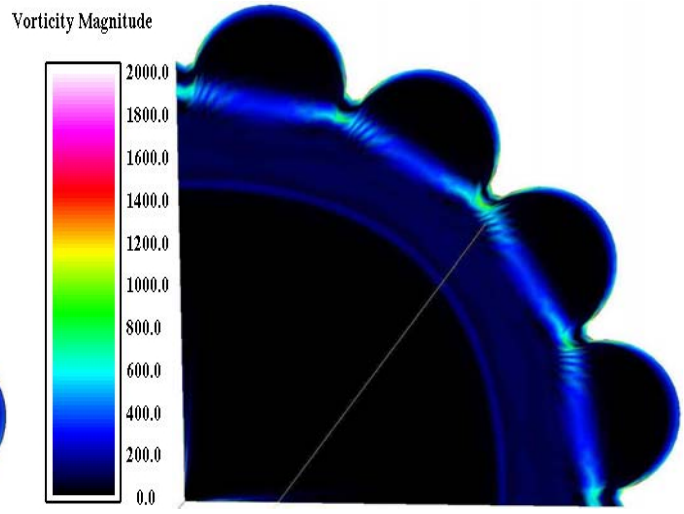

Figure 83. Vorticity Magnitude Plot of 2.75 inches Diameter Modified Scalloped Combustor (Left).
Figure 84. Vorticity Magnitude Plot of 3 inches Diameter Modified Scalloped Combustor (Right).

LIST OF REFERENCES

1. Kuo, K. K., Principles of Combustion, John Wiley & Sons, Inc., 1986.

2. Glassman, I., Combustion, Academic Press, Inc., 1987.

3. Bussing, T., Pappas, G., "An Introduction to Pulse Detonation Engines," 33rd AIAA Aerospace Sciences Meeting & Exhibit, Reno, Nevada, January 11-14, 1999, Paper No. AIAA 94-0263.

4. Williams, F.A., Combustion Theory, Addison-Wesley, Reading, Massachusetts, 1965.

5. Sexton, N.G., "Detonability of Hydrocarbon/Air Mixtures Using Combustion Enhancing Geometries for Pulse Detonation Engines", Master's Thesis, Naval Postgraduate School, 2001.

6. Roy, G.D., Frolov, S.M., Netzer D.W., Borisov A.A., High-Speed Deflagration and Detonation, ELEX-KM Publishers, 2001.

7. Brophy, C.M., LT Werner, S., Sinibaldi, J.O., "Performance Characterization of a Valveless Pulse Detonation Engine", 41st Aerospace Sciences Meeting & Exhibit, Reno, Nevada, January 6-9, 2003, Paper No. AIAA 2003-1344.

8. Roy, G.D., Frolov, S.M., Santoro, R.J., Tysganov, S.A., Confined Detonations and Pulse Detonation Engines, Torus Press, 2003.

9. Steinbrenner, J.P., Chawner, J.R., The GRIDGEN Version 9 Multiple Block Grid Generation Software, MDA Engineering, Inc., 1994.

10. Pomerantz, B., "Aerodynamic Analysis of a Modified, Pylon-Mounted JSOW/CATM Using Multi-Grid CFD Menu", Master's Thesis, Naval Postgraduate School, 1997.

11. Buning, P.G., Jespersen, D.C., Pulliam, T.H., Chan, W.M., Slotnick, J.P., Krist, S.E., Renze, K.J., Overflow User's Manual Version 1.8w, NASA Ames Research Center, 2002.

12. Walatka, P.P, Clucas, J., FAST User Guide, Computer Science Corp, Sterling Software, Inc., 1993.

THIS PAGE INTENTIONALLY LEFT BLANK

INITIAL DISTRIBUTION LIST

1. Defense Technical Information Center
   Ft. Belvoir, Virginia

2. Dudley Knox Library
   Naval Postgraduate School
   Monterey, California

3. Curriculum Office, Code MAE
   Department of Mechanical and Astronautical Engineering
   Naval Postgraduate School
   Monterey, California

4. Prof. Christopher M. Brophy, Code MAE/Br
   Department of Mechanical and Astronautical Engineering
   Naval Postgraduate School
   Monterey, California

5. Prof. Garth V. Hobson, Code MAE/Hg
   Department of Mechanical and Astronautical Engineering
   Naval Postgraduate School
   Monterey, California

6. Prof. Tat Soon Yeo
   Temasek Defense Systems Institute
   National University of Singapore
   Block E1, 1 Engineering Drive 2, #05-05
   Singapore 117576

7. Mr. Kwok Weng Jimmy Chan
   Block 765, Choa Chu Kang North 5, #06-315
   Singapore 680765